Spectroscopy and dynamics of small molecules in solid parahydrogen

Doctoral Thesis

Hiromichi Hoshina

Division of Chemistry, Graduate School of Science,
Kyoto University, Kyoto 606-8502, Japan.

June 4, 2003

Contents

Introduction

0.1 Salient features of solid parahydrogen for spectroscopic and chemical dynamics studies

Because of the symmetry requirement of the total wavefunction of hydrogen molecule, there are two modifications for hydrogen molecules in nature.[1] Hydrogen molecules, H_2, having the nuclear spin angular momentum of $I = 0$ are called *para*-hydrogen, and those having $I = 1$ are called *ortho*-hydrogen. *Para*-hydrogen in its ground electronic state is associated with the rotational states of even quantum numbers only, while *ortho*-hydrogen is associated with odd numbers exclusively. Since the interconversion between the $I = 0$ and $I = 1$ nuclear spin states is very slow in the absence of an external magnetic field, *para*-hydrogen and *ortho*-hydrogen can be considered to be different molecules under normal conditions.[2]

At room temperatures, the equilibrium population ratio between *ortho*-hydrogen and *para*-hydrogen is 3:1. At very low temperatures, *para*-hydrogen and *ortho*-hydrogen occupy their lowest rotational energy levels, that is, the $J = 0$ and 1 levels, respectively. Hereafter, the terms para and ortho are used to signify hydrogen molecules in the $J = 0$ and $J = 1$ rotational states, respectively, as we deal with hydrogen molecules at very low temperatures.

In this thesis, energy levels and dynamics of small molecules trapped in solid parahydrogen (p-H_2) are studied by high resolution spectroscopy. High-

resolution spectroscopy is a powerful technique to investigate details of energy levels and dynamics of atoms and molecules, but its application is generally limited to spectroscopy in the gas phase. In condensed media, relaxation of the excited state is fast due to strong intermolecular interactions to make the spectral line width very broad. In addition, inhomogeneous broadening of the line width is inevitable in condensed phase. Broadening of the line width makes the observation of fine structures in condensed media difficult. Solid p-H_2, however, allows us exceptionally high resolution spectroscopy, because of its properties enumerated in the following.

- Since the $J = 0$ rotational wavefunction has a completely spherical character, p-H_2 has no permanent electric moments of any order. Thus, the crystal of p-H_2 provides a homogeneous environment for a guest molecule embedded therein.

- As compared with rare gas solids, the lattice constant of solid p-H_2 is considerably larger (3.78 Å) because of the large zero-point lattice vibration due to the small mass of the H_2 molecules. The mean amplitude of the zero-point vibration in solid p-H_2 amounts to almost 20 % of the lattice constant.[3] The large lattice constant and the large amplitude of zero point lattice vibration of p-H_2 molecules in solid phase provides a free space for guest molecules which is significantly wider than other matrices.

- Because of the large lattice constants of solid p-H_2, interactions between the guest molecule and surrounding host molecules become weak compared with those in rare gas atom matrices, although the polarizability of hydrogen molecule is larger than that of Ne atom. As a result, the lifetime of excited states of a guest molecule in solid p-H_2 becomes much longer.

- Because of the softness of the crystal due to the large zero point lattice vibration, the self-repairing power of solid p-H_2[1] makes the imperfection of the crystal structure around the dopant molecules very small, which allows quantitative analyses of fine spectral structures of doped molecules as being trapped in the D_{3h} crystal field proper to the neat p-H_2 solid.[4]

By virtue of the above salient features of solid p-H_2, infrared spectra of molecules therein show surprisingly sharp linewidths associated with well-quantized, rotation-vibration states.[4] Thus, we have been able to perform high resolution spectroscopy of dopant molecules and to analyze fine spectral structures originating from subtle interactions by surrounding crystal lattice.[4,5] For example, CD_4 in solid p-H_2 shows extremely sharp absorption lines of the ν_3 and ν_4 ro-vibrational. The width of one of the two becomes as narrow as 0.015 cm^{-1} (45 MHz) at 3.7 K.[6] This width is one or two orders of magnitude smaller than the width of rovibrational lines in conventional matrix isolation spectroscopy. From the quantitative analysis of the ro-vibrational structure of CD_4, information on intermolecular interactions was successfully obtained. (See Chapter 1)

In addition to the advantages of the solid p-H_2 in high resolution spectroscopy, the solid is useful for the study of chemical reactions at cryogenic temperature; the absence of the cage effect in solid p-H_2 matrix is advantageous for studying photochemical reactions in condensed phase. In rare gas matrices, *in situ* photolysis is prohibitive, because the photolyzed species can not escape from the trapping site due to the cage effect. In contrast, the photofragment in the solid p-H_2 crystal can be separated utilizing the excess energy of photo-dissociation. Using these advantages of solid p-H_2, unstable molecules such as methyl radicals produced by the *in situ* photolysis of methyl iodide can be easily studied, for example.[7]

Solid p-H_2 matrix allows also a spectral measurement for a long period

of time, which is favorable for observation of slow secondary reactions which occur subsequent to the photolysis. Thus, we were able to monitor very slow chemical reactions by quantum mechanical tunneling.

0.2 Outlines of the spectroscopic study of rotating molecules trapped in solid parahydrogen

In Part I, foreign molecules executing rotational motion in solid p-H_2 are studied by analyzing their ro-vibrational spectra. This part consists of three chapters on the subjects of CD_4, CD_3 and C_3. The CD_3 radical was produced by *in situ* photolysis of CD_3I while C_3 was obtained from the photodissociation of acetylene cluster by using 193 nm ArF laser. The rovibrational spectra of CD_4 and CD_3 were successfully analyzed by taking into account the crystal field potential which is constructed by the summation of the pairwise potential between the trapped molecule and the surrounding hydrogen molecules. Although the rotational constants of CD_4 and CD_3 are slightly decreased in solid p-H_2 because of the renormalization of the dynamical motion of surrounding hydrogen molecules, they are almost freely rotating in the crystal. On the other hand, the obtained infrared spectra of C_3 did not show a rotational structure. The spectral structure of C_3 was explained not by the rotational motion but by the tunneling motion of C_3 in between the trapping sites of solid p-H_2. The difference of the dynamical motion between methanes (CH_4, CD_4) and C_3 originates from the difference in the size of molecules. As molecules become larger, the molecular rotation become hindered, and finally it stop rotating.

0.3 Outlines of the chemical dynamics study

Studies of cryo chemical reactions are important not only for analysis of the contribution of the tunneling effect to chemical reactions, but also for the reactions in interstellar clouds. In particular, chemical reactions of the type of $X + H_2 \rightarrow XH + H$ are regarded as constituting major links in molecular processes in the outer space because of the overwhelming abundance of hydrogen in the universe. Until recently, X was considered to be positive ions as in the examples of $CH^+ + H_2 \rightarrow CH_2^+ + H$ and $NH_3^+ + H_2 \rightarrow NH_4^+ + H$. This is because ion-molecule reactions proceed with temperature-independent Langevin rate coefficients so that they can be candidates for molecular evolution compatible with the environment in the outer space. However, as is reviewed by Herbst,[9] reactions between neutral radicals and molecules also appear surprisingly rapid at low temperatures. Under the circumstance the experimental investigation on the tunneling contribution to chemical reactions between neutral molecules is desired.[10]

In Part II, tunneling chemical reactions of molecules in solid parahydrogen are studied. Spectra of deuterated methyl radicals (CD_3, CHD_2, CH_2D, and CH_3) trapped in solid parahydrogen were observed by an FTIR spectrometer. The decrease in the absorption intensity of radicals and the increase in the intensity of methane were observed over a span of about one week. As a result of the study, it was found that radicals reacts with surrounding hydrogen molecules.

$$R + H_2 \rightarrow RH + H \tag{1}$$

$$(R = CD_3, CHD_2, CH_2D, CH_3)$$

The reaction (1) takes place at 5 K in solid *p*-H_2. Since the activation energy of this reactions is $\simeq 4000$ cm^{-1}, thermal activation for the reactions at 5 K is prohibitive. Therefore, the occurrence of the reaction (1) must be ascribed exclusively to quantum tunneling. To our knowledge the present work

provides the first direct spectral evidence for exclusive tunneling reaction between neutral molecules.

Assuming that the reactions can be expressed by a pseudo first-order rate law, the rate constants were determined by the least squares fitting to the temporal change of the intensities of radicals and methane. The obtained rate constants show different values for different species. As the mass of the radicals increases, the reaction rate increases. This correlation may reflect the density of state of the ground states of reactants and products.

Bibliography

[1] J. Van Kranendonk, *Solid Hydrogen, Theory of the properties of solid H_2, HD, and D_2*, (Plenum, New York, 1983).

[2] P.C. Souers, *Hydrogen Properties for Fusion Energy* (University of California Press, Berkeley, 1986).

[3] I.F. Silvera, *Rev. Mod. Phys.* **52** 393 (1980).

[4] T. Momose, T. Miki, T. Wakabayashi, T. Shida, M.-C. Chan, S.S. Lee, and T. Oka, *J. Chem. Phys.* **107**, 7707 (1997).

[5] S. Tam, M.E. Fajardo, H. Katsuki, H. Hoshina, T. Wakabayashi and T. Momose, *J. Chem. Phys.* **111**, 4191 (1999).

[6] H. Katsuki, and T. Momose, *Phys. Rev. Lett.* **84**, 3286 (2000).

[7] T. Momose, M. Miki, M. Uchida, T. Shimizu, I. Yoshizawa, and T. Shida, *J. Chem. Phys.* **103**, 1400 (1995).

[8] M. Hartmann, R.E. Miller, J. P. Toennies, and A. Vilesov, *Phys. Rev. Lett.* **75**, 1566 (1995).

[9] E. Herbst, *Annu. Rev. Phys. Chem.* **46**, 27 (1995).

[10] V.A. Benderskii, D.E. Makarov, and C.A. Wight, *Chemical Dynamics at Low Temperatures*, (John Wiley & Sons, Inc., New York, 1994).

Part I

Spectroscopy of small molecules trapped in solid parahydrogen

Chapter 1

Infrared spectroscopic study of rovibrational states of perdeuterated methane (CD_4) trapped in parahydrogen crystal

Abstract

The triply degenerate stretching (ν_3) and bending (ν_4) modes of CD_4 in solid parahydrogen at cryogenic temperatures are studied by Fourier transform infrared (FTIR) spectroscopy to reveal crystal field split rovibrational structures. The observed spectra are analyzed by taking into account the crystal field potential which is constructed by the summation of the pairwise (dispersive) potential between the methane and the surrounding hydrogen molecules. By the least-squares fitting of the observed to a theoretical model the molecular constants of CD_4 as well as the potential coefficient are determined as in the previous work on the CH_4/p-H_2 system. The potential is approximated to be proportional to the product of the polarizability of hydrogen molecule, the dipole-quadrupole polarizability of methane, and the inverse of the seventh power of the intermolecular distance between methane

and hydrogen molecules. From the ratio of the potential coefficients of CH_4 and CD_4 the dipole-quadrupole polarizability of CD_4 is found to be 0.875 times that of CH_4 under the assumption that the quantum renormalization effect is negligible. A novel temperature dependence of the lineshape of the ν_3 and ν_4 modes is discovered over the range of 4.5 and 8.0 K.

1.1 Introduction

Interaction between molecules is a broad concept ranging from vigorous chemical reactions to subtle perturbations perceptible only by way of the virial coefficient, for example. As any two molecules approach each other the dispersion force sets in to form van der Waals complexes which have long been studied. Recent progress in high-resolution spectroscopy in combination with the molecular beam technique has contributed greatly to the understanding of the interaction between molecules. Molecular clusters are one of the popular subjects of the current molecular science.

However, the research of the intermolecular interaction is almost exclusively confined in the gas phase system especially when quantitative assessment of the interaction is concerned. In condensed media the constituent molecules interact each other much more strongly and in complicated ways than in the isolated loose complex in the gas phase. The strong interaction results in a severe spectral line broadening and smears out subtle spectral information on the intermolecular interaction.

A turning point of this situation arrived in 1989 when Oka and his coworkers found that the linewidth of a high ΔJ rotational transition ($v = 0 \leftarrow 0$, $J = 6 \leftarrow 0$) of solid parahydrogen (p-H_2) was as narrow as 180 MHz ($\cong 0.006$ cm^{-1} at FWHM).[1] An even higher resolution of 0.0003 cm^{-1} was observed in a stimulated Raman gain spectroscopy of the solid.[2] These discoveries opened an avenue of high-resolution spectroscopy of the solid p-H_2

itself as well as of impurities in the solid.[3] The extreme sharpness of the spectral line in solid p-H_2 is due to the following intrinsic properties of the solid:

1. The average charge density in p-H_2 at cryogenic temperatures is spherical because the rotational quantum number $J = 0$ nullifies the expectation value of all the permanent multipole moments. This property leaves the feeble electrostatic perturbation due to the dispersion force as the only intermolecular interaction.

2. The distance between the two neighboring hydrogen molecules is as large as 3.783 Å and the zero-point lattice vibrational amplitude amounts to about 20 % of the nearest neighbor distance. This property brings forth a roomy and soft environment for molecules embedded in the solid.

3. Being the lightest molecule the rotational and the vibrational energy spacings of p-H_2 in the solid are very large compared with other molecular aggregates. The low density of state implies inefficient dissipation of energy of excited molecules in the solid p-H_2, and leads to remarkably narrow homogeneous linewidths.

4. As a quantum solid like solid ^{3}He and ^{4}He the solid p-H_2 has a propensity of self ordering and inhomogeneity caused by the accommodation of foreign molecules is minimized. This property mitigates the cumbersome problem of formation of multi-sites often encountered in conventional rare gas matrices.

By virtue of the above features of the solid p-H_2, foreign molecules embedded in the solid will find themselves in a nearly free and uniform environment with a low rate of energy relaxation. Moreover, they are free from the Doppler effect in contrast to molecules in the gas phase. Capitalizing on

these salient features we have been studying molecular spectroscopy of foreign molecules in the solid p-H_2 since 1995.[4–11] Fajardo's group also has been studying atoms and molecules in solid p-H_2.[12,13] In our high-resolution spectroscopic studies[8–11] we have found that the spectral resolution is high enough to resolve fine splittings due to the anisotropic interaction between a foreign molecule and hydrogen molecules. The rovibrational spectrum together with the fine splittings of foreign molecules in the p-H_2 crystal is subjected to an extensive quantitative analysis to obtain parameters to gauge the intermolecular interaction, in addition to the usual molecular constants such as the rotational constant and the Coriolis coupling constant.[8,9] The feasibility of the quantitative analysis of spectrum attaches great importance to high resolution spectroscopic studies in the p-H_2 crystal. The p-H_2 crystal used as the matrix allows us not only the high-resolution spectroscopy but also photochemical studies by monitoring the change of the unmistakable "fingerprint" rovibrational spectra of reactants and products in the photolysis,[4–7] as summarized in our review article.[11]

This chapter presents a high-resolution spectroscopic study on intermolecular interaction for the CD_4/p-H_2 system. The observed spectra of the ν_3 (triply degenerate C-D stretching) and the ν_4 (triply degenerate bending) modes of CD_4 are fully analyzed in terms of a model in which a CD_4 molecule substitutionally occupies a site of a p-H_2 molecule in the hexagonal close-packed (hcp) crystal of D_{3h} symmetry. In addition to the rovibrational structure, crystal field splittings are observed as in our previous study on the CH_4/p-H_2 system.[8,9] From the comparison of the molecular constants of CH_4 and CD_4 determined by the present and the previous work,[9] we are able to estimate the isotope effect on the dipole-quadrupole polarizability of methane quantitatively. Moreover, a remarkable dependence of the lineshape upon the temperature is found in the range of about 4.5 and 8.0 K. Such a dependence suggests an intrinsic nature of interaction between the

intramolecular rovibrational motion and the phonon of the p-H_2 crystal.

1.2 Experiment

The experimental procedure is essentially the same as the previous work on the CH_4/p-H_2 system.[9,11] The perdeuterated methane (CD_4) of 99.2 atomic % from Isotec Inc. was used as received. The admixture of the deuterated methane and p-H_2 with a contamination of about 0.1% of o-H_2 was in the volume ratio of about 1 to 10^5, which was introduced to a copper optical cell of a dimension of 1.7 cm in inner diameter and 3.0 cm in optical path length at about 8.5 K to yield a transparent mixed crystal in about 2 hours. The crystal was then cooled to 4.5±0.1 K, at which temperature all the spectral recording was performed except for the runs to investigate the temperature effect on the lineshape. In the latter, the whole ν_3 and the ν_4 band regions were recorded at several temperatures between 4.5 and 8.0 K.

A Fourier transform infrared (FTIR) spectrometer Bruker IFS 120HR was employed typically with 1000 scans in 10 hours at a resolution of 0.01 cm^{-1}. A globar source, a KBr beam splitter, and a liquid N_2 cooled HgCdTe detector were used as in the previous work on the CH_4/p-H_2 system.[9,11] In the investigation of the temperature effect on the lineshape a resolution of 0.1 cm^{-1} was employed.

1.3 Theory

In this section we briefly describe the theoretical framework to study the intermolecular interaction. We have already developed the theory for the prototype CH_4/p-H_2 system in our previous study where we have presented two approaches to express the intermolecular potential.[8,9] The first approach relies on the symmetry of the methane molecule (T_d) and of the crystal (D_{3h}). The second approach is based on the summation of pairwise intermolecular

interaction over the whole crystal. In the present work we will adopt the second approach because of its conceptual concreteness.

In order to analyze the rotational energy levels of methane interacting with surrounding hydrogen molecules, we need the interaction potential which depends on the orientation of methane. First, we describe the pairwise interaction between a methane and a hydrogen. Since both methane and p-H_2 molecules possess no permanent dipole nor quadrupole moment, the interaction between them is mainly due to the dispersion force. Among the potential due to the dispersion the first leading anisotropic term for a single pair of methane and p-H_2 with a separation of R is approximated as follows.[8,9,11]

$$v(\omega; R) = a_3(R)\frac{i}{\sqrt{2}}[D^{(3)}_{2,0}(\omega) - D^{(3)}_{-2,0}(\omega)] \tag{1.1}$$

The angle ω stands for the Euler angles of the methane relative to the intermolecular axis between the paired methane and hydrogen molecules. The distance-dependent coefficient $a_3(R)$ can be related to the term involving the polarizability of hydrogen α_{H_2} and the dipole-quadrupole polarizability of methane A in the classical expansion of the dispersion force as in the following. (See Appendix)

$$a_3(R) \propto \alpha_{H_2} A/R^7 \tag{1.2}$$

The terms in the square bracket in Eq.(1.1) represent Wigner's rotation matrices for the methane. The definition and the phase of Wigner's rotation matrices are the same as before.[8,14,15] The angular dependence of $v(\omega; R)$ is described by the bracketed factor only. The next order interaction term originating from the quadrupole polarizability of methane is negligibly small[8,9] so that we will ignore it in this chapter.

Next, we consider the interaction potential of methane surrounded by the infinite number of hydrogen molecules. Since we can safely assume the additivity of the dispersion, the potential for the central methane can be

simply obtained by summing the interactions in Eq.(1.1) for all the pairs between the methane and hydrogen molecules. The resultant potential can be concisely written as,

$$V(\Omega) = \epsilon_{3c} V_3(\Omega) \tag{1.3}$$

where the distance-dependent coefficient $a_3(R)$ in Eq.(1.1) is related to the coefficient ϵ_{3c} in Eq.(1.3) as,

$$\epsilon_{3c} = i\sqrt{2} a_3(R_0) \sum_{i=1}^{\infty} (R_0/R_i)^7 D^{(3)*}_{0,3}(\Omega_{\to i}) \tag{1.4}$$

and the angular part $V_3(\Omega)$ in Eq.(1.3), after the summation over the whole D_{3h} lattice, becomes as

$$V_3(\Omega) = \frac{1}{2}[D^{(3)}_{2,3}(\Omega) - D^{(3)}_{-2,3}(\Omega) + D^{(3)}_{2,-3}(\Omega) - D^{(3)}_{-2,-3}(\Omega)] \tag{1.5}$$

with the running number i in $\Omega_{\to i}$ in Eq.(1.4) over all the hydrogen molecules $1 \sim \infty$. R_0 and R_i in Eq.(1.4) stand for the nearest neighbor distance between the hydrogen molecules in the crystal and the distance between methane and a hydrogen molecule i, respectively. The angle Ω is the Euler angles of the central methane relative to the crystal axis (c-axis) and the angle $\Omega_{\to i}$ represents the orientation of the pair axis between the methane and the i-th hydrogen molecule relative to the crystal axis. The sum of $\sum_{i=1}^{\infty}(R_0/R_i)^7 D^{(3)*}_{0,3}(\Omega_{\to i})$ is calculated as $0.5290i$ for the hcp lattice.[9] Here, the crystal axis (XYZ) is defined such that the Z-axis is along the c-axis and Y-axis is parallel to one of the two-fold axes of the crystal. The potential thus obtained in Eq.(1.3) is, of course, invariant to all the symmetry operations of both methane (T_d) and the crystal (D_{3h}). We call the potential in Eq.(1.3) as the crystal field potential. Note that the crystal field is related to the pairwise intermolecular interaction of Eq.(1.1) as in Eq.(1.4), thus once the coefficient ϵ_{3c} is determined, we can deduce the pairwise interaction without ambiguity.

The rotational energy levels in the ground vibrational state can be calculated as the eigenvalue of the matrix of Hamiltonian $\mathscr{H} = B''\hat{J}^2 + V(\Omega)$ where $\hat{J}$ is the rotational angular momentum operator and B'' is the rotational constant of the ground state. The rotational levels in the triply degenerate excited vibrational states can be obtained with the Hamiltonian $\mathscr{H} = \nu_0 + B'\hat{J}^2 + \mathscr{H}_{cor} + V(\Omega)$ where ν_0 is the band origin, B' is the rotational constant of the excited vibrational states and $\mathscr{H}_{cor}$ is the Hamiltonian for the Coriolis interaction.

The interaction potential $V(\Omega)$ in Eq.(1.3) causes the splitting of the degenerate states of the spherical rotor in the free space into M sublevels. The split levels can be labeled by use of the irreversible representations of an extended group obtained from the direct product of the molecular symmetry group (T_d) and the crystal point group (D_{3h}) with a proper consideration of the parity of the whole system.[8]

1.4 Results and discussion

1.4.1 Spectral assignment

Figures 1.1 and 1.2 demonstrate typical recordings of the ν_3 and the ν_4 bands of CD_4 in p-H_2 at 4.5 K. The temporal change at this temperature due to the relaxation of the nuclear spin state was insignificant in contrast to the noticeable isothermal change of the spectral pattern in the CH_4/p-H_2 system.[9,11] The peaks are assigned to the crystal field split rovibrational transitions as a result of the analysis similar to that for the CH_4/p-H_2 system.[8,9] The sticks in the figures stand for the calculated transitions (see below). With the interaction potential in Section 1.3 the rovibrational states of CD_4 are determined with a total of 8 parameters, that is, the three rotational constants B'', B'_3, and B'_4, the two band origins ν_3 and ν_4, the two Coriolis constants ζ_3 and ζ_4, and one potential coefficient ϵ_{3c} in Eq.(1.3). The potential coefficient ϵ_{3c} is

assumed to be the same for the ground and the excited vibrational states as in the previous work.[9] By the least-squares fitting of the observed spectra, the parameters are determined as summarized in Table 1.1, where the previously determined values of CH_4 in the p-H_2 crystal as well as those in the gas phase are included for comparison. The spectral assignments attained by the least-squares fitting are summarized in Tables 1.2 and 1.3 for the ν_3 and ν_4 bands, respectively. It is seen that the residual errors between the observed and the calculated transition energies are satisfactorily small relative to the typical linewidth of 0.3 cm^{-1}. The sticks in Figs.1.1 and 1.2 represent the calculated transition energies in Tables 1.2 and 1.3, respectively.

Table 1.1: The optimized molecular constants of CD_4 and CH_4

	CD_4		CH_4[9]	
	Solid hydrogen	Gas phase[16,17]	Solid hydrogen	Gas phase
Ground state				
B''	2.301(36)	2.591	4.793(42)	5.241
ν_3 Excited state				
ν_3	2257.63(1)	2258.2	3017.26(11)	3019.491
B'_3	2.193(15)	2.577	4.603(18)	5.192
ζ_3	0.1335(85)	0.145	0.0450(51)	0.0558
ν_4 Excited state				
ν_4	994.31(9)	995.6	1303.62(11)	1310.761
B'_4	2.212(25)	2.574	4.591(40)	5.240
ζ_4	0.334(9)	0.355	0.4654(56)	0.4664
Crystal field				
$\lvert\epsilon_{3c}\rvert$	22.58(75)		25.80(37)	

The rotational constant B, the band origin ν, and the crystal field coefficient ϵ_{3c} of the ground and the ν_3 and ν_4 excited states are in units of cm^{-1} except for the Coriolis coupling constant ζ. The values of CH_4 are taken from Ref. 9, and the gas phase values in the third column are from Refs. 16 and 17.

We also tried to fit the spectrum by varying the potential coefficient ϵ_{3c} independently for the three states. However, the resultant values were the same within the standard deviation. Thus, the assumption of a common value for ϵ_{3c} for the three different states seems justified.

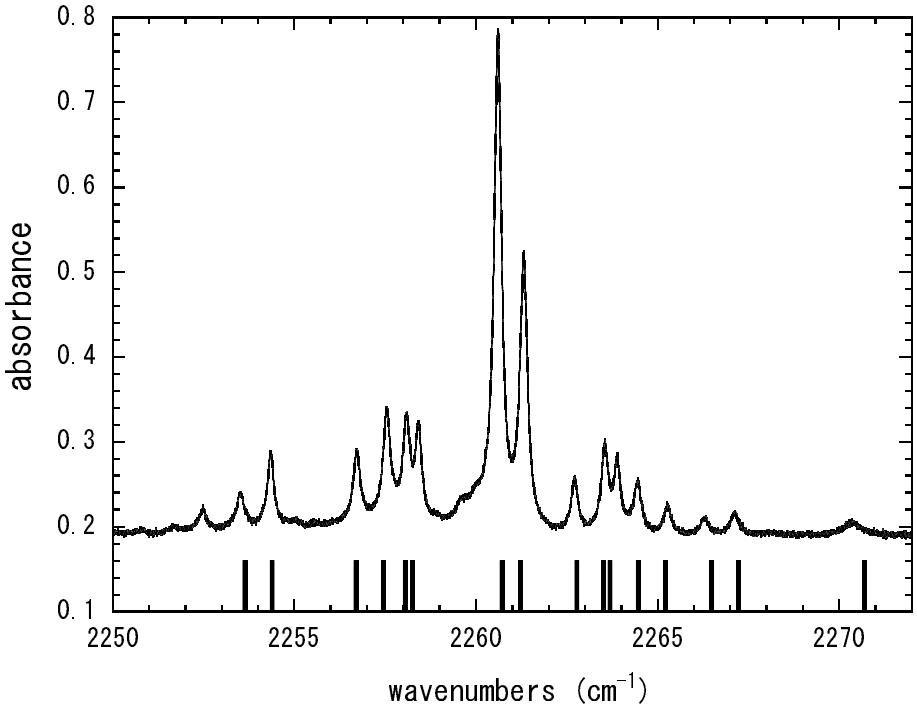

Figure 1.1: FTIR spectrum of the ν_3 fundamental band of CD_4 isolated in solid parahydrogen. The sticks show the calculated transition energies in Table 1.2.

Note that in Table 1.1 the absolute value of the coefficient $|\epsilon_{3c}|$ is given. In the previous paper[9] we reported a negative value for ϵ_{3c} as the best-fitting parameter because the theory[8] predicted the negativity of ϵ_{3c} so that in the least-squares fitting procedure in the previous work[9] we started from a negative initial value for ϵ_{3c}. However, since ϵ_{3c} appears only in off-diagonal elements of the Hamiltonian matrix, the sign of ϵ_{3c} is indeterminable in principle. For this reason we list only the absolute value of ϵ_{3c} in Table 1.1.

As shown by asterisks in the last column of Tables 1.2 and 1.3, several $\Delta R \neq 0$ transitions were observed where R stands for the sum of the quantum numbers of the rotational and vibrational angular momenta. These $\Delta R \neq 0$ become allowed transitions due to the interaction potential $V(\Omega)$ in Eq.(1.3). By virtue of these $\Delta R \neq 0$ transitions the rotational constants B_i'

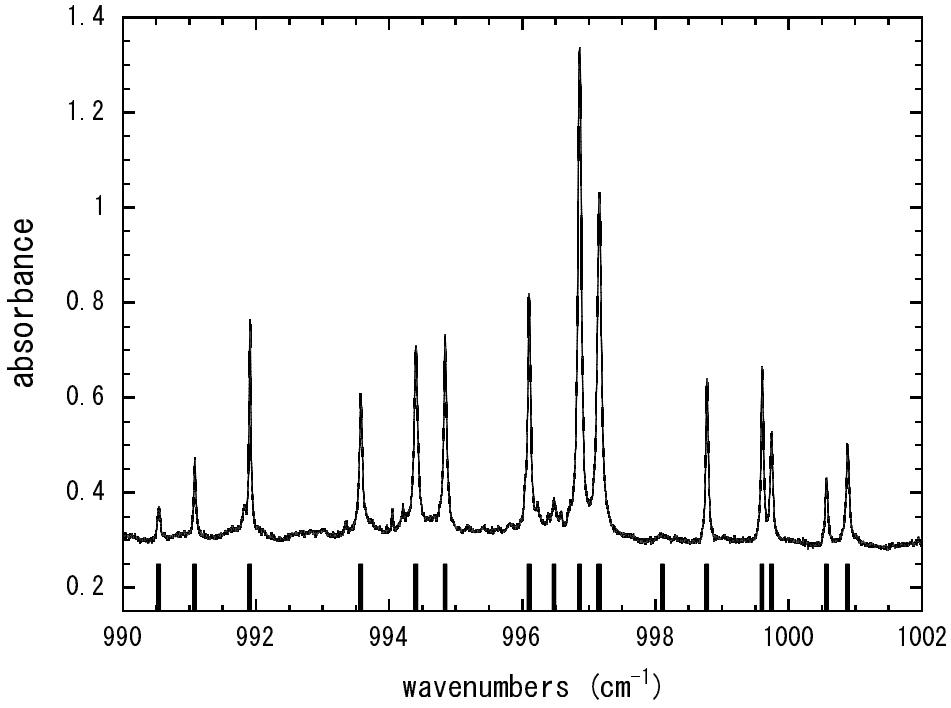

Figure 1.2: FTIR spectrum of the ν_4 fundamental band of CD_4 isolated in solid parahydrogen. The sticks show the calculated transition energies in Table 1.3.

and the Coriolis coupling constants ζ_i for the excited vibrational states can be determined independently as shown in Table 1.1.

1.4.2 Molecular constants

Comparison of the rotational constants and the Coriolis parameters in Table 1.1 reveals that the statement made on the rotational motion of the CH_4/*p*-H_2 system in our previous work is also true in the CD_4/*p*-H_2 system (see Section VI-A of Ref.9), that is, a CD_4 molecule in the *p*-H_2 crystal is rotating almost freely as in the gas phase with a slight increase of the effective mass for the rotation. The rotational constants of CD_4 in solid *p*-H_2 are about 10% smaller than in the gas phase. The decrease of the rotational constants should be attributed to the increase of the effective mass of methane caused

by the isotropic dispersion interaction between the methane and surrounding hydrogen molecules. Although we cannot evaluate the isotropic interaction directly from the rotational spectra, we can be sure that the isotropic interaction is stronger in the excited vibrational states than in the ground state, because the decreases of the rotational constants in the excited vibrational states are larger than the decrease in the ground state. Furthermore, the reduction of the constants is slightly larger for CD_4 than for CH_4, which suggests that the interaction is stronger for CD_4 than CH_4.

The decrease of the absolute values of ϵ_{3c} from CH_4 to CD_4 amounts to about 12 % relative to the value of CH_4. Two possibilities are conceivable for the cause of the decrease in ϵ_{3c}. One is to ascribe the decrease to the intrinsic molecular property of CH_4 and CD_4. The other is to associate with the renormalization effect. We first consider the possibility due to the molecular property. Since the coefficient ϵ_{3c} is related to the polarizability of p-H_2 and the dipole-quadrupole polarizability of methane as is seen from Eqs.(1.2) and (1.4), the difference in ϵ_{3c} for CH_4 and CD_4 may be attributed to the difference of the dipole-quadrupole polarizability of CH_4 and CD_4. If the renormalization effect is ignorable, the ratio of the dipole-quadrupole polarizability of CD_4 and CH_4 is obtained as $A_3(CD_4)/A_3(CH_4)$=0.875 from the values of ϵ_{3c} in Tables. In the above derivation of the ratio the implicit assumption is that the dispersion interaction is additive. However, the obtained ratio may not be seriously affected even if we admit some non-additivity. Thus, the ratio may well reflect the intrinsic molecular property of the two methanes. The isotope effect on the hyperpolarizabilities like A has never been discussed before. We are only aware of the work by Raynes et. al.[18] who calculated the dipole polarizability of CH_4 and CD_4. The difference of the polarizability of CH_4 and CD_4 was mainly attributed to the difference in the contribution of the zero point vibration, which led to a smaller polarizability of CD_4 than CH_4 with a ratio of 0.74. We may expect a similar

effect for the hyperpolarizability A.

Next, we consider the second possibility for the cause of the decrease in ϵ_{3c} as due to the quantum renormalization effect. Since CD_4 is heavier and is expected to have smaller mean amplitudes of phonon than CH_4, the average of $1/R^7$ may be smaller for CD_4 for this reason.

At the moment, we have no preference between the two possibilities above. However, we should like to emphasize that the quantitative isotope effect in the intermolecular interaction found in the present work is unprecedented. Reliable quantum chemical calculations on the isotope effect of the dipole-quadrupole polarizability of methane will allow the assessment of the contribution of the quantum renormalization effect in the crystal field potential of ϵ_{3c}.

1.4.3 Temperature dependence of lineshape

Figures 1.3 and 1.4 show the temperature dependence of the doublets of the R(0) lines of the ν_3 and ν_4 bands at about 2260.6/2261.3 and about 996.8/997.1 cm^{-1}. The spectral resolution in Figures 1.3 and 1.4 is 0.1 cm^{-1}. The change is found to be completely reversible. As the temperature rises from 4.5 to 8.0 K, the intensity of all the four lines decreases. A closer examination reveals that the maxima of the "red" component of ν_3 band at 2260.6 cm^{-1} do not shift nor broaden appreciably but the "blue" component at 2261.3 cm^{-1} shift towards blue but not broaden noticeably. On the other hand, the "red"component of ν_4 band at 996.8 cm^{-1} shift towards red and broaden while the "blue" component at 997.1 cm^{-1} shift towards blue and much broaden. Other transitions also show similar temperature dependence; some but not all the transitions shift with temperature. The width of the ν_3 transition does not broaden appreciably but that of the ν_4 transition broadens noticeably. These spectral changes with temperature for the CD_4/p-H_2 system are peculiar to the deuterated system because such a no-

ticeable change has not been observed for the CH_4/p-H_2 system so far. The change in the linewidth should be closely related to the coupling between the intramolecular rovibrational motion and the lattice motion, i.e., phonon. These are the most challenging problems to solve. Spectral changes with temperature in the solid state are, of course, not uncommon, and most of them are explained in terms of the populational change of phonon states. However, the drastic change of the intensity and the linewidth in such a narrow range of 4.5 to 8.0 K is remarkable and a new mechanism may be required for elucidation. We are planning to observe the temperature dependence on the lineshape of all the isotopes of methane under higher resolutions to obtain more quantitative information. Since the p-H_2 crystal can be characterized much better than any other molecular crystals, the observed spectral change in the present work may, hopefully, play a priming role for deeper understanding of microscopic dynamics of molecular aggregates.

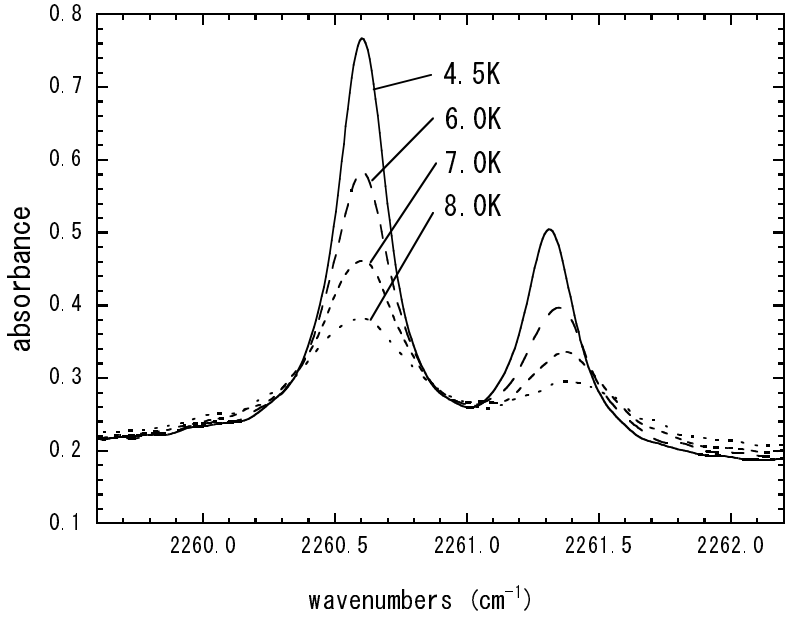

Figure 1.3: Temperature dependence of the ν_3 band of CD_4 trapped in solid parahydrogen. Only the spectral region of the R(0) transition is shown.

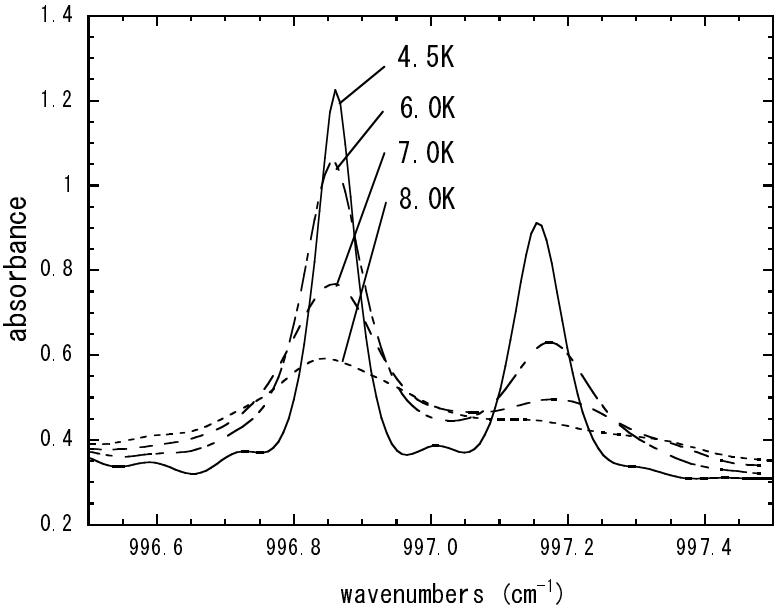

Figure 1.4: Temperature dependence of the ν_4 band of CD_4 trapped in solid parahydrogen. Only the spectral region of the R(0) transition is shown.

1.5 Concluding Remark

In this chapter, we have studied the rovibrational transition of CD_4 isolated in solid p-H_2. The quantitative analysis of the spectrum reveals the almost free rotation of CD_4 with a slight increase of the effective mass. From the ratio of potential coefficients of CH_4 and CD_4 the dipole-quadrupole polarizability of CD_4 is found to be 0.875 times that of CH_4. The novel temperature dependence of the lineshape and frequency is found over a small temperature range of 4.5 and 8.0 K, which is now under further study for more quantitative understanding.

Table 1.2: The observed transition energies, the assignments, and the calculated transition energies of the ν_3 transition of CD_4 in solid parahydrogen.

Observed		Calculated									
		Assignments									
		Upper state				Lower state					
Energy (cm^{-1})	Polarization	J'	R'	M'	Γ'	J''	M''	Γ''	Energy (cm^{-1})	Obs.-Calc.	Predicted Polarization	
2252.48												
2253.51	∥	0	1	0	$A_1\overline{F_2}$	1	0	$A_2\overline{F_1}$	2253.65	-0.14	∥	
2254.35	⊥	0	1	0	$A_1\overline{F_2}$	1	±1	$E\overline{F_2}$	2254.39	-0.04	⊥	
2256.71	⊥	1	1	±1	$E\overline{F_1}$	1	0	$A_2\overline{F_1}$	2256.71	0.00	⊥	
2257.54	∥	1	1	±1	$E\overline{F_1}$	1	±1	$E\overline{F_2}$	2257.45	0.09	∥	
2258.09	⊥	1	1	0	$A_2\overline{F_2}$	1	±1	$E\overline{F_2}$	2258.06	0.03	⊥	
2258.42	⊥	1	2	±1	$E\overline{F_2}$	1	±1	$E\overline{F_2}$	2258.26	0.16	⊥	*
2260.61	⊥	1	0	±1	$E\overline{A_1}$	0	0	$A_1\overline{A_1}$	2260.73	-0.12	⊥	
2261.32	∥	1	0	0	$A_2\overline{A_2}$	0	0	$A_1\overline{A_1}$	2261.23	0.09	∥	
2262.72	⊥	2	1	±1	$E\overline{F_1}$	1	0	$A_2\overline{F_1}$	2262.78	-0.06	⊥	
2263.55	∥	2	1	±1	$E\overline{F_1}$	1	±1	$E\overline{F_2}$	2263.52	0.03	∥	
2263.89		2	1	0	$A_1\overline{F_2}$	1	0	$A_2\overline{F_1}$	2263.70	0.19	∥	
2264.46		2	1	0	$A_1\overline{F_2}$	1	±1	$E\overline{F_2}$	2264.48	-0.02	⊥	
2265.26		2	3	±1	$E\overline{F_1}$	1	0	$A_2\overline{F_1}$	2265.22	0.04	⊥	*
2266.33		2	1	±1	$E\overline{F_1}$	1	±1	$E\overline{F_2}$	2266.49	-0.16	∥	
2267.14		2	3	0	$A_1\overline{F_2}$	1	0	$A_2\overline{F_1}$	2267.24	-0.10	∥	*
2270.37		2	1	±2	$E\overline{F_2}$	1	±1	$E\overline{F_2}$	2270.70	-0.33	⊥	
2275.70		2	3	±2	$E\overline{A_1}$	0	0	$A_1\overline{A_1}$	2275.78	-0.08	⊥	*

The columns of Γ' and Γ'' show the irreducible representation of the extended group G given in Ref.8.

The asterisk in the last column shows the transitions of $\Delta R \neq 0$

Table 1.3: The observed transition energies, the assignments, and the calculated transition energies of the ν_4 transition of CD_4 in solid parahydrogen.

Observed		Calculated									
		Assignments									
		Upper state				Lower state					
Energy (cm^{-1})	Polarization	J'	R'	M'	Γ'	J''	M''	Γ''	Energy (cm^{-1})	Obs.-Calc.	Predicted Polarization	
988.11												
990.54												
991.08	∥	0	1	0	$A_1\overline{F_2}$	1	0	$A_2\overline{F_1}$	991.19	-0.11	∥	
991.91	⊥	0	1	0	$A_1\overline{F_2}$	1	±1	$E\overline{F_2}$	991.93	-0.02	⊥	
993.58	⊥	1	1	±1	$E\overline{F_1}$	1	0	$A_2\overline{F_1}$	993.59	-0.01	⊥	
994.40	∥	1	1	±1	$E\overline{F_1}$	1	±1	$E\overline{F_2}$	994.33	0.07	∥	
994.84	⊥	1	1	0	$A_2\overline{F_2}$	1	±1	$E\overline{F_2}$	994.75	0.09	⊥	
996.10	⊥	1	2	±1	$E\overline{F_2}$	1	±1	$E\overline{F_2}$	996.10	0.00	⊥	*
996.86	⊥	1	0	±1	$E\overline{A_1}$	0	0	$A_1\overline{A_1}$	996.86	0.00	⊥	
997.16	∥	1	0	0	$A_2\overline{A_2}$	0	0	$A_1\overline{A_1}$	997.12	0.04	∥	
998.77	⊥	2	1	±1	$E\overline{F_1}$	1	0	$A_2\overline{F_1}$	998.91	-0.14	⊥	
999.60	∥	2	1	±1	$E\overline{F_1}$	1	±1	$E\overline{F_2}$	999.66	-0.06	∥	
999.75	∥	2	1	0	$A_1\overline{F_2}$	1	0	$A_2\overline{F_1}$	999.76	-0.01	∥	
1000.57	⊥	2	1	0	$A_1\overline{F_2}$	1	±1	$E\overline{F_2}$	1000.50	0.07	⊥	
1000.89	⊥	2	2	±1	$E\overline{F_2}$	1	±1	$E\overline{F_2}$	1000.82	0.07	⊥	*
1006.56												
1007.18												
1025.92												

The columns of Γ' and Γ'' show the irreducible representation of the extended group G given in Ref.8

The asterisk in the last column shows the transitions of $\Delta R \neq 0$

Bibliography

[1] M. Okumura, M.-C. Chan, and T. Oka, *Phys. Rev. Lett.* **62**, 32 (1989).

[2] T. Momose, D.P. Weliky, and T. Oka, *J. Mol. Spectrosc.* **153**, 760 (1992).

[3] T. Oka, *Annu. Rev. Phys. Chem.* **44**, 299 (1993).

[4] T. Momose, M. Miki, M. Uchida, T. Shimizu, I. Yoshizawa, and T. Shida, *J. Chem. Phys.* **103**, 1400 (1995).

[5] T. Momose, M. Uchida, N. Sogoshi, M. Miki, S. Masuda, and T. Shida, *Chem. Phys. Lett.* **246**, 583 (1995).

[6] M. Miki T. Wakabayashi, T. Momose, and T. Shida, *J. Phys. Chem.* **100**, 12135 (1996).

[7] N. Sogoshi, T. Wakabayashi, T. Momose, and T. Shida, *J. Phys. Chem.* **101**, 522 (1997).

[8] T. Momose, *J. Chem. Phys.* **107**, 7695 (1997).

[9] T. Momose, T. Miki, T. Wakabayashi, T. Shida, M.-C. Chan, S.S. Lee, and T. Oka, *J. Chem. Phys.* **107**, 7707 (1997).

[10] T. Momose, H. Katsuki, H. Hoshina, N. Sogoshi, T. Wakabayashi, and T. Shida, *J. Chem. Phys.* **107**, 7717 (1997).

[11] T. Momose and T. Shida, *Bull. Chem. Soc. Jpn.* **71**, 1 (1998).

[12] S. Tam, M. Macler, and M.E. Fajardo, *J. Chem. Phys.* **106**, 8955 (1997).

[13] M.E. Fajardo and S. Tam, *J. Chem. Phys.* **108**, 4237 (1998).

[14] E.P. Wigner, *Group Theory*, (Academic Press, New York, 1959).

[15] J.T. Hougen, *International Review of Science,* Physical Chemistry Vol 3, Ser 2, Spectroscopy, edited by D. A. Ramsay (Butterworths, London, 1976) pp. 75-125.

[16] G. Herzberg, *Molecular Spectra and Molecular Structure II*, (Krieger Publishing Company Malabar, Florida, 1991).

[17] L. H. Jones and R. S. McDowell, *J. Mol. Spectrosc.* **3**, 632 (1959).

[18] W.T. Raynes, P. Lazzeretti, and R. Zanasi, *Mol. Phys.* **64**, 1061 (1988).

Chapter 2

Infrared spectroscopy of rovibrational transition of methyl radicals (CH_3, CD_3) in parahydrogen crystal

Abstract

The ν_3 and ν_4 vibrational transitions of CH_3 and CD_3 embedded in solid parahydrogen was studied by high-resolution infrared spectroscopy. The observed spectra showed clear fine structures due to quantized rotational motion, which is subjected to the perturbation from the electrostatic field of the crystal. The spectral structures of the ν_3 transition of CD_3 were analyzed by the use of the crystal field theory we have developed previously. The rotational constant B of CD_3 determined by the least squares fitting method was found to be 6 % smaller than that in the gas phase, while the C constant was 15 % smaller. Intermolecular interaction between the radicals and surrounding hydrogen molecules are discussed based on the crystal field potential parameters.

2.1 Introduction

In a series of papers, we have demonstrated that solid parahydrogen is an exceptional matrix for isolation spectroscopy, because of its high spectral resolutions.[1–20] Infrared absorption spectra of molecules embedded in solid parahydrogen exhibits linewidths as narrow as 100MHz ($\simeq$0.003cm^{-1}),[12] which is sharp enough to resolve fine structures originated in subtle interaction by surrounding crystal lattice.

Due to the weak intermolecular interaction between hydrogen molecules, and the large lattice constant of solid parahydrogen,[22,23] small molecules such as diatomic molecules,[13,14,18] water[15] and methane[4,9,10] rotate almost freely in the crystal. These small molecules occupy a single substitutional site of the hexagonal close packed (*hcp*) lattice of solid parahydrogen. Self-repairing nature of solid parahydrogen as a quantum crystal[22] makes the crystal structure around the dopant molecules still perfect irrespective of the substitution, allowing for the quantitative analysis of the fine spectral structure with the use of the crystal field theory.[21,24] The analysis of the ro-vibrational spectra of CH_4 and CD_4 in solid parahydrogen revealed that the rotational constants of methane in solid parahydrogen were about 10 % smaller than those in the gas phase. The reduction of the rotational constants must be a result of the interaction between the rotational motion of the central molecule and the dynamical motion of the surrounding lattice. However, physical origin of the reduction is yet to be understood well. A similar reduction of the rotational constants has been observed for molecules in superfluid He nano-droplets, whose origin is still under discussion.[25–28]

In this paper, we have studied ro-vibrational transitions of CH_3 and CD_3 in solid parahydrogen aiming to understand the energy levels and dynamics of molecules in the condensed phase in more details. Infrared spectra of the methyl radicals in solid Ar have been extensively studied by Jacox et. al.[29,30]

They found that the rotational levels of the radicals do not undergo major perturbation in the Ar matrix environment. In this study, we found that the rotational levels of the methyl radicals in parahydrogen matrix were less perturbed than those in other matrices. Herein, the quantitative analysis of rotation-vibration transitions of methyl radicals in solid parahydrogen is discussed.

2.2 Experiments

The methyl radicals, CH_3 and CD_3, were produced by *in-situ* photolysis of methyl iodides in solid parahydrogen. Details of our experimental setups were described in previous papers.[1,31,32] Briefly, parahydrogen gas containing less than 0.05 % orthohydrogen was mixed with a small amount ($\sim$10 ppm) of methyl iodide (CH_3I,CD_3I) and the mixed gas was continuously run into a copper optical cell kept at about 8.5 K to grow a transparent crystal. The size of the optical cell was 3.0 cm in length and 1.7 cm in diameter. A low pressure 20 W mercury lamp was used without filters for the photolysis of the methyl iodides. A UV irradiation of about 2 hours was enough to produce sufficient numbers of methyl radicals. A Fourier-transform infrared (FTIR) spectrometer (Bruker IFS 120HR) was used for the recording of infrared absorption. A globar source, a KBr beam splitter, and a liquid N_2 cooled HgCdTe detector were used for the FTIR measurements.

2.3 Observed spectra

Figure 2.1 shows the infrared absorption spectra of CH_3 in solid parahydrogen observed at 4.5 K. Traces (a) and (b) show spectra of the doubly degenerate stretching (ν_3) transition and the doubly degenerate bending (ν_4) transition, respectively. In each transition, only a doublet was observed. The transition wavenumbers and its polarization are listed in Table 2.1. The assignment of

quantum numbers in Table 2.1 is discussed in later sections. No temporal change of the intensities was observed for a period of a week.

Figure 2.2 shows the absorption of CD_3 in solid parahydrogen at 4.5K. Traces (a) and (b) are the spectra of the doubly degenerate stretching (ν_3) transition and the doubly degenerate bending (ν_4) transition, respectively. The transition wavenumbers and its polarization are listed in Tables 2.2 and 2.3. The total intensity of the whole band decreased in a few days resulting from the tunneling reaction of $CD_3 + H_2 \rightarrow CD_3H + H$.[32,33] Nevertheless, intensity alternation among each transition was not observed for a week within our detection limit.

As clearly seen in Figs.2.1 and 2.2, the ν_4 transition is much shaper than the ν_3 transition of both the CH_3 and CD_3 radicals. The widths (FWHM; full width at half maximum) of CH_3 at 4.5 K were 0.6 cm^{-1} and 0.1 cm^{-1} for the ν_3 and ν_4 transitions, respectively, while the widths of CD_3 were 0.2 cm^{-1} and 0.02 cm^{-1} for the ν_3 and ν_4, respectively.

2.4 Theory

Analysis of rotation-vibration spectra of molecules in crystals is significantly different from that in gaseous phase. In this section, we describe details of the theory for the quantitative analysis of the observed spectra. As is discussed previously,[21,24] we assume that each radical occupies a single substitutional site of the hexagonal-close-packed lattice. It is also assumed that the iodine atom dissociated from the radical is trapped far from the radical so that perturbations of the iodine atom to the ro-vibrational energy levels of the radicals is negligibly small.[19] We first discuss the extended group pertinent to the present system in the subsection 2.4.1. Classification of the rotational wavefunctions in terms of the irreducible representations of the extended group is given in 2.4.2. Then, the Hamiltonian of the present system for the

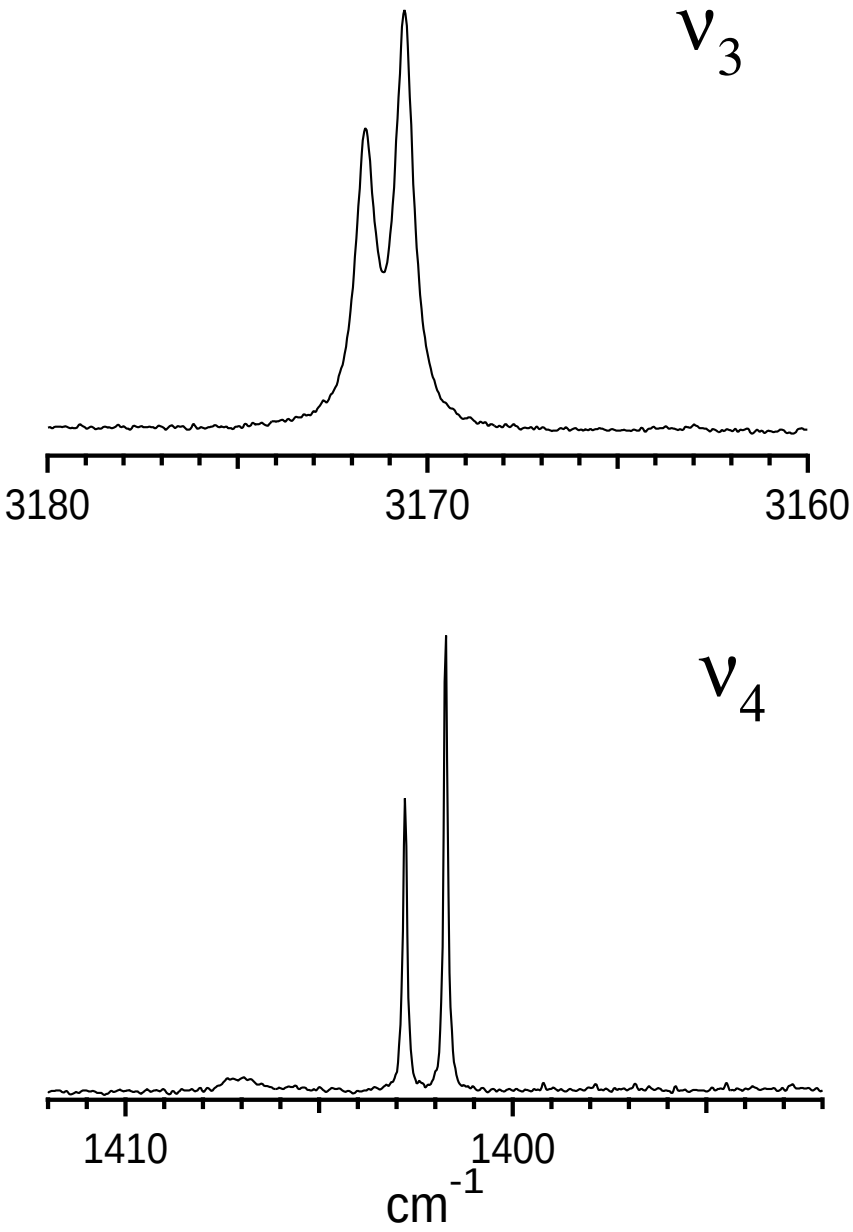

Figure 2.1: FTIR spectrum of the ν_3 (upper panel) and ν_4 (lower panel) fundamental transitions of CH_3 isolated in solid parahydrogen.

Table 2.1: The observed transition wavenumbers and the assignments of CH_3 in solid parahydrogen.

	wavenumbers	polarization	assignments								
			N'	$\|k'\|$	$\|M'\|$	l	Γ'	N''	$\|k''\|$	$\|M''\|$	Γ''
ν_3	3170.5	$\perp$	1	1	1	+	$E\overline{A_1'}(+E\overline{A_2'})$	0	0	0	$A_1\overline{A_1'}$
	3171.5	$\parallel$	1	1	0	+	$A_2\overline{A_1''}(+A_2\overline{A_2''})$	0	0	0	$A_1\overline{A_1'}$
ν_4	1401.7	$\perp$	1	1	1	+	$E\overline{A_1'}(+E\overline{A_2'})$	0	0	0	$A_1\overline{A_1'}$
	1402.8	$\parallel$	1	1	0	+	$A_2\overline{A_1''}(+A_2\overline{A_2''})$	0	0	0	$A_1\overline{A_1'}$

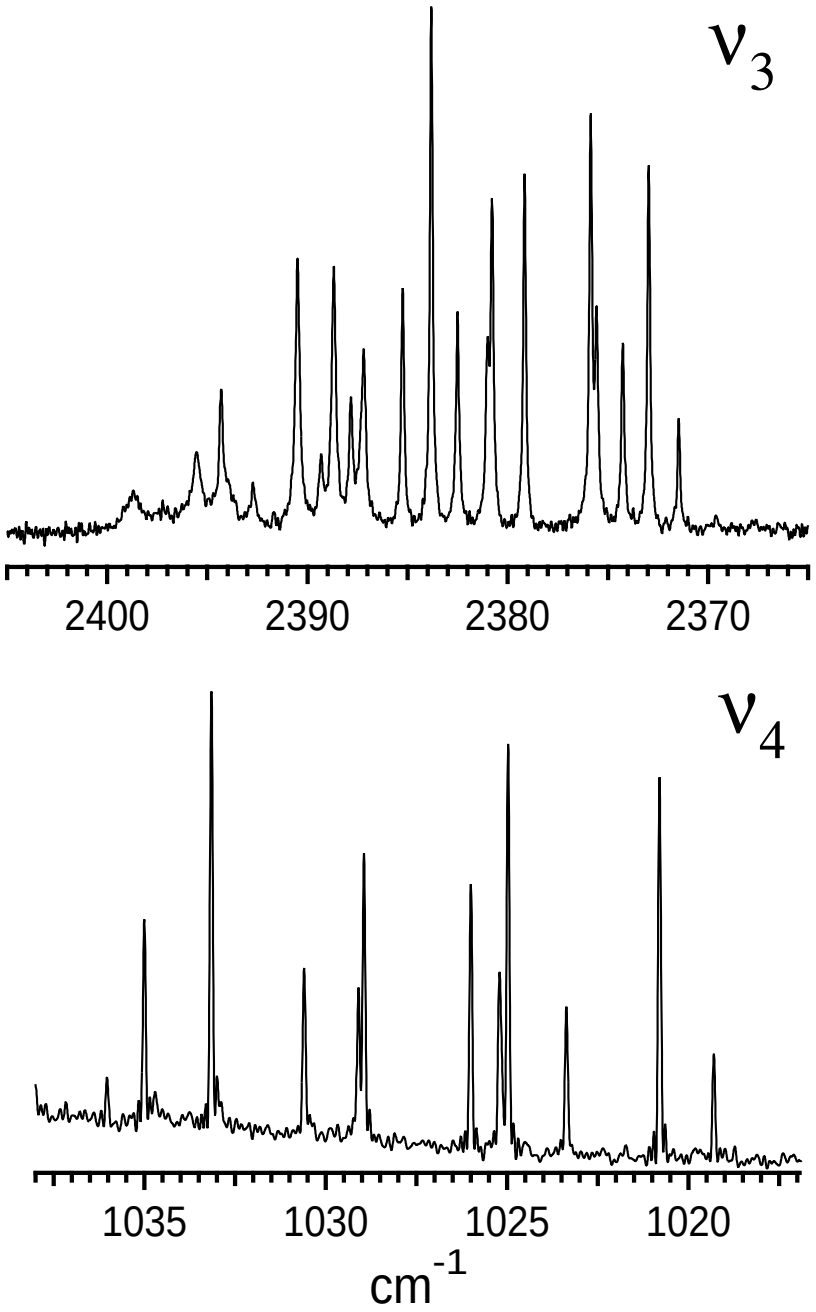

Figure 2.2: FTIR spectrum of the ν_3 (upper panel) and ν_4 (lower panel) fundamental transitions of CD_3 isolated in solid parahydrogen.

Table 2.2: The observed transition wavenumbers, the assignments, and the calculated transition wavenumbers of the ν_3 transition of CD_3 in solid parahydrogen. The columns of Γ' and Γ'' show irreducible representations of rotation-vibration wavefunction in the extended group G.

Obserbed		Calculated											
Transition		Assignments									Transition		
wavenumbers		Upper state					Lower state				wavenumbers	Obs.	Predicted
(cm^{-1})	Polarization	N'	$\|k'\|$	$\|M'\|$	l	Γ'	N''	$\|k''\|$	$\|M''\|$	Γ''	(cm^{-1})	- Calc.	polarization
2371.44	$\parallel$	0	0	0	−	$A_1\overline{E'}$	1	1	0	$A_2\overline{E''}$	2371.6	-0.1	$\parallel$
2372.96	$\perp$	0	0	0	−	$A_1\overline{E'}$	1	1	1	$E\overline{E'}$	2372.9	0.1	$\perp$
2374.24	$\parallel$	1	1	1	+	$E\overline{A_1'}(+E\overline{A_2'})$	1	0	1	$E\overline{A_2''}$	2374.1	0.1	$\parallel$
2375.56	$\perp$	1	1	0	+	$A_2\overline{A_2''}(+A_2\overline{A_1''})$	1	0	1	$E\overline{A_2''}$	2375.5	0.1	$\perp$
2375.86	$\perp$	1	1	1	+	$E\overline{A_1'}(+E\overline{A_2'})$	1	0	0	$A_2\overline{A_2'}$	2376.1	-0.2	$\perp$
2379.15	$\perp$	2	2	2	−	$E\overline{E'}$	2	2	0	$A_1\overline{E'}$	2379.0	0.2	$\perp$
2380.77	$\perp$	1	0	0	−	$A_2\overline{E'}$	1	1	1	$E\overline{E'}$	2380.5	0.3	$\perp$
2381.01	$\perp$	1	0	1	−	$E\overline{E''}$	1	1	0	$A_2\overline{E''}$	2381.2	-0.2	$\perp$
2382.51	$\parallel$	1	0	1	−	$E\overline{E''}$	1	1	1	$E\overline{E'}$	2382.5	0.0	$\parallel$
2383.82	$\perp$	1	1	1	+	$E\overline{A_1'}(+E\overline{A_2'})$	0	0	0	$A_1\overline{A_1'}$	2383.8	0.0	$\perp$
2385.25	$\parallel$	1	1	0	+	$A_2\overline{A_1''}(+A_2\overline{A_2''})$	0	0	0	$A_1\overline{A_1'}$	2385.2	0.0	$\parallel$
2387.19	$\perp$	2	2	1	+	$E\overline{A_2''}(+E\overline{A_1''})$	1	1	0	$A_2\overline{E''}$	2387.3	-0.1	$\perp$
2387.84	$\parallel$	2	2	0	+	$A_1\overline{A_1'}(+A_1\overline{A_2'})$	1	1	0	$A_2\overline{E''}$	2387.9	-0.1	$\parallel$
2388.70	$\parallel$	2	2	1	−	$E\overline{E''}$	1	1	1	$E\overline{E'}$	2388.6	0.1	$\parallel$
2389.34		2	2	0	−	$A_1\overline{E'}$	1	1	1	$E\overline{E'}$	2389.3	0.0	$\perp$
2390.51	$\perp$	3	3	3		$A_2\overline{E'}$	2	2	2	$E'\overline{E'}$	2390.3	0.2	$\perp$
2392.65		2	1	1	+	$E\overline{A_1'}(+E\overline{A_2'})$	1	0	1	$E\overline{A_2''}$	2392.8	-0.1	$\parallel$
2394.31		2	2	2	+	$E\overline{A_1'}(+E\overline{A_2'})$	0	0	0	$A_1\overline{A_1'}$	2394.1	-0.1	$\perp$
2395.51													

Table 2.3: The observed transition wavenumbers and the assignments of the ν_4 transition of CD_3 in solid parahydrogen. The columns of Γ' and Γ'' show the irreducible representations of rotation-vibration wavefunction in the extended group G.

Obserbed		Calculated								
Transition wavenumbers		Assignments								
		Upper state					Lower state			
(cm^{-1})	Polarization	N'	$\|k'\|$	$\|M'\|$	l	Γ'	N''	$\|k''\|$	$\|M''\|$	Γ''
1019.296	$\parallel$	0	0	0	–	$A_1\overline{E'}$	1	1	0	$A_1\overline{E''}$
1020.801	$\perp$	0	0	0	–	$A_1\overline{E'}$	1	1	1	$E\overline{E'}$
1023.360	$\parallel$	1	1	1	+	$E\overline{A_1'}(+E\overline{A_2'})$	1	0	1	$E\overline{A_2''}$
1024.976	$\perp$	1	1	1	+	$E\overline{A_1'}(+E\overline{A_2'})$	1	0	0	$A_2\overline{A_2'}$
1025.201	$\perp$	1	1	0	+	$A_2\overline{A_2''}(+A_2\overline{A_1''})$	1	0	1	$E\overline{A_2''}$
1026.003	$\perp$									
1028.947	$\perp$	1	0	0	–	$A_2\overline{E'}$	1	1	1	$E\overline{E'}$
1029.102	$\perp$	1	0	1	–	$E\overline{E''}$	1	1	0	$A_2\overline{E''}$
1030.602	$\parallel$	1	0	1	–	$E\overline{E''}$	1	1	1	$E\overline{E'}$
1033.154	$\perp$	1	1	1	+	$E\overline{A_1'}(+E\overline{A_2'})$	0	0	0	$A_1\overline{A_1'}$
1035.009	$\parallel$	1	1	0	+	$A_2\overline{A_1''}(+A_2\overline{A_2''})$	0	0	0	$A_1\overline{A_1'}$

analysis of the observed spectra is described in subsection 2.4.3.

2.4.1 Extended Group

We consider a methyl radical occupying a single substitutional site of a hexagonal-close-packed crystal (see Fig.2.3). In order to analyze the rotation vibration spectra of molecules in crystals, it is necessary to take into account the symmetries of both the crystal and the molecule. For this purpose, it is convenient to introduce the extended group[34] as discussed previously.[4,21,24]

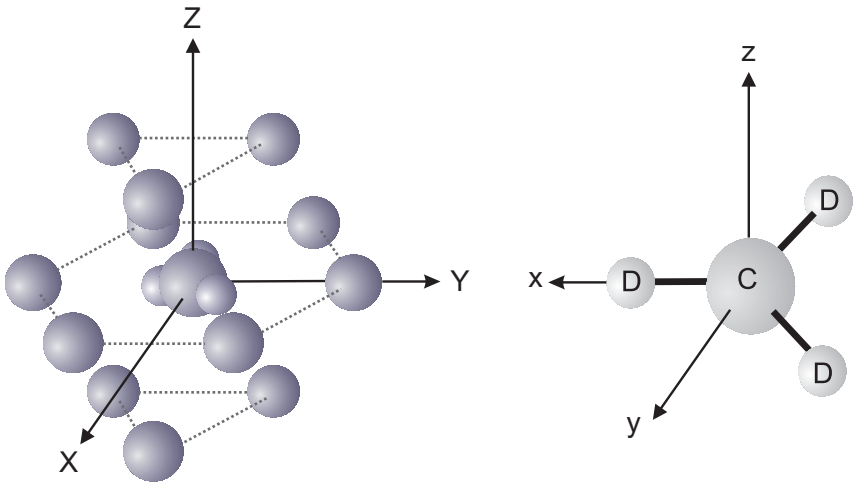

Figure 2.3: A methyl radical molecule occupying a substitutional site of the *hcp* lattice of parahydrogen (left). Crystal-fixed axes are designated as XYZ (left) and molecule-fixed axes are designated as xyz (right).

The crystal structure belongs to D_{3h} point group, which is composed of 12 symmetry operations,

$$D_{3h} = \{E, 2C_3, 3C_2, \sigma_h, 2S_3, 3\sigma_v\}.$$

Notations of symmetry operations are standard.

The radical belongs to the same D_{3h} point group, but it is more convenient to use the permutation-inversion group G_{12}, whose symmetry operations are

given below.

$$G_{12}(M) = \{E, 2(123), 3(23), E^*, 2(123)^*, 3(23)^*\}$$

Here, E represents the identity operator, (123) a cyclic permutation of identical nuclei and $(123)^*$ a cyclic permutation followed by the space-fixed inversion.[35]

The extended group appropriate to the present system is a subgroup of the direct product group of the space symmetry group D_{3h} and the molecular symmetry group G_{12}. Explicit express of the symmetry operations are given below.

$$\begin{aligned} G \;=\; & \{E\overline{E}, 2E\overline{(123)}, 3E\overline{(23)}, 2C_3\overline{E}, 4C_3\overline{(123)}, 6C_3\overline{(23)}, \\ & 3C_2\overline{E}, 6C_2\overline{(123)}, 9C_2\overline{(23)}, \sigma_h\overline{E^*}, 2\sigma_h\overline{(123)^*}, 3\sigma_h\overline{(23)^*}, \\ & 2S_3\overline{E^*}, 4S_3\overline{(123)^*}, 6S_3\overline{(23)^*}, 3\sigma_v\overline{E^*}, 6\sigma_v\overline{(123)^*}, 9\sigma_v\overline{(23)^*}\} \end{aligned}$$

In the above, symmetry operations on the molecule are represented with overbars.[34] The operations $\{E, 2C_3, 3C_2\}$ of the space symmetry couple only to the symmetry operations $\{\overline{E}, 2\overline{(123)}, 3\overline{(23)}\}$ of the molecule, whereas the operations $\{\sigma_h, 2S_3, 3\sigma_v\}$ of the space couple to $\{\overline{E^*}, 2\overline{(123)^*}, 3\overline{(23)^*}\}$. These restrictions are introduced because any operation that includes the space inversion operation either in space operation or in molecular operation, but not in both, is not a feasible operation in the present system. The group G is isomorphic to the direct product group $D_3 \otimes G_{12}$. The character table of the group G is listed in Table 2.4. The symmetry species of space fixed components of the dipole moment μ are also listed.

2.4.2 Symmetry Classification

Rotational wavefunction of the radical is conveniently expressed as a linear combination of Wigner's rotation matrix $D^l_{k,m}(\chi, \theta, \phi)$.[36] In addition, anisotropic potential of intermolecular interaction is usually expanded as a

Table 2.4: Character table of group G.

	$1E\overline{E}$	$2E\overline{(123)}$	$3E\overline{(23)}$	$2C_3\overline{E}$	$4C_3\overline{(123)}$	$6C_3\overline{(23)}$	$3C_2\overline{E}$	$6C_2\overline{(123)}$	$9C_2\overline{(23)}$	$1\sigma_h\overline{E^*}$	$2\sigma_h\overline{(123)^*}$	$3\sigma_h\overline{(23)^*}$	$2S_3\overline{E^*}$	$4S_3\overline{(123)^*}$	$6S_3\overline{(23)^*}$	$3\sigma_v\overline{E^*}$	$6\sigma_v\overline{(123)^*}$	$9\sigma_v\overline{(23)^*}$	
$A_1\overline{A_1'}$	1	1	1	1	1	1	1	1	1	1	1	1	1	1	1	1	1	1	
$A_1\overline{A_2'}$	1	1	-1	1	1	-1	1	1	-1	1	1	-1	1	1	-1	1	1	-1	
$A_1\overline{E'}$	2	-1	0	2	-1	0	2	-1	0	2	-1	0	2	-1	0	2	-1	0	
$A_1\overline{A_1''}$	1	1	1	1	1	1	1	1	1	-1	-1	-1	-1	-1	-1	-1	-1	-1	
$A_1\overline{A_2''}$	1	1	-1	1	1	-1	1	1	-1	-1	-1	1	-1	-1	1	-1	-1	1	
$A_1\overline{E''}$	2	-1	0	2	-1	0	2	-1	0	-2	1	0	-2	1	0	-2	1	0	
$A_2\overline{A_1'}$	1	1	1	1	1	1	-1	-1	-1	1	1	1	1	1	1	-1	-1	-1	
$A_2\overline{A_2'}$	1	1	-1	1	1	-1	-1	-1	1	1	1	-1	1	1	-1	-1	-1	1	
$A_2\overline{E'}$	2	-1	0	2	-1	0	-2	1	0	2	-1	0	2	-1	0	-2	1	0	
$A_2\overline{A_1''}$	1	1	1	1	1	1	-1	-1	-1	-1	-1	-1	-1	-1	-1	1	1	1	μ_z
$A_2\overline{A_2''}$	1	1	-1	1	1	-1	-1	-1	1	-1	-1	1	-1	-1	1	1	1	-1	
$A_2\overline{E''}$	2	-1	0	2	-1	0	-2	1	0	-2	1	0	-2	1	0	2	-1	0	
$E\overline{A_1'}$	2	2	2	-1	-1	-1	0	0	0	2	2	2	-1	-1	-1	0	0	0	(μ_x, μ_y)
$E\overline{A_2'}$	2	2	-2	-1	-1	1	0	0	0	2	2	-2	-1	-1	1	0	0	0	
$E\overline{E'}$	4	-2	0	-2	1	0	0	0	0	4	-2	0	-2	1	0	0	0	0	
$E\overline{A_1''}$	2	2	2	-1	-1	-1	0	0	0	-2	-2	-2	1	1	1	0	0	0	
$E\overline{A_2''}$	2	2	-2	-1	-1	1	0	0	0	-2	-2	2	1	1	-1	0	0	0	
$E\overline{E''}$	4	-2	0	-2	1	0	0	0	0	-4	2	0	2	-1	0	0	0	0	

linear combination of Wigner's rotation matrices. Therefore it is useful to compose symmetry adapted functions of linear combination of the rotation matrix D under the extended group G.

Explicit expression of the symmetry adapted functions depends on the definition of both crystal-fixed and molecule-fixed axes. The definitions of the crystal-fixed axes (XYZ) and molecule-fixed axes (xyz) are shown in Fig.2.3. Crystal c axis is taken as the Z axes, and one of the C_2 symmetry axes of the crystal (as shown in Fig.2.3) is taken as the X axis of the crystal-fixed axes. The crystal-fixed axis are identical to the laboratory-fixed axes. The C_3 symmetry axis of the radical is taken as the z axis, and one of the C_2 symmetry axis of the molecule (as shown in Fig.2.3) is taken as the x axis of the molecule-fixed axes.

The symmetry adapted functions under the extended group G can be obtained by considering the transformation of the rotational matrix $D^l_{k,m}(\chi, \theta, \phi)$ under each operation of the extended group.[21,24] The symmetry adapted functions up to the third rank tensors are classified into each irreducible representation in Table 2.5.

2.4.3 Hamiltonian

We assume that perturbation from the surrounding lattice to the dopant molecules is weak enough so that the rotation-vibration Hamiltonian of the system is well described as a sum of the standard rotation-vibration Hamiltonian $H_{rot-vib}$ and a crystal field potential V as

$$H = H_{rot-vib} + V. \tag{2.1}$$

The rotational Hamiltonian of the radical in the vibrational ground state is written as

$$H_{rot-vib} = B''\hat{N}^2 + (C'' - B'')\hat{N}_c^2 \tag{2.2}$$

Table 2.5: Symmetry adapted functions of linear conbination of Wigner's rotation matrix $D^l_{k,m}(\chi,\theta,\phi)$ in the extenden group G. The definitions of Wigner's rotaiton matrix is that introduced by Wigner.[36]

rank	irreducible representation	wavefunctions $D^l_{k,m}$
l=0	$A_1\overline{A'_1}$	$D^0_{0,0}$
l=1	$A_2\overline{A'_2}$	$D^1_{0,0}$
	$A_2\overline{E''}$	$D^1_{-1,0}$, $D^1_{1,0}$
	$E\overline{E'}$	$D^1_{-1,-1}$, $D^1_{-1,1}$, $D^1_{1,-1}$, $D^1_{1,1}$
	$E\overline{A''_2}$	$D^1_{0,-1}$, $D^1_{0,1}$
l=2	$A_1\overline{A'_1}$	$D^2_{0,0}$
	$A_1\overline{E'}$	$D^2_{-2,0}$, $D^2_{2,0}$
	$A_1\overline{E''}$	$D^2_{-1,0}$, $D^2_{1,0}$
	$E\overline{A'_1}$	$D^2_{0,-2}$, $D^2_{0,2}$
	$E\overline{E'}$	$D^2_{-2,-2}$, $D^2_{-2,2}$, $D^2_{2,-2}$, $D^2_{2,2}$, $D^2_{-1,-1}$, $D^2_{-1,1}$, $D^2_{1,-1}$, $D^2_{1,1}$
	$E\overline{A''_1}$	$D^2_{0,-1}$, $D^2_{0,1}$
	$E\overline{E''}$	$D^2_{-1,-2}$, $D^2_{1,-2}$, $D^2_{-2,-1}$, $D^2_{2,-1}$, $D^2_{-2,1}$, $D^2_{2,1}$, $D^2_{-1,2}$, $D^2_{1,2}$
l=3	$A_1\overline{A'_1}$	$\frac{1}{2}\{D^3_{-3,-3} - D^3_{3,-3} - D^3_{-3,3} + D^3_{3,3}\}$
	$A_1\overline{A'_2}$	$\frac{1}{2}\{D^3_{-3,-3} + D^3_{3,-3} - D^3_{-3,3} - D^3_{3,3}\}$
	$A_1\overline{E'}$	$\frac{1}{\sqrt{2}}\{D^3_{-1,-3} - D^3_{-1,3}\}$, $\frac{1}{\sqrt{2}}\{D^3_{1,-3} - D^3_{1,3}\}$
	$A_1\overline{A''_2}$	$\frac{1}{\sqrt{2}}\{D^3_{0,-3} - D^3_{0,3}\}$
	$A_1\overline{E''}$	$\frac{1}{\sqrt{2}}\{D^3_{-2,-3} - D^3_{-2,3}\}$, $\frac{1}{\sqrt{2}}\{D^3_{2,-3} - D^3_{2,3}\}$
	$A_2\overline{A'_1}$	$\frac{1}{2}\{D^3_{-3,-3} - D^3_{3,-3} + D^3_{-3,3} - D^3_{3,3}\}$
	$A_2\overline{A'_2}$	$\frac{1}{2}\{D^3_{-3,-3} + D^3_{3,-3} + D^3_{-3,3} + D^3_{3,3}\}$, $D^3_{0,0}$
	$A_2\overline{E'}$	$\frac{1}{\sqrt{2}}\{D^3_{-1,-3} + D^3_{-1,3}\}$, $\frac{1}{\sqrt{2}}\{D^3_{1,-3} + D^3_{1,3}\}$, $D^3_{-2,0}$, $D^3_{2,0}$
	$A_2\overline{A''_1}$	$\frac{1}{\sqrt{2}}\{D^3_{-3,0} - D^3_{3,0}\}$, $\frac{1}{\sqrt{2}}\{D^3_{-3,0} + D^3_{3,0}\}$
	$A_2\overline{A''_2}$	$\frac{1}{\sqrt{2}}\{D^3_{0,-3} + D^3_{0,3}\}$, $\frac{1}{\sqrt{2}}\{D^3_{0,-3} + D^3_{0,3}\}$
	$A_2\overline{E''}$	$\frac{1}{\sqrt{2}}\{D^3_{-2,-3} + D^3_{-2,3}\}$, $\frac{1}{\sqrt{2}}\{D^3_{2,-3} + D^3_{2,3}\}$, $D^3_{-1,0}$, $D^3_{1,0}$
	$E\overline{A'_1}$	$\frac{1}{\sqrt{2}}\{D^3_{-3,-1} - D^3_{3,-1}\}$, $\frac{1}{\sqrt{2}}\{D^3_{-3,1} - D^3_{3,1}\}$
	$E\overline{A'_2}$	$\frac{1}{\sqrt{2}}\{D^3_{-3,-1} + D^3_{3,-1}\}$, $\frac{1}{\sqrt{2}}\{D^3_{-3,1} + D^3_{3,1}\}$, $D^3_{0,-2}$, $D^3_{0,2}$
	$E\overline{E'}$	$D^3_{-2,-2}$, $D^3_{-2,2}$, $D^3_{2,-2}$, $D^3_{2,2}$, $D^3_{-1,-1}$, $D^3_{1,-1}$, $D^3_{-1,1}$, $D^3_{1,1}$
	$E\overline{A''_1}$	$\frac{1}{\sqrt{2}}\{D^3_{-3,-2} - D^3_{3,-2}\}$, $\frac{1}{\sqrt{2}}\{D^3_{-3,2} - D^3_{3,2}\}$
	$E\overline{A''_2}$	$\frac{1}{\sqrt{2}}\{D^3_{-3,-2} + D^3_{3,-2}\}$, $\frac{1}{\sqrt{2}}\{D^3_{-3,2} + D^3_{3,2}\}$, $D^3_{0,-1}$, $D^3_{0,1}$
	$E\overline{E''}$	$D^3_{-1,-2}$, $D^3_{1,-2}$, $D^3_{-2,-1}$, $D^3_{2,-1}$, $D^3_{-2,1}$, $D^3_{2,1}$, $D^3_{-1,2}$, $D^3_{1,2}$

where $\hat{N}$ and $\hat{N}_c$ are the total and projection rotational angular momentum operators, respectively, and B'' and C'' are the rotational constants of the vibrational ground state. We ignored the centrifugal distortion term and other higher order terms, since the transitions we observed were only those between $J = 0$, 1 or 2. The rotation-vibration Hamiltonian in the doubly degenerate vibrational excited states is written as

$$H_{rot-vib} = h\nu_i + B'_i\hat{N}^2 + (C'_i - B'_i)\hat{N}_c^2 + H_{cor} \tag{2.3}$$

where ν_0 is the frequency of the band origin of the i-th vibrational transition, B'_i and C'_i are the rotational constants in the i-th vibrational excited states, and H_{cor} is the Hamiltonian for the Coriolis interaction.

As for the potential V in Eq.(2.1), we only consider anisotropic potentials that are a function of the Euler angle Ω of the radical relative to the crystal-fixed axes, since the isotropic potential does not change relative energies of rotational states of the radical. Conservation of total energy requires that the anisotropic potential has to be invariant under any symmetry operation of the extended group G, i.e. the potential needs to belong to the $A_1\overline{A'_1}$ irreducible representation of the group G (see Table 2.5). The first two anisotropic terms are given as

$$V(\Omega) = \epsilon_2 D^2_{0,0}(\Omega) + \frac{1}{2}\epsilon_3[D^3_{-3,-3}(\Omega) - D^3_{3,-3}(\Omega) - D^3_{-3,3}(\Omega) + D^3_{3,3}(\Omega)] \tag{2.4}$$

where Ω is the orientation of the radical relative to the crystal-field axes and ϵ_2 and ϵ_3 are the coefficients that we call crystal field parameters.

2.4.4 Rovibrational energy

In order to understand the effect of the crystal field potential, $V(\Omega)$, to the rovibrational energy levels of the radicals, energy shifts and splittings of the $N = 0$ and $N = 1$ rotational levels in the vibrational ground state are depicted in Fig. 2.4.

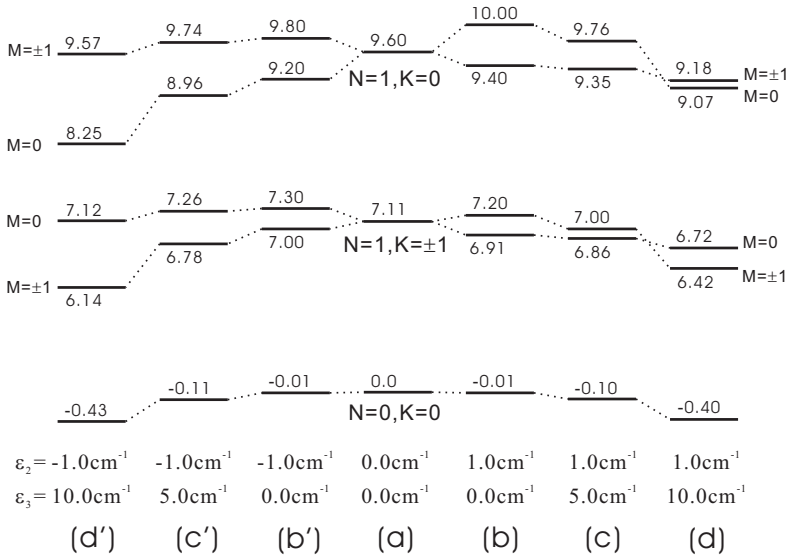

Figure 2.4: Energy levels of the $N = 0$ and $N = 1$ rotational states in the vibrational ground state. (a): $\epsilon_2 = 0$, $\epsilon_3 = 0$ (correspond to the gaseous phase). (b)$\sim$(d): $\epsilon_2 = 1.0$ cm^{-1}. (b')$\sim$(d'): $\epsilon_2 = -1.0$ cm^{-1}. (b) and (b'): $\epsilon_3 = 0.0$ cm^{-1}. (c) and (c'): $\epsilon_3 = 5.0$ cm^{-1}. (d) and (d'): $\epsilon_3 = 10.0$ cm^{-1}.

The degeneracy of the $M = \pm 1$ and $M = 0$ levels is lifted due to the second order potential $\epsilon_2 D^2_{00}(\Omega)$. The first order perturbation theory tells that the second order potential shifts the $N = 1$, $|k| = 1$, $M = 0$ and the $N = 1$, $|k| = 1$, $|M| = 1$ by $-\frac{1}{5}\epsilon_2$ and $\frac{1}{10}\epsilon_2$, respectively, while the $N = 1$, $k = 0$, $M = 0$ and the $N = 1$, $k = 0$, $|M| = 1$ levels by $\frac{2}{5}\epsilon_2$ and $-\frac{1}{5}\epsilon_2$, respectively. Therefore, when the value of ϵ_2 is positive, the $M = 0$ level is lower than $M = \pm 1$ level for the $N = 1$, $k = \pm 1$ state, while the $M = \pm 1$ level is lower than the $M = 0$ level for the $N = 1$, $k = 0$ state. On the other hand, when the value of ϵ_2 is negative, the $M = \pm 1$ level is lower than $M = 0$ level for the $N = 1$, $k = \pm 1$ state, while the $M = 0$ level is lower than the $M = \pm 1$ level for the $N = 1$, $k = 0$ state.

The effect of the third order potential is complicated, but it is smaller than that of second order potential. The $M = 1$ and $M = -1$ levels are yet degenerated due to the axial symmetry of the *hcp* structure.

2.4.5 Optical selection rule

There are optical selection rules of the M sublevels in addition to the standard selection rule of N and k quantum numbers. In general, transitions between the $M = 0$ and $M = 0$ levels are active for the radiation polarized parallel to the c-axis of the crystal, while the transitions between the $M = 0$ and $M = \pm 1$ levels are active for the radiation polarized perpendicular to the c axis. Transition between the $M = \pm 1$ and $M = \pm 1$ levels are active for both polarization. More strict selection rule can be derived easily by the use of the character table in Table 2.4 and the symmetry classification of each rotational state shown in Table 2.5. For example, the selection rule for the Q(1) transition is as follows. The overall symmetries of the rotation-vibration wavefunction of the $N = 1$ states in the vibrational ground state are $A_2\overline{A_2'}$ and $E\overline{A_2''}$ for the ($N = 1$, $k = 0$, $M = 0$), and ($N = 1$, $k = 0$, $|M| = 1$) states, respectively, while $A_2\overline{E''}$ and $E\overline{E'}$ for the ($N = 1$, $|k| = 1$, $M = 0$), and ($N = 1$, $k = |1|$, $|M| = 1$) states, respectively. In the doubly degenerate vibrational excited state (E'), the symmetries are $A_2\overline{E'}$ and $E\overline{E''}$ for the ($v = 1$, $N = 1$, $k = 0$, $M = 0$) and ($v = 1$, $N = 1$, $k = 0$, $|M| = 1$) states respectively, while $A_2\overline{A_1''}$ or $A_2\overline{A_2''}$ for the ($v = 1$, $N = 1$, $|k| = 1$, $M = 0$, $+l$) states, $E\overline{A_1'}$ or $E\overline{A_2'}$ for the ($v = 1$, $N = 1$, $|k| = 1$, $|M| = 1$, $+l$) states, $A_2\overline{E''}$ for the ($v = 1$, $N = 1$, $|k| = 1$, $M = 0$, $-l$) states and $E\overline{E'}$ for the ($v = 1$, $N = 1$, $|k| = 1$, $|M| = 1$, $-l$) states, where ($+l$) and ($-l$) designate Coriolis doublet.[37] Therefore, by taking into account of the symmetry of the dipole operators, the active transitions for the radiation polarized perpendicular to the c-axis are

$$(v = 1, N = 1, |k| = 1, |M| = 1, +l; E\overline{A_2'}) \leftarrow (v = 0, N = 1, k = 0, M = 0; A_2\overline{A_2'})$$

$$(v = 1, N = 1, |k| = 1, M = 0, +l; A_2\overline{A_2''}) \leftarrow (v = 0, N = 1, k = 0, |M| = 1; E\overline{A_2''})$$

$$(v = 1, N = 1, k = 0, |M| = 1; E\overline{E''}) \leftarrow (v = 0, N = 1, |k| = 1, M = 0; A_2\overline{E''})$$

and

$$(v=1, N=1, k=0, M=; A_2\overline{E'}) \leftarrow (v=0, N=1, |k|=1, |M|=1; E\overline{E'}),$$

while the transitions of

$$(v=1, N=1, |k|=1, |M|=1, +l; E\overline{A_2'}) \leftarrow (v=0, N=1, k=0, |M|=1; E\overline{A_2''})$$

and

$$(v=1, N=1, k=0, |M|=1; E\overline{E''}) \leftarrow (v=0, N=1, |k|=1, |M|=1; E\overline{E'})$$

are active for the radiation polarized parallel to the c-axis. All other transitions such as

$$(v=1, N=1, k=0, M=0; A_2\overline{E''}) \leftarrow (v=0, N=1, |k|=1, M=0; A_2\overline{E'})$$

are inactive.

2.5 Analysis

2.5.1 CD_3

Comparison of the polarization dependence of the observed transitions with theoretically predicted polarization dependence, the spectra shown in Fig.2.2 can be analyzed qualitatively. For example, the transitions at 2371.44 cm^{-1} and 2372.96 cm^{-1} in the ν_3 mode showed polarization dependence of parallel and perpendicular, respectively. If the perturbation due to the crystal field is small, these two transitions must be those of $(v=1, N=0, k=0, M=0) \leftarrow (v=0, N=1, |k|=1, M'')$. Referring to the observed polarization dependence, these two transitions are attributable to $(v=1, N=0, |k|=0, M=0; A_1\overline{E'}) \leftarrow (v=0, N=1, |k|=1, M=0; A_2\overline{E''})$ and $(v=1, N=0, |k|=0, M=0; A_1\overline{E'}) \leftarrow (v=0, N=1, |k|=1, |M|=1; E\overline{E''})$, respectively.

The spacing between these two transitions; that is, 1.52 cm^{-1} corresponds to the spacing between $M=0$ and $M=\pm 1$ levels in the $N=1$, $|k|=1$

state of the vibrational ground state. The $M = \pm 1$ level is lower in energy than the $M = 0$ level. The assignment is also supported from the fact that the spacing between the lowest two transitions of the ν_4 mode (1019.296 cm^{-1} and 1020.801 cm^{-1}) are 1.555 cm^{-1}, which is in good agreement with the spacing in the ν_3 mode of 1.52 cm^{-1}, as these two transitions are also assigned to those from the $M = 0$ and $M = \pm 1$ levels, respectively, in the $v = 0$, $N = 1$, $|k| = 1$ state to the $(v = 1, N = 0, k = 0, M = 0)$ level.

In the same way, the third, fourth and fifth transitions from the lowest frequency side of both modes (ν_3: 2374.24, 2375.56 and 2375.86 cm^{-1}, ν_4: 1023.360, 1024.976 and 1025.201 cm^{-1}) can be assigned to the transitions from the $(v = 0, N = 1, k = 0, |M| = 0 \text{ or } 1)$ levels to the $(v = 1, N = 1, |k| = 1, |M| = 0 \text{ or } 1, +l)$ levels. Only three transition are allowed among the four possible transitions as discussed in Sec. 2.4.5. By taking differences of the transition wavenumbers, it is obtained that the spacing between the $|M| = 1$ and $M = 0$ levels in the $N = 1$, $k = 0$ state of the vibrational ground state is 1.62 cm^{-1}.

Referring to the qualitative assignments discussed above, the spectrum shown in Fig.2.2 can be analyzed quantitatively with the use of the Hamiltonian in Eq.(2.3). We employed the least squares fitting method to determine the parameters in the Hamiltonian. Unfortunately, it was found that the number of observed transitions in the ν_4 mode was not enough to determine molecular parameters, we focuse only on the analysis of the ν_3 mode in this paper. The observed frequencies of the ν_3 transition were taken into account to determine total of 7 parameters; that is, the rotational constant of the ground state (B'', C''), and of the ν_3 (B'_3, C'_3) excited states, the band origin (ν_3), and two coefficients ϵ_2 and ϵ_3 of the crystal field parameters in Eq.(2.4). The crystal field potential parameters ϵ_2 and ϵ_3 were assumed to be the same for the ground and the ν_3 vibrational excited states.[5,9] Since the Coriolis parameter ζ_i and the rotational constants were unable to determine

independently, we fixed the Coriolis parameter to the value in the gas phase ($\zeta_3 = 0.201$). The assumption is based on the fact that the Coriolis parameter of methane in solid parahydrogen is almost the same value as that in the gas phase. Table 2.6 summarizes the determined parameters. The gas phase values[38–40] are also listed in Table 2.6 for comparison.

Table 2.6: Molecular constants of CD_3 in solid parahydrogen. The values except for the Coriolis parameters are given in units of cm^{-1}. The Coriolis coupling constant ζ is fixed to the value of gas phase data. The gas phase values are taken from Refs. 33 and 34.

	Solid *para*-H_2	Gas Phase[33,34]
Ground state		
B''	4.529(60)	4.802
C''	2.033(77)	2.390
ν_3 excited states		
ν_3	2378.81(11)	2381.09
ζ	0.201†	0.201
B'_3	4.479(60)	4.759
C'_3	2.018(32)	2.373
Crystal field		
ϵ_2	-2.44(21)	
$\lvert\epsilon_3\rvert$	8.37(58)	

†: fixed to the gas phase values.

Comparison of the observed transition frequencies and the theoretical frequencies are given in Table 2.2. The residual errors between the observed and the calculated transition frequencies are fairly small compared to the typical linewidth of 0.2 cm^{-1} for the ν_3 transition.

Figure 2.5 depicts the energy levels and the observed transitions. The observed transitions are indicated by solid and dashed lines; the solid lines are the transitions for radiation polarized parallel to the c axis, while dashed lines are the transitions polarized perpendicular to the c axis. The mixing

of different rotational states due to the crystal field potential allowed us to observe a few forbidden transitions as shown in Fig.2.5.

2.5.2 CH_3

Because of the large rotational constants of CH_3 (B=9.58 cm^{-1}, and C=4.74 cm^{-1}in the gas phase[40]), the population in the ground $N = 0$,$k = 0$ state is expected to be more than 99.9% at 4.5 K. Therefore, only the ${}^rR(0)$ transition should be observed. The doublet in Figure 2.1 is assigned to the ${}^rR(0)$ transition with the spacing of the doublet corresponds to the energy splitting between the $M = 0$ and $M = \pm 1$ levels of the $N = 1$, $|k| = 1$ states in the vibrational excited state.

Unfortunately, it is not possible to determine molecular constants of CH_3 from only the doublet shown in Fig.2.1 because of the lack of sufficient information. The only information we obtain from the spectrum is that the splittings of the doublets of 1.0 cm^{-1} for the ν_3 transition and of 1.1 cm^{-1} for the ν_4 transition are related to the crystal field parameters ϵ_2 and ϵ_3 in Eq.(2.4). The splittings are smaller than those of CD_4 (1.4 cm^{-1} for the ν_3 and 1.9 cm^{-1} for the ν_4). If the crystal field parameters of ϵ_2 is dominant, the spacing is roughly equal to $\frac{3}{10}\epsilon_2$. Thus. the small splittings of CH_3 indicate that the absolute value of the crystal field parameter ϵ_2 of CH_3 is smaller than that of CD_3. Apparently, we need additional information to discuss further.

2.6 Discussion

2.6.1 Analysis

As shown in Table 2.2, the agreement between observed frequencies and theoretically predicted frequencies is not as good as that for methane in solid parahydrogen.[4,9] In the present analysis we ignored the coupling between the

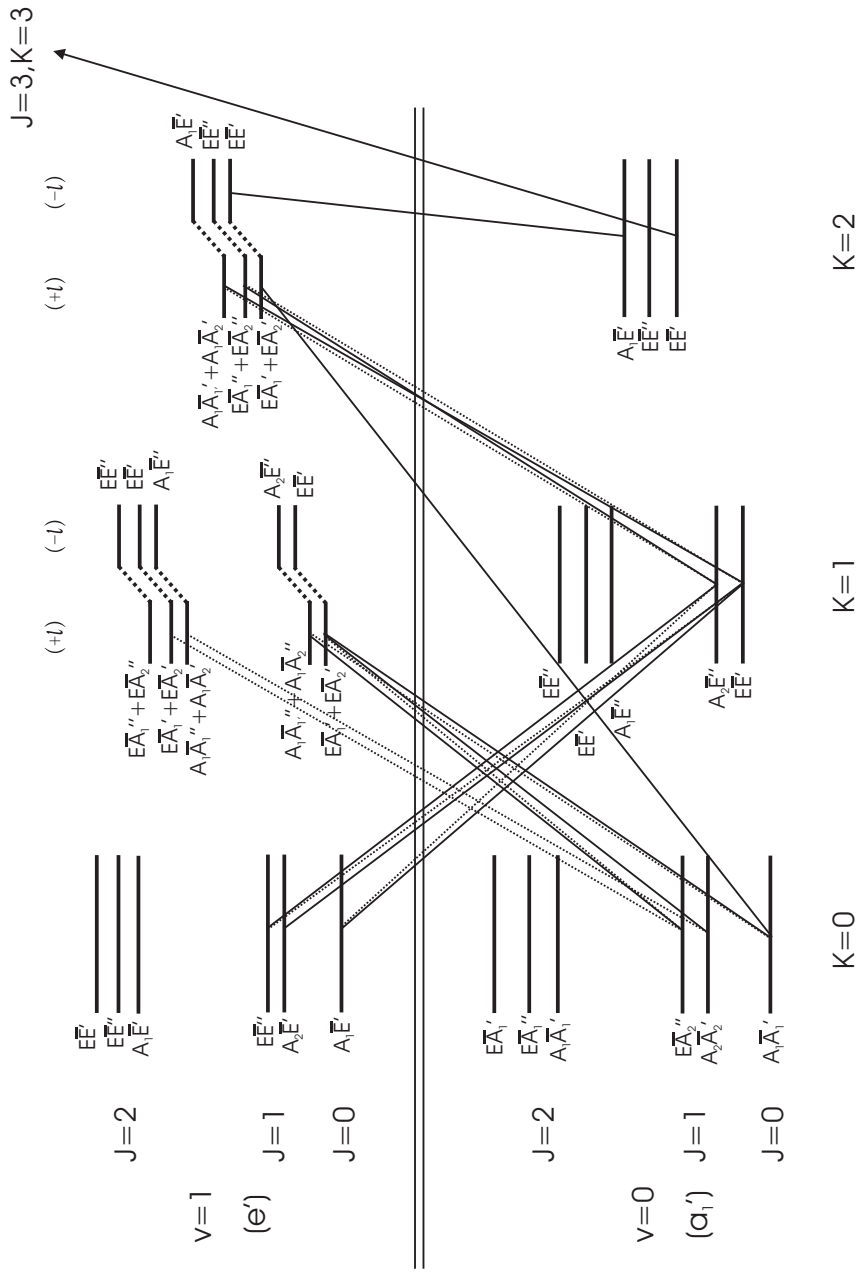

Figure 2.5: The rovibrational levels of the ground vibrational ($v = 0$) and doubly degenerate vibrational excited states ($v = 1$). Each energy levels are labeled by the irreducible representation $\Gamma\overline{\Gamma}$ of rotation-vibration wavefunction in the extended group G. The solid lines between the ground and vibrational excited states indicate the allowed transitions for radiation polarized parallel to the c axis, while dashed lines indicate transitions polarized perpendicular to the c axis.

rotational motion and translational motion of the radical in the crystal. Such effect has been discussed in the case of diatomic molecules.[41–43] The rotation-translation coupling might be more important for symmetric top molecules than for spherical top molecules. Modification of the present Hamiltonian by including the rotation-translation coupling is now underway.

2.6.2 Rotational Constants

The rotational constants of CD_3 in solid parahydrogen were found to be smaller than those in the gas phase. The constant B is about 6% smaller than the value in the gas phase, while the constant C is about 15% smaller. The reduction is the same orders of magnitude as that of methane in solid parahydrogen, where the reduction is about 10%.

The reduction of the rotational constants corresponds to the increase of the effective moment of inertia. The increases of the moment of inertia have been reported for molecules embedded in superfluid helium droplets. There are several different explanations for the origin of the increase in He droplets. They include a hydrodynamic model[27] and rigid cluster model.[28] Neither model however, can be applied to molecules in solid parahydrogen, because hydrogen molecules are bounded at their lattice sites. We will discuss the origin of the increase of the moment of inertia of molecules in solid parahydrogen in a separate paper.[44]

2.6.3 Crystal Field Parameter

The crystal field parameters ϵ_2 and ϵ_3 in Eq.(2.4) contain information on the intermolecular interaction between the radical and surrounding hydrogen molecules. As a first order approximation, we analyze the parameters in terms of the pair type dispersion interaction between the radical and hydrogen molecule.

Since both the methyl radical and the parahydrogen molecule have no

permanent dipole moment, the anisotropic interaction between them mainly comes from dispersion forces. The anisotropic potential of pairwise dispersion interaction between the i-th parahydrogen molecule and the methyl radical can be written as

$$v(\omega_i, R_i) = a_2(R_i) D^{(2)}_{0,0}(\omega_i) + a_3(R_i)[D^{(3)}_{3,0}(\omega_i) - D^{(3)}_{-3,0}(\omega_i)] \tag{2.5}$$

where ω_i is the Euler angles of the methyl radical relative to the intermolecular axis between the radical and i-th hydrogen molecule and R_i is the distance between the radical and the hydrogen molecule. The coefficients $a_2(R_i)$ and $a_3(R_i)$ are the functions of the distance R_i. Here, we ignore the orientational dependence of the hydrogen molecule on the potential, since all hydrogen molecules occupy the $J = 0$ rotational state. Assuming the additivity of the dispersion interaction, the crystal field potential in Eq.(2.4) is obtained by summing up all the pairwise interaction in Eq.(2.5) between the radical and all hydrogen molecules in the crystal as

$$\begin{aligned} V(\Omega) &= \sum_{i=1}^{\infty} v(\omega_i, R_i) \\ &= \sum_{i=1}^{\infty} a_2(R_i) \sum_m {D^{(2)}_{0,m}}^*(\Omega_{\to i}) D^{(2)}_{0,m}(\Omega) \\ &\quad + \sum_{i=1}^{\infty} a_3(R_i) \sum_m {D^{(3)}_{0,m}}^*(\Omega_{\to i}) \frac{1}{\sqrt{2}} \left[D^{(3)}_{-3,m}(\Omega) - D^{(3)}_{3,m}(\Omega) \right] \end{aligned} \tag{2.6}$$

where the angle $\Omega_{\to i}$ represents the orientation of the i-th pair axis relative to the c axis of the crystal, and Ω is the orientation of the radical relative to the crystal axis. If the hydrogen molecule are completely fixed at the equilibrium position of the crystal lattice, the crystal field parameters ϵ_2 and ϵ_3 are expressed as follows.

$$\epsilon_2 = a_2(R_0) \sum_{i=1}^{\infty} \left(\frac{R_0}{R_i} \right)^6 D^{(2)*}_{0,0}(\Omega_{\to i}) = a_2(R_0) S^{(2)}_6 \tag{2.7}$$

$$\epsilon_3 = i\sqrt{2} a_3(R_0) \sum_{i=1}^{\infty} \left(\frac{R_0}{R_i} \right)^7 D^{(3)*}_{0,3}(\Omega_{\to i}) = i\sqrt{2} a_3(R_0) S^{(3)}_7 \tag{2.8}$$

Here, R_0 is the lattice constant of the crystal ($R_0 = 3.783\mathring{A}$). The parameters $S_6^{(2)} = \sum_{i=1}^{\infty}(R_0/R_i)^6 D_{0,0}^{(2)*}(\Omega_{\to i})$ and $S_7^{(3)} = \sum_{i=1}^{\infty}(R_0/R_i)^7 D_{0,3}^{(3)*}(\Omega_{\to i})$ are calculated to be $S_6^{(2)} = 0.003048$ and $S_7^{(3)} = 0.52901i$ for the hcp lattice.

From the classical multipole expansion of the dispersion interaction potential,[45] the distance dependent coefficients $a_2(R)$ and $a_3(R)$ in Eqs.(2.7) may be written as,

$$a_2(R) = -\frac{1}{(4\pi\epsilon_0)^2}\frac{I_{\mathrm{H}_2} I_{\mathrm{CD}_3}}{2(I_{\mathrm{H}_2} + I_{\mathrm{CD}_3})}\left\langle \frac{1}{R^6} \right\rangle \alpha_{\mathrm{H}_2}\gamma_{\mathrm{CD}_3} \tag{2.9}$$

$$a_3(R) = \sqrt{\frac{1}{15}}\frac{1}{(4\pi\epsilon_0)^2}\frac{I_{\mathrm{H}_2} I_{\mathrm{CD}_3}}{I_{\mathrm{H}_2} + I_{\mathrm{CD}_3}}\left\langle \frac{1}{R^7} \right\rangle \alpha_{\mathrm{H}_2} A_{\mathrm{CD}_3} \tag{2.10}$$

where I_{H_2} and I_{CD_3} are ionization energy of hydrogen and CD_3, respectively, α_{H_2} is the dipole polarizability of hydrogen, γ_{CD_3} is the anisotropic dipole polarizability of CD_3, A_{CD_3} is the anisotropic quadrupole polarizability of CD_3, and $\langle 1/R^n \rangle$ ($n = 6, 7$) is the mean value of $1/R^n$. To derive Eqs.(2.9) and (2.10), we used the London approximation.[45]

If the effect of the zero point vibration of parahydrogen molecules in the lattice is negligibly small, $\langle 1/R^6 \rangle$ and $\langle 1/R^7 \rangle$ can be replaced with $1/R_0^6$ $1/R_0^7$, respectively, where R_0 is the lattice constant of solid parahydrogen. Then the values of ϵ_2 and ϵ_3 are estimated to be

$$\begin{aligned}
\epsilon_2 &= a_2(R) S_6^{(2)} \\
&= -\frac{1}{(4\pi\epsilon_0)^2}\frac{I_{\mathrm{H}_2} I_{\mathrm{CD}_3}}{2(I_{\mathrm{H}_2} + I_{\mathrm{CD}_3})}\frac{1}{R_0^6}\alpha_{\mathrm{H}_2}\gamma_{\mathrm{CD}_3} S_6^{(2)} \\
&= -1.49 \times 10^{-4} \ (\mathrm{cm}^{-1})
\end{aligned} \tag{2.11}$$

$$\begin{aligned}
\epsilon_3 &= i\sqrt{2} a_3(R) S_7^{(3)} \\
&= i\sqrt{\frac{2}{15}}\frac{1}{(4\pi\epsilon_0)^2}\frac{I_{\mathrm{H}_2} I_{\mathrm{CD}_3}}{I_{\mathrm{H}_2} + I_{\mathrm{CD}_3}}\frac{1}{R_0^7}\alpha_{\mathrm{H}_2} A_{\mathrm{CD}_3} S_7^{(3)} \\
&= -1.81 \ (\mathrm{cm}^{-1})
\end{aligned} \tag{2.12}$$

where we used the known values of $I_{\mathrm{H}_2} = 15.426(\mathrm{eV})$,[46] $I_{\mathrm{CD}_3} = 9.831(\mathrm{eV})$,[47] $R_0 = 3.783 \times 10^{-10}(\mathrm{m})$,[23] $\alpha_{\mathrm{H}_2} = 8.926 \times 10^{-41}(\mathrm{C \cdot m^2/V})$,[23] and $\gamma_{\mathrm{CD}_3} =$

$0.0811 \times 10^{-41}(\mathrm{C \cdot m^2/V})$.[48] As for the dipole-quadrupole polarizability A, we used the value of methane ($A_{\mathrm{CH_4}} = 2.97 \times 10^{-50}$ $\mathrm{C \cdot m^3/V}$).[49]

The order of the estimated value for the coefficient ϵ_3 is the same as the determined value from the observed spectra as seen in Table 2.6. On the other hand, the estimated value of ϵ_2 is four orders of magnitude smaller than the observed value in Table 2.6. Part of the discrepancy in the coefficients ϵ_2 is due to the large zero-point vibration of parahydrogen crystal we have neglected. Since the amplitude of zero-point lattice vibration of solid parahydrogen crystal is about 20 % of the lattice constant, the average of $\langle 1/R^6 \rangle$ may be different from the value of $1/R_0^6$.

2.6.4 Nuclear Spin Conversion

In the case of CH_4 and CD_4 in solid parahydrogen, we have observed the nuclear spin conversion between different nuclear spin states. The intensity alternation of the observed transitions has been observed in a time scale of a day, which has been interpreted as to the change of nuclear spin population from the equilibrium ratio at high temperatures to the ratio at liq. He temperature. Contrary to the case of methane, we observed any intensity alternation for neither CH_3 nor CD_3. The nuclear spin conversion of the radical may be too fast to observe in the timescale of our observation.

Bibliography

[1] T. Momose, M. Miki, M. Uchida, T. Shimizu, I. Yoshizawa, T. Shida, J. Chem. Phys. 103, (1995) 1400-1405.

[2] D. P. Weliky, K. E. Kerr, T. J. Byers, Y. Zhang, T. Momose, T. Oka, J. Chem. Phys. 105 (1996) 4461-4481.

[3] M. Miki, T. Wakabayashi, T. Momose, T. Shida, J. Phys. Chem. 100 (1996) 12135-12137.

[4] T. Momose, T. Miki, T. Wakabayashi, T. Shida, M.-C. Chan, S.S. Lee, T. Oka, J. Chem. Phys. 107 (1997) 7707-7716.

[5] T. Momose, H. Katsuki, H. Hoshina, N. Sogoshi, T. Wakabayashi, T. Shida, J. Chem. Phys. 107 (1997) 7717-7720.

[6] S. Tam, M. Macler, M.E. Fajardo, J. Chem. Phys. 106 (1997) 8955-8963.

[7] T. Momose, T. Shida, Bull. Chem. Soc. Jpn. 71 (1998) 1-15.

[8] M.E. Fajardo, S. Tam, J. Chem. Phys. 108 (1998) 4237-4241.

[9] H. Hoshina, T. Wakabayashi, T. Momose, T. Shida, J. Chem. Phys. 110 (1999) 5728-5733.

[10] S. Tam, M.E. Fajardo, H. Katsuki, H. Hoshina, T. Wakabayashi and T. Momose, J. Chem. Phys. 111 (1999) 4191-4198.

[11] S. Tam, M.E. Fajardo, Rev. Sci. Instrum. 70 (1999) 1926-1932.

[12] H. Katsuki, T. Momose, Phys. Rev. Lett. 84 (2000) 3286-3289.

[13] M. Fushitani, T. Shida, T. Momose, M. Räsänen, J. Phys. Chem. A 104 (2000) 3635-3641.

[14] S. Tam, M. Macler, M.E. DeRose, M.E. Fajardo, J. Chem. Phys. 113 (2000) 9067-9078.

[15] M.E. Fajardo and S. Tam, J. Chem. Phys. 115 (2001) 6807-6810.

[16] H. Katsuki, T. Momose, T. Shida, J. Chem. Phys. 116 (2002) 8411-8417.

[17] H. Katsuki, T. Nakamura, T. Momose, J. Chem. Phys. 116 (2002) 8881-8892.

[18] D.T. Anderson, R.J. Hinde, S. Tam, M.E. Fajardo, J. Chem. Phys. 116 (2002) 594-607.

[19] M. Fushitani, T. Momose, T. Shida, Chem. Phys. Lett. 356 (2002) 375-382.

[20] M. Fushitani, T. Momose, J. Chem. Phys. 116 (2002) 10739-10743.

[21] T. Momose, H. Hoshina, M. Fushitani, H. Katsuki, Vib. Spectrosc. in press.

[22] J.Van Kranendonk, Solid Hydrogen, Theory of the Properties od Solid H_2, HD, D_2. Plenum, New York, 1983.

[23] P.C. Souers, Hydrogen Properties for Fusion Energy. University of California Press, Berkeley, 1986.

[24] T. Momose, J. Chem. Phys. 107 (1997) 7695-7706.

[25] R. Fröchtenicht, J.P. Toennis, A. Vilesov, Chem. Phys. Lett. 229 (1994) 1-7.

[26] M. Hartmann, R.E. Miller, J.P. Toennies, A. Vilesov, Phys. Rev. Lett. 75 (1995) 1566-1569.

[27] C. Callegari, A. Conjusteau, I. Reinhard, K.K. Lehmann, G. Scoles, Phys. Rev. Lett. 83 (1999) 5058-5061.

[28] S. Grebenev, M. Hartmann, M. Havenith, B. Sartakov, J.P. Toennies, A.F. Vilesov, J. Chem. Phys. 112 (2000) 4485-4495.

[29] M.E. Jacox, J. Mol. Spectrosc. 66 (1977) 272-287.

[30] D.E. Milligan, M.E. Jacox, J. Chem.Phys. 47 (1967) 5146-5156.

[31] M. Fushitani, N. Sogoshi, T. Wakabayashi, T. Momose and T. Shida, J. Chem. Phys. 109 (1998) 6346-6350.

[32] T. Momose, H. Hoshina, N. Sogoshi, H. Katsuki, T. Wakabayashi, T. Shida, J. Chem. Phys. 108 (1998) 7334-7338.

[33] H. Hoshina, M. Fushitani, T. Momose, T. Shida, J. Chem. Phys. submitted.

[34] R.E. Miller, J. C. Decius, J. Chem. Phys. 59 (1973) 4871-4883.

[35] P.R. Bunker, P. Jensen, Molecular Symmetry and Spectroscopy. NRC Research Press, Ottawa, 1998.

[36] E.P. Wigner, Group Theory. Academic Press, New York, 1959.

[37] G. Herzberg, Molecular Spectra Molecular Structure, Vol. II Infrared and Raman Spectra of Polyatomic Molecules, Krieger Publishing, New York, 1991.

[38] J. M. Frye, T. J. Sears, D. Leiner, J. Chem. Phys. 88 (1988) 5300-5306.

[39] W. M. Fawzy, T. J. Sears, P. B. Davies, J. Chem. Phys. 92 (1988) 7021-7026.

[40] C. Yamada, E. Hirota, K. Kawaguchi, J. Chem. Phys. 75 (1981) 5256-5264.

[41] H. Friedmann, S. Kimel, J. Chem. Phys. 43 (1965) 3925-3939.

[42] L.F. Keyser, G.W.Robinson, J. Chem. Phys. 44 (1966) 3225-3239.

[43] H. Friedmann, S. Kimel, J. Chem. Phys. 47 (1967) 3589-3605.

[44] H. Hoshina, H. Katsuki, T. Momose, to be published.

[45] A.D. Buckingham, Adv. Ghem. Phys. 12 (1967) 107-142.

[46] D. Shiner, J.M. Gilligan, B.M. Cook, W. Lichten, Phys. Rev. A 47 (1993) 4042-4047.

[47] J. Dyke, N. Jonathan, E. Lee, A. Morris, J. Chem. Soc. Faraday Trans. 2, 72 (1976) 1385-1396.

[48] The anisotropic dipole polarizability of CD_3 was calcurated by the ab-initio calcuration by using Gaussian 98 for Windows NT with MP2/6-311++G basis set.

[49] U. Buck, J. Schleusener, D.J. Malik, D. Secrest, J. Chem. Phys. 74 (1981) 1707-1717.

Chapter 3

The UV and IR absorption spectra of C_3 trapped in solid parahydrogen.

Abstract

We present UV and IR absorption spectroscopy of small carbon molecules of C_3 using a by high-resolution Fourier-transform spectrometer. Extremely sharp UV absorption features with multiplet structures were observed in the $\tilde{A}^1\Pi_u \leftarrow \tilde{X}^1\Sigma_g^+$ electronic transition. The sharp UV absorption lines demonstrates the potential of solid parahydrogen as a matrix for high-resolution spectroscopy of UV-VIS electronic transitions. Details of observed spectra are discussed.

3.1 Introduction

Small carbon molecules of C_3 have attracted considerable attention of many spectroscopists since the first identification of the molecule by Herzberg.[1] The researchers' interests cover not only the basic science but also its applications to chemical reactions in combustion flame and interstellar space.[2,3] Both the ground $\tilde{X}^1\Sigma_g^+$and the first excited $\tilde{A}^1\Pi_u$electronic states have been extensively

studied in the gas phase[4–11] as well as in rare gas matrices.[12–20]

In this paper, we report high-resolution UV spectra of C_3 embedded in solid parahydrogen (p-H_2). The popularity of solid p-H_2 crystals as a host for matrix isolation spectroscopy has grown steadily in last several years.[21–24] The favorable properties of solid p-H_2 as a matrix host include astonishingly sharp infrared absorption lines[24,25] and feasibility of *in-situ* photolysis.[22] For example, high-resolution infrared spectroscopy of methane[26,27] and methyl radical[28] in solid p-H_2 revealed fully resolved ro-vibrational spectra of the dopant molecules in single substitutional sites of a hexagonal-close-packed (*hcp*) crystal. So far, the application of high-resolution matrix isolation spectroscopy in solid p-H_2 has been limited to the spectroscopy in infrared (IR) region. The aim of the present paper is to demonstrate the applicability of the solid p-H_2 matrix to the high-resolution spectroscopy of electronic transitions of dopant molecules as well.

In previous papers,[29–31] small carbon molecules C_n (n=3, 5, 7 and 9) produced by laser ablation of graphite were successfully isolated in a solid p-H_2 matrix, and the IR absorption spectra of these molecules were identified. Herein, we present the high-resolution UV absorption spectrum of the $\tilde{A}^1\Pi_u \leftarrow \tilde{X}^1\Sigma_g^+$ electronic transition of C_3 in solid p-H_2. IR absorption spectra of C_3 in solid p-H_2 observed with higher spectral resolution than that we employed in previous papers[29–31] are also discussed.

3.2 Experiment

In the present study, C_3 molecules were produced by *in-situ* UV photolysis of acetylene (C_2H_2) clusters embedded in solid p-H_2. The UV photolysis of the C_2H_2 clusters was found to produce C_3 molecules more efficiently than laser ablation of graphite that we employed in the previous papers.[29,30] We also performed UV photolysis of benzene (C_6H_6) as well as laser ablation

of fullerene (C_{60})[31] to produce C_3 molecules in solid p-H_2. Irrespective of the precursor molecules, the absorption spectra of the C_3 molecules were, including fine spectral structures, exactly the same for all the samples as discussed below.

Pure parahydrogen gas containing less than 0.05 % orthohydrogen was obtained by passing normal hydrogen gas (ortho:para=3:1) through ferric hydroxide catalysts kept at 14 K.[22,23,25] Small amount of precursor molecules (C_2H_2 or C_6H_6) were mixed with the p-H_2 gas at room temperatures. Subsequently, the premixed gas was introduced into an optical cell kept at $\sim$ 8 K in a liquid-helium cryostat to grow transparent crystals. The cell was made of copper. Both ends of the cell was sealed with BaF_2 windows using indium gaskets. For the UV photolysis, the crystals were irradiated by laser pulses of an ArF excimer laser (MBX-100, 193 nm 30 mJ/pulse, $\sim$10 ns pulse width, 50 Hz) for a few hours without using any focusing lens.

The UV and IR absorption spectra of the C_3 molecules were observed by using a Fourier-transform spectrometer (Bruker IFS 120 HR). A KBr beamsplitter, a glober source, and a liquid N_2 cooled HgCdTe (MCT) detector were used for the recording of the IR spectra, while a quartz beamsplitter, a tungsten lamp, and a photomultiplier were used for the UV spectra. The spectral resolution was 0.1 cm^{-1} for the UV spectroscopy, and 0.1 $\sim$ 0.01 cm^{-1} for the IR spectroscopy.

3.3 Results and discussion

3.3.1 UV spectra

The band origin of the $\tilde{A}^1\Pi_u$-$\tilde{X}^1\Sigma_g^+$ transition

Figure 3.1 shows the UV spectrum of C_2H_2/p-H_2 system after an irradiation with 193 nm photons. A strong absorption at 24,499 cm^{-1} (408 nm) is assigned to the origin band of the $\tilde{A}^1\Pi_u$-$\tilde{X}^1\Sigma_g^+$ transition, as the transition

wavelength is close to that in solid Ar (410 nm),[12] in solid Ne (405 nm),[12,20] and in the gas phase (405 nm).[7–9] In Fig.3.1, the origin band is designated as $\tilde{A}(000)$-$\tilde{X}(000)$, where the numbers in parenthesis ($\nu_1\nu_2\nu_3$) indicate three vibrational quantum numbers in the upper or lower electronic state. The linear C_3 molecule has one symmetric (stretching ν_1) and two asymmetric (bending ν_2 and stretching ν_3) vibrational modes.

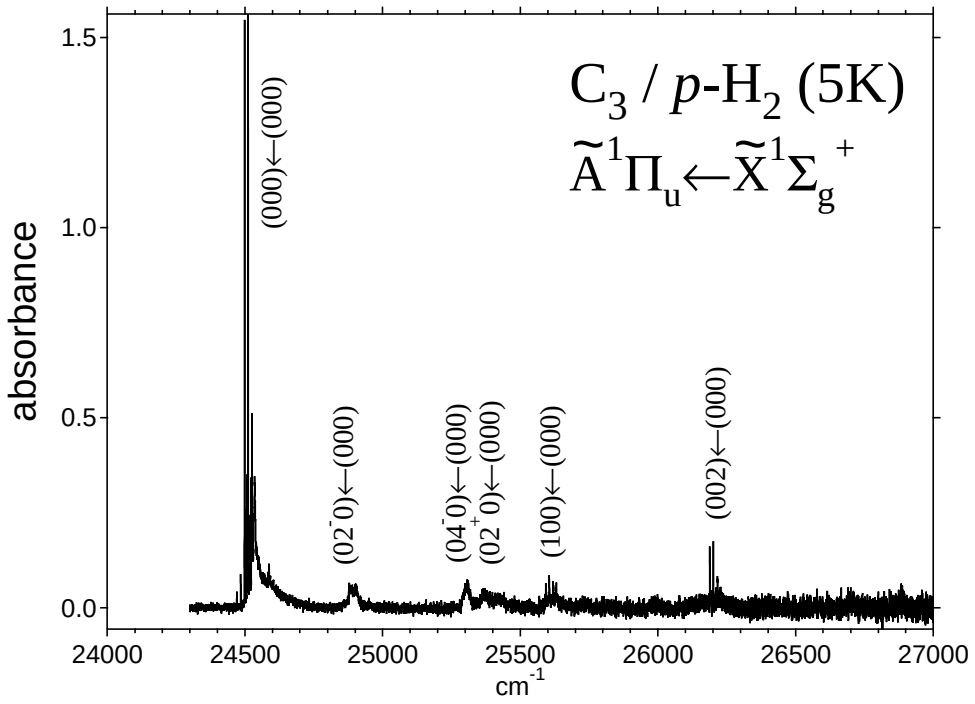

Figure 3.1: UV absorption spectrum of the $\tilde{A}^1\Pi_u \leftarrow \tilde{X}^1\Sigma_g^+$ transition of C_3 in solid p-H_2 at 5 K. The spectrum was recorded after the solid p-H_2 sample containing acetylene molecules (p-H_2/C_2H_2=1000) was irradiated with laser pulses at 193 nm from an ArF excimer laser (30 mJ/pulse at 30 Hz) for 3 hours.

Vibronic bands

In the higher-frequency region to the origin band, several absorption bands were observed at 24,879, 25,292, 25,372, 25,593, and 26,188 cm^{-1} as shown in Fig.3.1. These bands are assigned to vibronic transitions of C_3 in solid

p-H_2. The separations of each vibronic band measured from the origin band at 24,499 cm^{-1} were 380, 793, 873, 1,094, and 1,690 cm^{-1}, respectively. All the observed frequencies are listed in Table 3.1.

For the Π-Σ type electronic transition of a linear concentric molecule such as C_3, asymmetric vibrational excitations are allowed when the quantum numbers of both the upper and lower states are even or odd.[32] Since C_3 molecules at 5 K are in the $v = 0$ vibrational ground state, transitions to even-numbered vibronic states, that is $v = 2n$, are expected to be observed. In the bending mode of the $\tilde{A}^1\Pi_u$ upper electronic state, relatively large Renner-Teller coupling was reported. Referring to the transition frequencies of gas phase LIF spectra,,[9] the absorption bands at 24,879, 25,372 and 25,292 cm^{-1} in Fig.3.1 are assigned to $\tilde{A}(02^-0)\leftarrow\tilde{X}(000)$, $\tilde{A}(02^+0)\leftarrow\tilde{X}(000)$ and $\tilde{A}(04^-0)\leftarrow\tilde{X}(000)$ vibronic transitions, respectively. The Renner-Teller splitting of the $v = 2$ level in the $\tilde{A}$ state of C_3 in solid *p*-H_2 is 493 cm^{-1}, which is in good agreement with the splitting of 491 cm^{-1} in the gas phase.[9]

Similarly to the case of the bending excitations, asymmetric-stretching excitations are allowed when even-numbered ν_3 state is excited. The observed frequency difference of 1,690 cm^{-1} between the absorption band at 26,188 cm^{-1} and the origin band at 24,999 cm^{-1} is in good agreement with the frequency difference of 1,671 cm^{-1} for the emission band of $\tilde{A}(002)\rightarrow\tilde{X}(000)$ and that of $\tilde{A}(000)\rightarrow\tilde{X}(000)$ in the gas phase LIF spectra.[9] Thus, the absorption band at 26,188 cm^{-1} in Fig.3.1 is assigned to the $\tilde{A}(002)\leftarrow\tilde{X}(000)$ vibronic transition of C_3.

As for the excitation of symmetric vibrations, transitions with any combination of quantum numbers are allowed. The band at 25,593 cm^{-1} in Fig.3.1 is attributable to the $\tilde{A}(100)\leftarrow\tilde{X}(000)$ transition, because the separation of 1,094 cm^{-1} measured from the band origin in Fig.3.1 is in good agreement with the gas-phase vibrational frequency of 1,085 cm^{-1} for the ν_1 mode in the upper state.[9]

Table 3.1: Observed frequencies of the UV absorption spectrum of C_3 in solid p-H_2.

observed frequency[a] cm^{-1}		difference[b] cm^{-1}	assignment	
24,470.0	w	(-28.6)		
24,484.8	w	(-13.8)		
24,498.6	s	0	band origin	$\tilde{A}^1\Pi_u \leftarrow \tilde{X}^1\Sigma_g^+$
24,500.7	w	(2.1)		
24,501.7	w	(3.1)		
24,504.5	m	(5.9)		
24,507.7	m	(9.1)		
24,511.1	s	(12.5)		
24,513.2	w	(14.6)		
24,515.4	w	(16.8)		
24,516.1	w	(17.5)		
24,517.0	w	(18.4)		
24,518.4	m	(19.8)		
24,519.1	w	(20.5)		
24,521.3	m	(22.7)		
24,525.7	s	(27.1)		
24,535.1	m,b	(36.5)		
24,550.7	w	(51.5)		
24,587.2	w	(88.6)		
24,878.6∼24,902.0	w,b	380.0	$(02^-0)\leftarrow(000)$	asymm. bending
25,291.8∼25,306.8	w,b	793.2	$(04^-0)\leftarrow(000)$	asymm. bending
25,371.5	w,b	872.9	$(02^+0)\leftarrow(000)$	asymm. bending
25,592.9	w	1094.3	$(100)\leftarrow(000)$	symm. stretching
25,605.1	w	(12.2)		
25,619.6	w	(26.7)		
25,630.4	w,b	(37.5)		
26,188.4	m	1689.8	$(002)\leftarrow(000)$	asymm. stretching
26,201.1	m	(12.7)		
26,216.2	w	(27.8)		

[a]Abbreviations: s,strong; m,medium; w,weak; b,broad.

[b]The numbers in parenthesis are the difference in frequency measured from the lowest-frequency peak within each vibronic band. The numbers without parenthesis are those measured from the band origin at 24,498.6 cm^{-1}.

Band shape

Figure 3.2 compares the fine structures of the band origin with those of both asymmetric and symmetric stretching excitations. Almost exactly the same spectral structures were observed for all the samples made with various conditions of crystal growth as well as various precursor molecules. Therefore, the spectral structures shown in Fig.3.2 must be intrinsic to the properties of C_3 molecules in solid p-H_2.

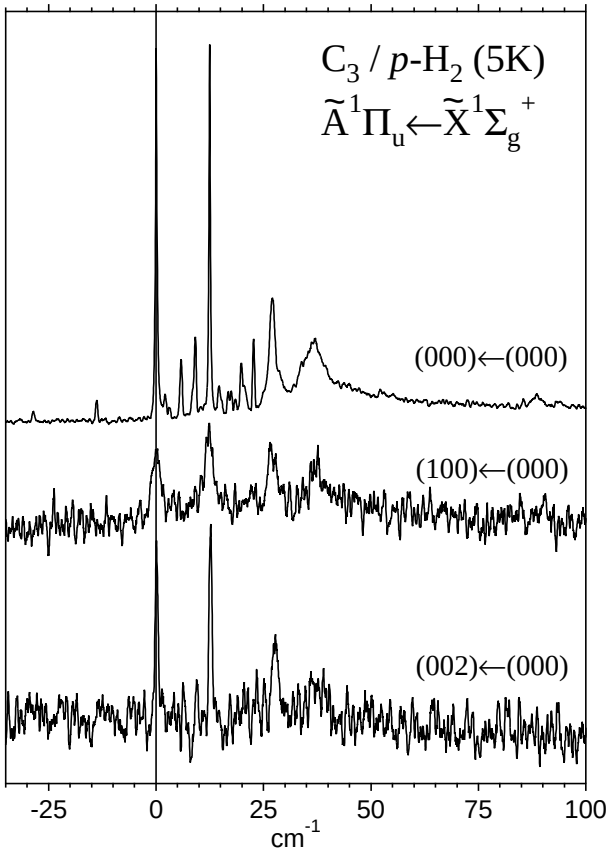

Figure 3.2: Expansion of parts of the absorption spectrum in Fig.3.1. From the upper to the bottom panels; fine structures of the band origin, the $\tilde{A}(100)\leftarrow\tilde{X}(000)$ symmetric stretching band, and the $\tilde{A}(002)\leftarrow\tilde{X}(000)$ asymmetric stretching band of the $\tilde{\mathrm{A}}^1\Pi_\mathrm{u}\leftarrow\tilde{\mathrm{X}}^1\Sigma_\mathrm{g}^+$ transition of C_3 in solid p-H_2. The offsets for the upper, middle, and lower panels are 24,498.6, 25,592.9, and 26,188.4 cm^{-1}, respectively.

In the $\tilde{A}(000)\leftarrow\tilde{X}(000)$ transition (upper panel in Fig.3.2), multiple sharp lines were observed whose width was $\sim$0.8 cm^{-1}, (full width at half maximum: FWHM). The strongest transition was observed at 24,498.6 cm^{-1}. In addition, two major sharp peaks were seen at 12.5 and 27.1 cm^{-1} above the strongest transition. A broad peak, which is probably a phonon band, was seen at 36.5 cm^{-1} above the strongest transition. The separations of the first three sharp peaks are nearly equal. We consider that the fine structure is due to quantized energy levels of hindered rotation or librational motion of linear C_3 in the p-H_2 crystal (see Sec.3.3). Contrary to the case in solid p-H_2, only a single peak accompanied by a phonon band were observed in the band origin of C_3 in solid Ar[12] and in solid Ne,[12,14,18–20] though peaks attributable to different trapping sites were observed.[18,19]

Vibronic bands of $\tilde{A}(100)\leftarrow\tilde{X}(000)$ at 25,592.9 cm^{-1} and $\tilde{A}(002)\leftarrow\tilde{X}(000)$ at 26,188.4 cm^{-1} in Fig.3.1 also showed fine structures composed of equally separated three to four peaks as shown in the middle and lower panels in Fig.3.2. These spectral patterns resemble to the pattern of the $\tilde{A}(000)\leftarrow\tilde{X}(000)$ band origin. The width of each sharp peak in the $\tilde{A}(100)\leftarrow\tilde{X}(000)$ transition was $\sim$3cm^{-1} (FWHM), while those of the $\tilde{A}(002)\leftarrow\tilde{X}(000)$ transition was $\sim$1cm^{-1} (FWHM). The symmetric stretching transition gave broader absorption lines than the asymmetric transition. The difference in the width must result from different relaxation processes in each excited state.

In contrast to the sharp, well-resolved spectral structures in the origin and the stretching-excited vibronic bands, three vibronic bands associated with bending excitations of $\tilde{A}(02^-0)$-$\tilde{X}(000)$ at 24,878.6 cm^{-1}, $\tilde{A}(04^-0)$-$\tilde{X}(000)$ at 25,291.8 cm^{-1}, and $\tilde{A}(02^+0)$-$\tilde{X}(000)$ at 25,371.5 cm^{-1} were much more broadened to 15$\sim$25 cm^{-1} FWHM (see Fig.3.1). Bondybey and English observed a series of vibronic bands of C_3 in a Ne matrix by laser induced fluorescence (LIF) excitation spectra.[14] They found that each vibronic band in Ne matrices was composed of a single peak of a linewidth of $\sim$2 cm^{-1}

FWHM accompanied by a phonon band at higher frequencies.[14] No broadening in the linewidth of the bending excitation transitions was observed in the Ne matrix, contrary to the case in solid p-H_2. The broadness of the bending bands in p-H_2 must originate in the strong coupling between the bending motion of C_3 and the lattice of p-H_2 matrix.

3.3.2 IR spectra

The ν_3 fundamental

After UV irradiation of C_2H_2/p-H_2 system, new absorption lines appeared in the C-C stretching region as shown in Fig.3.3. The absorption feature is assigned to the ν_3 fundamental of C_3. A strong doublet at 2,034.5 and 2,035.9 cm^{-1} was observed with nearly equal intensity. The spectral width was less than 0.01 cm^{-1} FWHM. The separation of the doublet was 1.4 cm^{-1}. The transition frequency and spectral pattern agree well with those in the previous studies in solid p-H_2.[27,29,31]

In addition to the strong doublet, a weak doublet was observed at 2,020.1 and 2,021.7 cm^{-1} as shown in Fig.3.3. Another weak doublet was observed at 1,983.5 and 1,985.0 cm^{-1} as depicted in the inset in Fig.3.3. The splitting width of each doublet was 1.6 and 1.5 cm^{-1} which are similar to that of the strong doublet (1.4 cm^{-1}) at 2,935 cm^{-1}. Since ^{13}C isotopes were contained to its natural abundance of 1.1% in precursor acetylene molecules, part of C_3 must be isotopomers of $^{13}C^{12}C^{12}C$ ($\sim$2%) and $^{12}C^{13}C^{12}C$ ($\sim$1%). According to isotopic substitution studies of laser vaporized C_3 in Ar matrices,[15–17,19] the ν_3 fundamental of $^{13}C^{12}C^{12}C$ was detected at 2,026.2 cm^{-1} and that of $^{12}C^{13}C^{12}C$ was at 1,987.4 cm^{-1}. Therefore, the weak doublet in Fig.3.3 and that in the inset in Fig.3.3 are assigned to the ν_3 fundamental of the monosubstituted isotopomers of $^{13}C^{12}C^{12}C$ and $^{12}C^{13}C^{12}C$, respectively. Matrix shifts of these isotopomeric peaks between p-H_2 and Ar matrices were -5.3 and -3.2 cm^{-1}, respectively. The observed transition frequencies of C_3 in

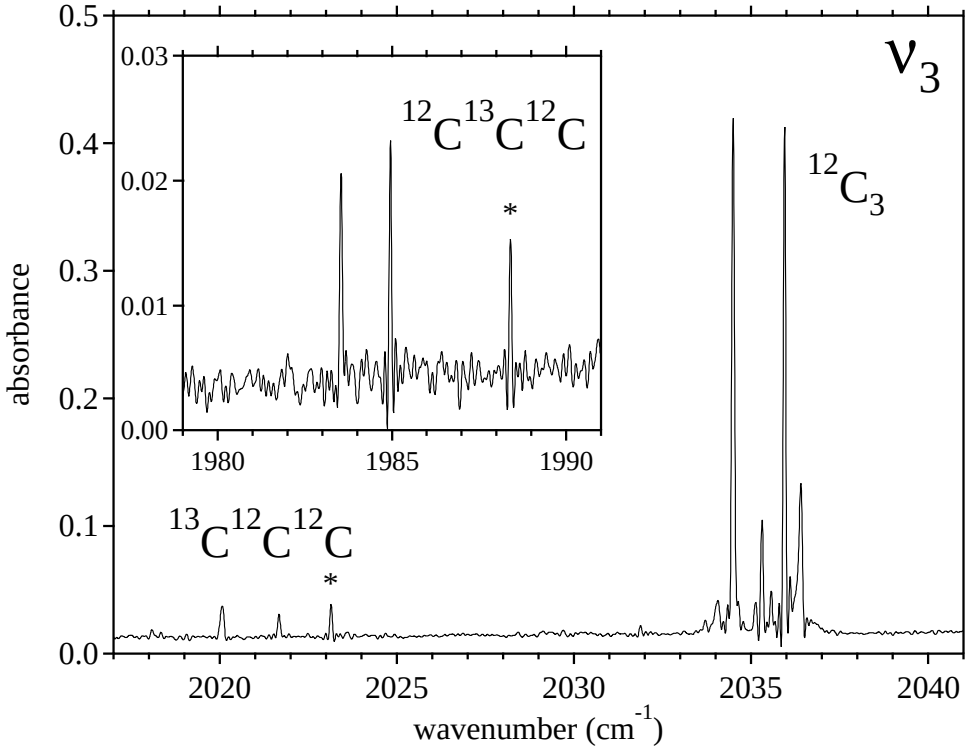

Figure 3.3: IR absorption spectrum of the ν_3 fundamental transition of C_3 in solid p-H_2. The spectral resolution was 0.1 cm^{-1}. The left inset shows a low-frequency region of the spectrum. Peaks with asterisks are due to absorption of water vapor in the laboratory air.

solid p-H_2 are summarized in Table 3.2.

The $\nu_1 + \nu_3$ combination band

An absorption band near 3,244 cm^{-1} shown in Fig.3.4 appeared concomitantly with the ν_3 band of C_3 by the UV irradiation. The transition frequency is close to that of the $\nu_1 + \nu_3$ combination band in solid Ar (3,245.2 cm^{-1}).[15–17] Thus, we assigned the band in Fig.3.4 to the $\nu_1 + \nu_3$ combination of C_3 in solid p-H_2. By using the observed frequency of the ν_3 and the $\nu_1 + \nu_3$ band, the ν_1 symmetric stretching frequency of the ground-state C_3 in solid p-H_2 is calculated to be $\sim$1,209 cm^{-1}.

Table 3.2: Observed IR frequencies of C_3 in solid p-H_2.

frequency cm^{-1}	assignment	splitting width cm^{-1}
1983.5	ν_3 ^{12}C-^{13}C-^{12}C	
1985.0		1.5
2020.1	ν_3 ^{13}C-^{12}C-^{12}C	
2021.7		1.6
2034.5	ν_3 $^{12}C_3$	
2035.3	site peak[a]	
2035.9		1.4
2036.4	site peak[a]	
3244.3	$\nu_1 + \nu_3$ $^{12}C_3$[a]	
3244.5		0.2

[a]Tentative assignments.

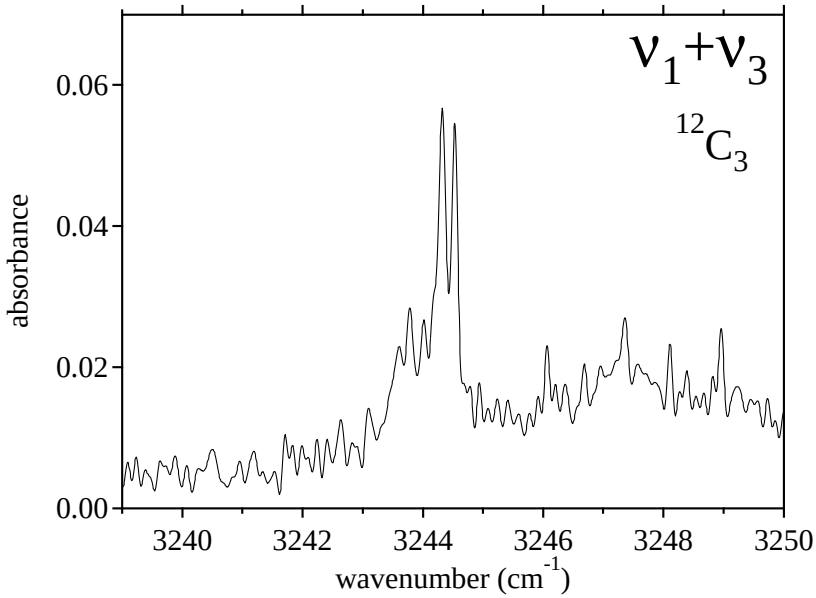

Figure 3.4: IR absorption spectrum of $\nu_1 + \nu_3$ combination band of C_3 in solid p-H_2.

3.3.3 Fine spectral structure

In the ν_3 infrared absorption spectra, a doublet with the splitting of ∼1.5 cm^{-1} was observed. Each component of the doublet was found to show different polarization dependence relative to the crystal axis. Since the spectral pattern and the splitting width were almost exactly the same for all the samples prepared by different conditions or precursors, the doublet must originate in the intrinsic energy levels of C_3 in solid p-H_2.

Although the size of the C_3 molecule (∼4 Å) is still comparable or even smaller than the space of a single substitutional site of the p-H_2 lattice, the spectral structure may not be attributed to the free rotation of the C_3 molecule in solid p-H_2, since there should be more than two rotational branches to be observed at 5K if the molecule is rotating freely. Instead, we propose a model that the doublet originates in the tunneling motion of orientation of the C_3 molecule relative to the crystal. There are three sta-

ble orientations for the C_3 molecule in a single substitutional site of the *hcp* crystal lattice. The potential barrier among these three orientations may be too high to make the C_3 molecule rotate freely. However the potential barrier could be small enough to connect the three orientations each other by a tunneling effect. The situation is similar to the case of tunneling splitting of a methyl group in some molecules.[33] In this model, two transitions are expected, that is A-A and E-E transitions, where A and E represent $k = 0$ and $k = \pm 1$ tunneling levels, respectively (see Ref. 33 for details). Namely, the splitting of $\sim$1.5 cm^{-1} observed in Fig.3.3 corresponds to the difference in energies between the A-A and E-E transitions.

Figure 3.5 shows the high resolution spectrum of the ν_3 transition of C_3 in solid p-H_2. The higher component of the doublet (2,035.9 cm^{-1}) showed a sharp peak, while the lower component (2,034.5 cm^{-1}) split into two peaks. The splitting in the lower component may be attributed to the spectral structure originated in the lift of the degeneracy in the E state. Perturbations of C_3 molecules could partly destroy the axial symmetry of the crystal lattice that makes the E state slightly non-degenerated. We believe the fine structure shown in Fig.3.5 supports the model of the tunneling motion as the origin of the spectral structures seen in all the transitions.

In the $\tilde{A}^1\Pi_u \leftarrow \tilde{X}^1\Sigma_g^+$ electronic transition, fine structures of about 12.5 cm^{-1} spacing were observed as seen in Fig.3.2. The structure must result from the same origin as that of the spectral structure of the IR spectra. Almost one order of magnitude larger spacing in the electronic transition ($\sim$ 12.5 cm^{-1}) compared with that in the vibrational transition ($\sim$ 1.5 cm^{-1}) is worth noting. The large spacing must originate in large energy separation between the A and E states in the electronic excited state. A reliable quantum chemical calculation of the potential is needed to discuss the model further.

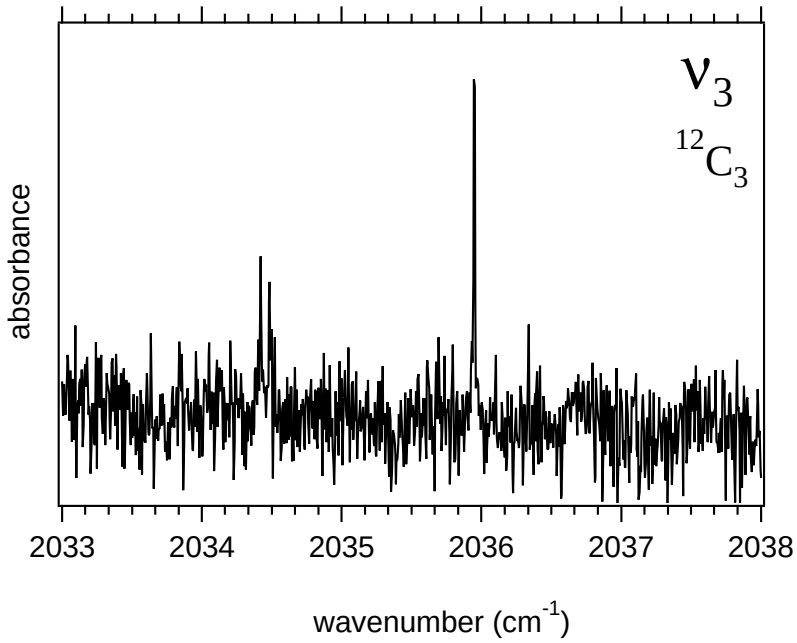

Figure 3.5: A high resolution (0.01 cm^{-1}) spectrum of the ν_3 fundermental transition of C_3 in solid p-H_2.

3.4 Conclusion

The electronic absorption spectrum of C_3 in solid p-H_2 is reported for the first time. The origin band of the $\tilde{A}^1\Pi_u \leftarrow \tilde{X}^1\Sigma_g^+$ transition of C_3 was found at 24,499 cm^{-1} (408 nm). The remarkably narrow linewidth (< 1 cm^{-1}) of the electronic transition allowed us to observe rich spectral structures. Several vibronic bands were also observed in the A-X transition. Among them, the vibronic bands related to bending excitations were much broadened compared with the bands of stretching excitations. In the IR spectrum of the ν_3 fundamental of C_3, a doublet was observed with a narrow linewidth (< 0.01 cm^{-1}). Spectral fine structures observed in both the UV and IR transitions could originate in the tunneling motion of orientation of the C_3 molecule in solid p-H_2. The present work clearly demonstrate the usefulness of solid p-H_2 for high-resolution matrix isolation spectroscopy of electronic

transitions of dopant molecules.

Bibliography

[1] G. Herzberg, *Astrophys. J.* **96**, 314 (1942).

[2] W. Weltner Jr., and R.J. Van Zee, *Chem. Rev.* **89**, 1713 (1989).

[3] A. Van Orden, and R.J. Saykally, *Chem. Rev.* **98**, 2313 (1998).

[4] K.H. Hinkle, J.J. Keady, and P.F. Bernath, *Science* **241**, 1319 (1988).

[5] K. Kawaguchi, K. Matsumura, H. Kanamori, and E. Hirota, *J. Chem. Phys.* **91**, 1953 (1989).

[6] N. Moazzen-Ahmadi, and A.R.W. McKellar, *J. Chem. Phys.* **98**, 7757 (1993).

[7] E.A. Rohlfing, and J.E.M. Goldsmith, *J. Opt. Soc. Am.* **B 7**, 1915 (1990).

[8] F.J. Northrup, and T.J. Sears, *J. Opt. Soc. Am.* **B 7**, 1924 (1990).

[9] W.J. Balfour, J. Cao, C.V.V. Prasad, and C.X.W. Qian, *J. Chem. Phys.* **101**, 10343 (1994).

[10] J. Baker, S.K. Bramble, and P.A. Hamilton, *J. Mol. Spectrosc.* **183**, 6 (1997).

[11] M. Izuha, and K. Yamanouchi, *J. Chem. Phys.* **109**, 1810 (1998).

[12] W. Weltner Jr., and D. McLeod, Jr., *J. Chem. Phys.* **45**, 3096 (1966).

[13] M.E. Jacox, and D.E. Milligan, *Chem. Phys.* **4**, 45 (1974).

[14] V.E. Bondybey, and J.H. English, *J. Chem. Phys.* **68**, 4641 (1978).

[15] J. Szczepanski, and M. Vala, *J. Chem. Phys.* **99**, 7371 (1993).

[16] J. Almlöf, P. Jensen, F.J. Northrup, C.M. Rohlfing, E.A. Rohlfing, and T.J. Sears, *J. Chem. Phys.* **101**, 5413 (1994).

[17] J. Szczepanski, and M. Vala, *J. Chem. Phys.* **101**, 5414 (1994).

[18] I. Čermák, M. Förderer, I. Čermáoková, S. Kalhofer, H. Stopka-Ebeler, G. Monninger, W. Krätschmer, and *J. Chem. Phys.* **108**, 10129 (1998).

[19] A.M. Smith, J. Agreiter, C. Engel, and V.E. Bondybey, *Chem. Phys. Lett.* **207**, 531 (1993).

[20] A.M. Smith, J. Agreiter, M. Härtle, C. Engel, and V.E. Bondybey, *Chem. Phys.* **189**, 315 (1994).

[21] T. Oka, *Ann. Rev. Phys. Chem.* **44**, 299 (1994).

[22] T. Momose, and T. Shida, *Bull. Chem. Soc. Jpn.* **71**, 1 (1998).

[23] M.E. Fajardo, and S. Tam, *Rev. Sci. Instrum.* **70**, 1926 (1999).

[24] T. Momose, H. Hoshina, M. Fushitani, and H. Katsuki, *Vib. Spectrosc.* in press.

[25] H. Katsuki, and T. Momose, *Phys. Rev. Lett.* **84**, 3286 (2000).

[26] T. Momose, M. Miki, T. Wakabayashi, T. Shida, M.C. Chan, S.S. Lee, and T. Oka, *J. Chem. Phys.* **107**, 7707 (1997).

[27] S. Tam, M.E. Fajardo, H. Katsuki, H. Hoshina, T. Wakabayashi, and T. Momose, *J. Chem. Phys.* **111**, 4191 (1999).

[28] H. Hoshina, M. Fushitani, and T. Momose, *J. Mol. Spectrosc.* submitted.

[29] M. Miki, T. Wakabayashi, T. Momose, and T. Shida, *J. Phys. Chem.* **100**, 12135 (1996).

[30] S. Tam, M. Macler, and M.E. Fajardo, *J. Chem. Phys.* **106**, 8955 (1997).

[31] N. Sogoshi, Y. Kato, T. Wakabayashi, T. Momose, S. Tam, M.E. DeRose, and M.E. Fajardo, *J. Phys. Chem.* **104**, 3733 (2000).

[32] G. Herzberg, *Molecular Spectra Molecular Structure, Vol. III Electronic Spectra Electronic Structure of Polyatomic Molecules* (Krieger Publishing, New York, 1991).

[33] J.H. Freed, *J. Chem. Phys.* **43**, 1710 (1965).

Part II

Tunneling chemical reactions of molecules in solid parahydrogen

Chapter 4

Tunneling chemical reactions in solid parahydrogen: Direct measurement of rate constants of $R + H_2 \rightarrow RH + H$ ($R = CD_3$, CD_2H, CDH_2, CH_3) at 5K.

Abstract

Tunneling chemical reactions between deuterated methyl radicals ($R = CD_3$, CD_2H, CDH_2) and the hydrogen molecule in a parahydrogen crystal have been studied by FTIR spectroscopy. The rate constants of the reactions $R + H_2 \rightarrow RH + H$ were determined directly from the temporal change in the intensity of the rovibrational absorption bands of the reactants and products in each reaction. It was found that the rate of each reaction differs definitely depending upon the degree of deuteration in the methyl radicals.

4.1 Introduction

Tunneling effect becomes important in chemical reactions at low temperature because of the suppression of thermally activated reaction processes. Such a situation is expected to be realized in interstellar clouds, for example.[1] How-

ever, the determination of bimolecular rate constants for cryogenic reactions is not easy because most systems are immobilized.

Compared with this difficulty inherent in bimolecular reactions, unimolecular reactions involving intramolecular tunneling processes are relatively easy to study. For example, a long-range hydrogen transfer by tunneling in a radiation damaged dimethylglyoxime crystal was studied by ESR spectroscopy.[2] Hydrogen atom exchange by tunneling was also studied by microwave spectroscopy for a malonaldehyde crystal.[3] More recently, a cis-trans isomerization of formic acid in rare gas matrices was studied in connection with the matrix effect on the tunneling process in the isomerization.[4]

As for the bimolecular reaction, the reaction

$$CH_3 + CH_3OH \rightarrow CH_4 + CH_2OH$$

was studied extensively by ESR spectroscopy.[5,6] Another example of the bimolecular reaction by tunneling was reported between hydrogen atoms and molecules.[7,8] We ourselves have been studying the reaction between the methyl radical and the parahydrogen molecule (p-H_2) at cryogenic temperatures.[9,10]

In the present work we extend our previous studies by covering all isotopomeric radicals CD_3, CD_2H, CDH_2 and CH_3. The aim of the present study is to shed more light on the intrinsic nature of the reactions promoted by tunneling. In order to give a general background of our study, we will first recapitulate our previous work.

During the past decade we have been studying rovibrational spectra of molecules embedded in solid p-H_2 which has several salient features in both high resolution spectroscopic and *in situ* photolytic studies.[9–18] The p-H_2 matrix is capable of providing not only high resolution spectroscopic information of embedded molecules but also subtle intermolecular interaction between trapped molecules and the matrix hydrogen molecule.[12,13,15–18] The feasibil-

ity of the study of *in situ* photolysis stems from the fact that molecules in solid p-H_2 happen to be free from the cage effect, which allows us to study photolytically produced fragments such as radicals originating from the parent molecule.[9,14,19–21]

In a previous paper we have observed FTIR spectra of the CD_3 radical trapped in solid p-H_2 crystal.[9] The decrease in the absorption intensity of CD_3 and the increase in the intensity of CD_3H were observed over a span of about one week at 5 K. As a result of that study, it was found that CD_3 reacts with surrounding hydrogen molecules by tunneling as follows.

$$CD_3 + H_2 \rightarrow CD_3H + H$$

Since the activation energy of the above reaction has been estimated to be 11∼14 kcal/mol ($\simeq 5500 \sim 7000$ K),[22,23] the occurrence of the above reaction at 5 K must be ascribed exclusively to pure tunneling. Assuming that the reaction can be expressed by a pseudo first-order rate law, the tunneling rate constant was determined as $(4.7 \pm 0.5) \times 10^{-6}$ s^{-1}. In the same experiment no appreciable spectral change was observed for the CH_3/p-H_2 system under the same conditions. This difference between the two systems was explained in terms of the enthalpic difference including the zero point energies of the reactants and products.

In the present work we have improved the spectroscopic resolution from 0.25 cm^{-1} for the previous work to 0.1-0.01 cm^{-1} and compared all the four isotopomeric systems. As a result, a systematic difference in the rate constant of the reaction with the matrix hydrogen molecule was disclosed. In order to get hints on the quantum level dependence of the tunneling reaction a preliminary test on the effect of the monitoring IR beam on the reaction rate was also attempted.

4.2 Experiment

Solid parahydrogen used as the matrix was prepared by the same technique described in our previous papers.[9,20] The methyl radicals, CH_3, CH_2D, CHD_2 and CD_3, were produced by *in-situ* photolysis of the corresponding methyl iodides CH_3I, CH_2DI (> 98 atom %D), CHD_2I (> 98 atom %D) and CD_3I (> 99 atom %D), which were premixed with the *p*-H_2 gas containing less than 0.05% of orthohydrogen. The admixture was introduced into a copper optical cell kept at about 8.2 K to grow a transparent mixed crystal. The size of the optical cell was 3.0 cm in length and 1.7 cm in diameter. BaF_2 was used as the windows of the optical cell and the cryostat. A low pressure 20W Hg lamp emitting both 253.7 nm and 184.9 nm photons was employed for photolysis of the iodides. A 4-hour long UV irradiation gave sufficient concentrations of the methyl radicals.

An FTIR spectrometer Bruker IFS 120HR was used throughout the work. To cover both the mid IR and near IR spectral regions two types of the light source were employed: for the mid IR region (10-2 μm) a glober source was used while for the near IR region (2-1 μm) a tungsten lamp was used. A KBr beam splitter and a liquid nitrogen cooled HgCdTe (MCT) detector were used in common to the measurements of the two spectral regions.

After the UV irradiation, the following three modes of measurement were performed in order to examine any possible effect of the light source on the samples.

1. The IR spectra were measured with no optical filter between the light sources and the sample. Since the sample was exposed for a long period to the monitoring IR beam covering a range of 700 cm^{-1}, which was a limit of transmission of the BaF_2 windows, through 7500 cm^{-1}, a limit of the KBr beam splitter, it was suspected that the light sources might have some effect on the sample in this mode of measurement.

The result of the measurement was listed in the second row of Tables 4.2 and 4.3.

2. To test the suspect mentioned for the mode 1, spectral recording was carried out with several IR filters being inserted between the light sources and the sample. Depending upon the spectral bands of our interest several filters were selected as summarized in the third, fourth and fifth rows of Tables 4.2 and 4.3. To be more specific IR filters passing either ranges of 785-1390 cm^{-1} or 2170-3905 cm^{-1} were used for CD_3I, a filter of 2170-3905 cm^{-1} for CHD_2I, and a filter of 1330-2240 cm^{-1} for CH_2DI, respectively.

3. To test further the possible effect of exposing sample to the monitoring beam, measurements of mode 3 were also made, where the light sources were turned off except for the period of spectral scanning which took about 1 or 2 hours for both the mid IR (with a globar source) and the near IR (with a tungsten lamp). During the rest of time a day, that is, about 23 to 22 hours, the sample was kept dark completely. This type of measurement was repeated every day during the whole recording lasting about 1 week. Since the effect of this turning off the light sources turned out to be little, the measurement was performed only for the CD_3I/p-H_2 system as shown in the last row of Tables 4.2 and 4.3.

The temperature of the crystal was kept all the way at 5.0±0.1 K.

4.3 Results and discussion

4.3.1 Obserbed spectra

Figures 4.1 through 4.4 show the results of the systems of CD_3I/p-H_2, CHD_2I/p-H_2, CH_2DI/p-H_2 and CH_3I/p-H_2 recorded by the mode 1 stated in Section

II.

In these figures trace (I) shows spectra as deposited at 5K, trace (II) after a 4 hour UV irradiation, and trace (III) the same as (II) after one week. In each figure spectra due to methane (CHD_3, CH_2D_2, CH_3D, CH_4) are shown at the bottom for the convenience of comparison with the spectra of products seen in (II) and (III). The symbols I, R, and M stands for methyl iodide, methyl radical, and methane, respectively. The observed frequencies of the vibrational fundamental bands of the iodides, the radicals, and the methanes are summarized in Table 4.1 along with the values observed in the gas phase[22,23] or the values obtained by an *ab initio* calcurations.[26] In the table, frequencies at the center of the band are adopted as the frequency of the band origin in solid p-H_2. The details of the result of each system will be discussed below.

Table 4.1: The observed wavenumbers of the vibrational absorption bands of deuterated methyl iodides, methyl radicals, and methanes in solid *p*-H_2. Labels in the parenthesis represent the character of the vibrational modes.

	CH_3I		CH_2DI		CHD_2I		CD_3I	
	p-H_2	gas[a]	*p*-H_2	gas[b]	*p*-H_2	gas[b]	*p*-H_2	gas[a]
ν_1	(a_1)		(a_1)		(a_1)		(a_1)	
(sym. stretch)	2979	2970	2237	2241	2189	2194	2151	2155
ν_2	(a_1)		(a_1)		(a_1)		(a_1)	
(sym. deform.)	1249	1252	1171	1172	1016	1018	947	951
ν_3	(a_1)		(a_1)		(a_1)		(a_1)	
(CI stretch)	N/A	533	N/A	518	N/A	508	N/A	501
	(e)		(a_1)		(a_1)		(e')	
ν_4	3059	3061	2997	3002	3027	3030	2298	2298
(deg. stretch)			(a_1')		(a_1')			
			3055	3057	2341	2336		
	(e)		(a_1)		(a_1)		(e')	
ν_5	1433	1436	1402	1415	1170	1170	1047	1049
(deg. deform.)			(a_1')		(a_1')			
			1234	1240	1280	1287		
	(e)		(a_1)		(a_1)		(e')	
ν_6	886	882	N/A	710	N/A	754	N/A	656
(rock)			(a_1')		(a_1')			
			866	862	N/A	659		

	CH_3		CH_2D		CHD_2		CD_3	
	p-H_2	gas[a]	*p*-H_2	calc[c]	*p*-H_2	calc[c]	*p*-H_2	gas[a]
ν_1	(a_1')		(a_1)		(a_1)		(a_1')	
(sym. stretch)	–	3004	–	2985	–	2135	–	2158
ν_2	(a_2'')		(b_1)		(b_1)		(a_2'')	
(sym. deform.)	–	606	–	553	–	505	–	458
	(e')		(a_1)		(a_1)		(e')	
ν_3	3171	3161	2285	2220	3121	3040	2379	2381
(deg. stretch)			(b_2)		(b_2)			
			3071	3080	2228	2295		
	(e')		(a_1)		(a_1)		(e')	

(*continue to the next page*)

(*continued from the previous page*)

ν_4	1402	1396	1393	1365	1035	1015	1034	1029
(deg. deform.)			(b_2)		(b_2)			
			1179	1145	1281	1210		

	CH_4		CH_3D		CH_2D_2		CHD_3	
	p-H_2	gas[a]	p-H_2	gas[a]	p-H_2	gas[a]	p-H_2	gas[a]
ν_1	(a_1)		(a_1)		(a_1)		(a_1)	
(sym. stretch)	N/A	2917	2972	2945	2973	2976	2990	2993
	(e)		(e)		(a_1)		(e)	
ν_2	N/A	1534	1472	1471	N/A	1436	1290	1291
(sym. deform.)					(a_2)			
					N/A	1333		
	(f_2)		(a_1)		(a_1)		(a_1)	
	3017.3	3019	2198	2200	N/A	2202	2140	2142
ν_3			(e)		(b_1)		(e)	
(deg. stretch)			3015	3017	3010	3013	2248	2263
					(b_2)			
					2231	2234		
	(f_2)		(a_1)		(a_1)		(a_1)	
	1303.6	1306	1304	1300	1031	1033	1002	1003
ν_4			(e)		(b_1)		(e)	
(deg. deform.)			1155	1155	1090	1090	1035	1036
					(b_2)			
					1234	1234		

[a] Reference 24
[b] Reference 25
[c] Reference 26

CD_3I

Trace (I) of Fig.4.1 shows the ν_2 and ν_4 fundamental bands of CD_3I peaking at 947 cm^{-1} and 2298 cm^{-1}. These are close to the reference values in the gas phase.[24] Trace (II) shows the spectra due to the perdeuterated methyl radical (R) and the residual iodide (I).

$$CD_3I \xrightarrow{253.7\text{ nm}+184.9\text{ nm}} CD_3 + I \tag{4.1}$$

The ν_3 and ν_4 bands of CD_3 were observed at 2379 cm^{-1} and 1034 cm^{-1} respectively. Contrary to the previous paper where the ν_3 band of CD_3 was heavily overlapped with the absorption band of CO_2, spectrum in trace (II) of Fig.4.1 shows an uncontaminated ν_3 band of CD_3 because the residual air in the spectrometer was rigorously evacuated in the present experiment. Structures of the ν_3 and ν_4 bands are attributed to the molecular rotation and to the crystal field splitting as in the case of the previous work.[28]

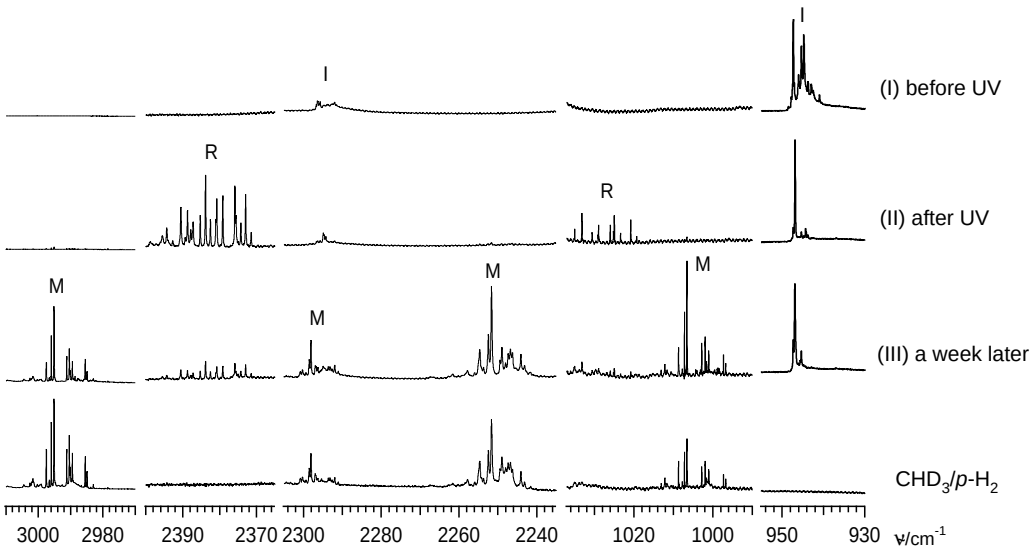

Figure 4.1: Infrared absorption spectra of CD_3I in solid p-H_2. (I) As deposited at 5K. (II) Same as (I) after a 240 min UV irradiation. (III) Same as (II) after one week. The spectra at the bottom is CHD_3 in solid p-H_2 at 4.8K. The symbols, I, R and M stand for the methyl iodide (CD_3I), methyl radical (CD_3) and methane (CHD_3) respectively. Spectra (I)$\sim$(III) are displayed in the same scale.

Although almost unrecognizable in trace (II) of Fig.4.1 very weak signals due to CH_2D_2 were observed at 2973 cm^{-1}. This methane was produced via the following

reactions[20] (cf.bottom of Fig.4.2).

$$\begin{aligned} CD_3 &\xrightarrow{184.9\ nm} CD_2 + D \\ CD_2 + H_2 &\longrightarrow CH_2D_2 \end{aligned} \tag{4.2}$$

Trace (III) of Fig.4.1 recorded after one week long exposition to the light source beam demonstrates sharp peaks at 2990 cm^{-1}, 2298 cm^{-1}, 2248 cm^{-1}, 1035 cm^{-1}, and 1002 cm^{-1}, all of them being attributable to CHD_3 as is supported by nice matching with the authentic spectrum shown at the bottom of Fig.4.1.

CHD_2I

The 3027 cm^{-1} band in trace (I) of Fig.4.2 assigned to the ν_4 absorption of CHD_2I/p-H_2 is in good agreement with the gas phase spectrum.[25] The absorption bands around 3121 cm^{-1}, 2228 cm^{-1}, and 1035 cm^{-1} in trace (II) are close to those of CHD_2 radical observed in the gas phase. They also compare favorably with the results of *ab initio* calculation for the radical[26] and can be assigned as ν_{3a}, ν_{3b}, ν_{4a} bands of CHD_2, respectively. Comparison of trace (III) with the spectrum at the bottom of Fig.4.2 clearly indicates that the peaks at about 3010 cm^{-1}, 2973 cm^{-1}, 2265 cm^{-1}, 2231 cm^{-1}, and 1031 cm^{-1} are associated with ν_{3b}, ν_1, $\nu_{4a} + \nu_{4c}$, ν_{3c}, and ν_{4a} of CH_2D_2, respectively.

CH_2DI

In trace (I) the ν_4, ν_1, and ν_5 bands of CH_2DI are observed at 2997 cm^{-1}, 2237 cm^{-1}, and 1402 cm^{-1} which are close to those in the gas phase.[25] The bands at around 2285 cm^{-1}, 3071 cm^{-1}, and 1393 cm^{-1} in trace (II) are close to those of ν_{3a}, ν_{3b}, ν_{4a}bands of the CH_2D radical, respectively, observed in the gas phase. They are also comparable with the result of an *ab initio* calculation.[26] Reference to the spectrum at the bottom of Fig.4.3 supports the assignment of the bands at

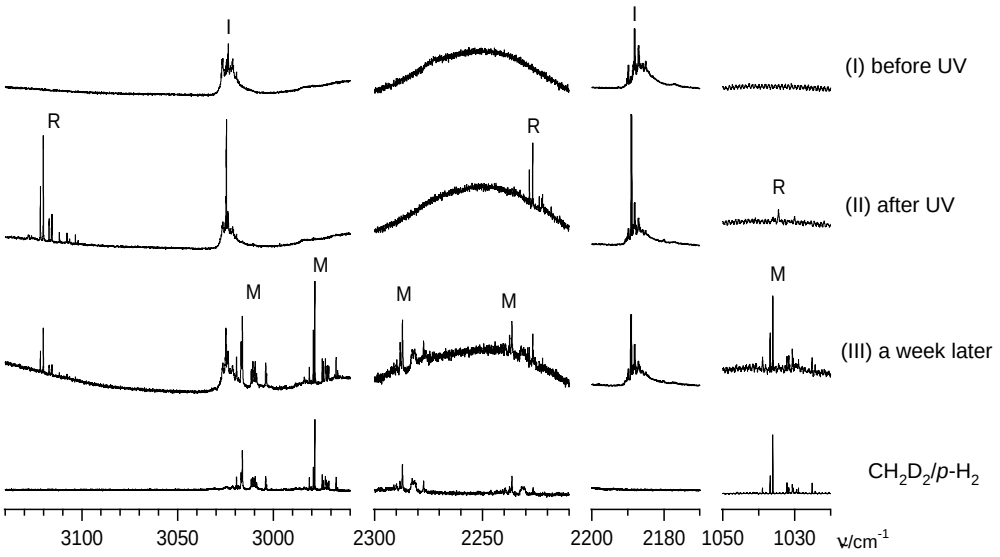

Figure 4.2: Infrared absorption spectra of CHD_2I in solid *p*-H_2. (I) As deposited at 5K. (II) Same as (I) after a 240 min UV irradiation. (III) Same as (II) after one week. The spectra at the bottom is CH_2D_2 in solid *p*-H_2 at 4.8K. The symbols, I, R and M stand for the methyl iodide (CHD_2I), methyl radical (CHD_2) and methane (CH_2D_2) respectively. Spectra (I)∼(III) are displayed in the same scale.

about 3015 cm^{-1}, 2198 cm^{-1}, and 1304 cm^{-1} in trace (III) to the ν_{3b}, ν_{3a}, and ν_{4a} bands of CH_3D, respectively.

CH_3I

Figure 4.4 for the prototypical system is shown for the sake of the integrity of all the isotopomeric systems. The result in Fig.4.4 is in complete agreement with the result of our previous work.[12,20] In brief, the conversion from the CH_3 radical (R) to methane (M) is almost ignorable during the one week standing (cf. (II) and (III) in Fig.4.4). The decrease in the intensity of R is counter balanced by the increase in the intensity of the methyl iodide (I). This result suggests that only some of the radicals recombine with the geminately produced iodine atom. This recombination will be shown to be relatively fast (see below).

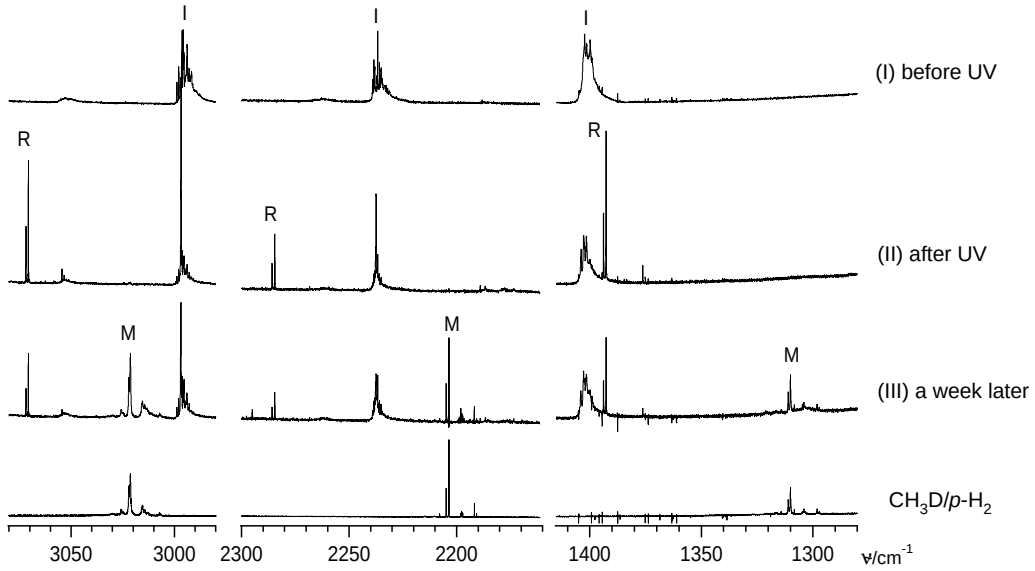

Figure 4.3: Infrared absorption spectra of CH_2DI in solid p-H_2. (I) As deposited at 5K. (II) Same as (I) after a 240 min UV irradiation. (III) Same as (II) after one week. The spectra at the bottom is CH_3D in solid p-H_2 at 4.8K. The symbols, I, R and M stand for the methyl iodide (CH_2DI), methyl radical (CH_2D) and methane (CH_3D) respectively. Spectra (I)$\sim$(III) are displayed in the same scale.

4.3.2 Spectral change

A common feature throughout Figs.4.1 to 4.3 is that the absorption of the radicals observed in trace (II) diminished to be replaced with the appearing absorption of the respective methanes in trace (III). From this result the following reaction scheme is immediately derived in accordance with our previous study.[9]

$$\mathrm{R} + \mathrm{H_2} \xrightarrow{k} \mathrm{RH} + \mathrm{H} \tag{4.3}$$

$$(\mathrm{R} = \mathrm{CD_3}, \mathrm{CHD_2}, \mathrm{CH_2D})$$

In sharp contrast to Figs.4.1-4.3, the all protiated system shown in Fig.4.4 showed almost no measurable change in one week. This result indicates that the reaction between CH_3 radical and parahydrogen does not occur or is too slow to detect by

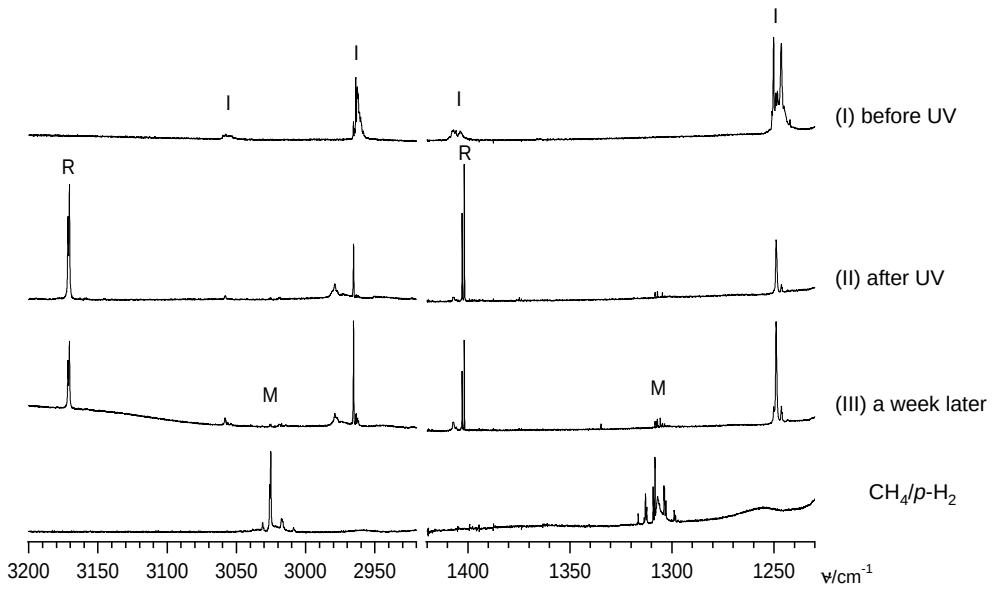

Figure 4.4: Infrared absorption spectra of CH_3I in solid p-H_2. (I) As deposited at 5K. (II) Same as (I) after 240 min UV irradiation. (III) Same as (II) after one week. The spectra at the bottom is CH_4 in solid p-H_2 at 4.8K. The symbols, I, R and M stand for the methyl iodide (CH_3I), methyl radical (CH_3) and methane (CH_4) respectively. Spectra (I)$\sim$(III) are displayed in the same scale.

our experiment.

$$CH_3 + H_2 \not\rightarrow CH_4 + H \tag{4.4}$$

Figures 4.5 and 4.6 demonstrate the temporal change in the intensity of the absorption band of various methyl radicals and the corresponding methanes produced by the irradiation of CD_3I, CHD_2I and CH_2DI systems. Since the baseline determination was not very reliable owing to the long term fluctuation of the background signal, the absorption intensity was estimated by assuming a lorentzian line shape to which the recorded spectral bands were least-squares fitted. In each panel the upper half shows the temporal changes of the methyl radicals and the counterpart methanes in arbitrary units, the latter change being multiplied by an arbitrary constant so as to make the decay of the radicals and the increase of the methanes

look approximately as a mirror image.

In order to interpret the results shown in the upper part of each panel of Figs.4.5 and 4.6 we have attempted the following two analyses. As will be shown later, the second method of analysis adopted for own discussion. Hence, however, the result of both methods is explained. In the first analysis it was assumed that the temporal changes of the radicals and the methanes were due to the reactions in Eq.(4.3). In this case the sum of the numbers of disappearing radicals and appearing methanes should remain constant as expressed in Eq.(4.5), where I_R and I_M represent the integrated intensities and A_R and A_M stand for the absorption coefficients of the radicals and methanes, respectively.

$$\frac{I_R}{A_R} + \frac{I_M}{A_M} = const. \tag{4.5}$$

The unknown parameters A_R and A_M were determined by least-squares fittings. The result of the fittings, however, disproved totally the constancy of the above equation.

As a next trial, it was presumed that some of the radicals were formed and decayed independently of the counterbalancing reaction (3). This presumption is based on the graphical features seen in the lower part of each panel which show the summation of the intensities of the methanes in black area and the radicals in grey. It is seen that the level of the summation becomes quickly (within less than 2×10^5 s) horizontal as shown in broken lines and that in the early stage a rapidly decaying component of the radical exists. It was found that the rapidly decaying component fits roughly an exponential curve, the exponents being summerized in Table 4.2. The variance of the exponents is admittedly large. It is unclear whether this rapid decay process is affected by the monitoring IR beam. All what can be said is that a small fraction of the methyl radicals is subjected to a first decay process, perhaps, a geminate recombination with the counterpart iodine atom produced from the

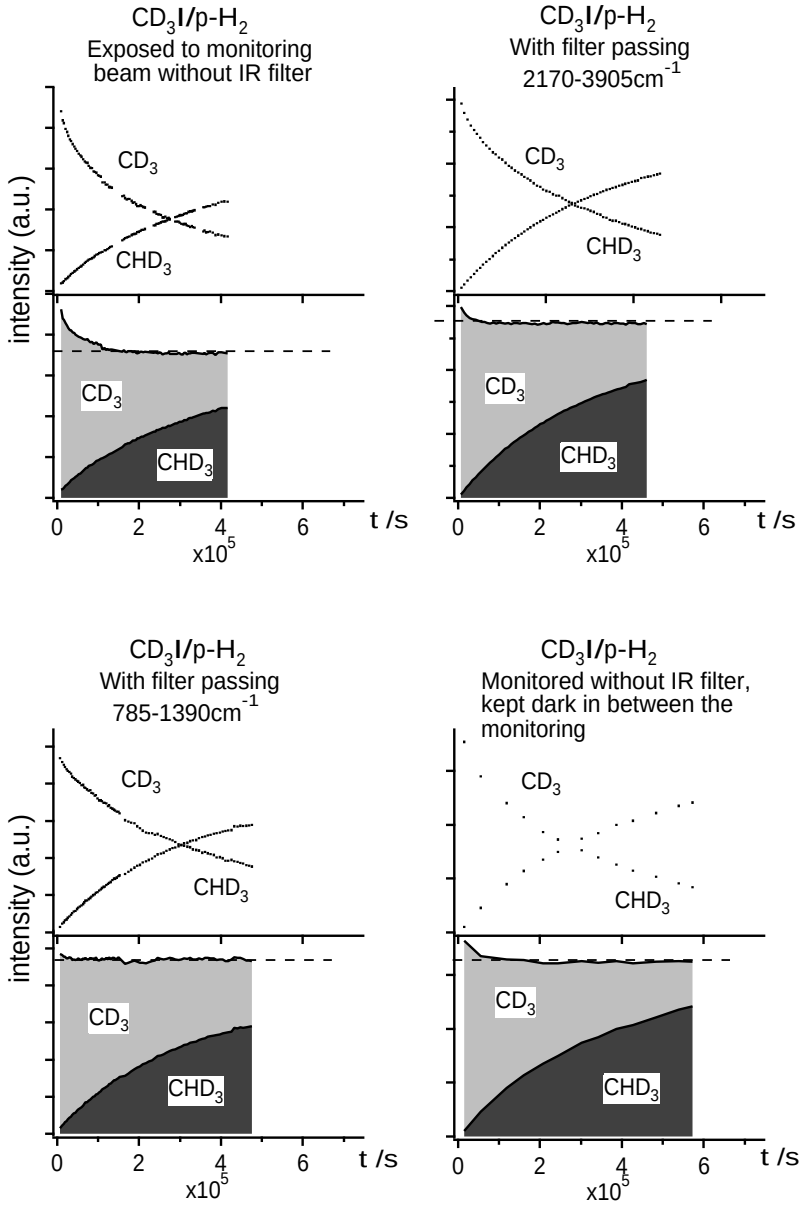

Figure 4.5: The temporal change of CD_3 and CD_3H in solid p-H_2 at 5K after UV irradiation. Upper left: The sample was exposed to the monitoring IR beam throughout the experiment with no IR filter being inserted. Lower left: Same as above with a filter passing 785-1390 cm^{-1}. Upper right: Same as the lower left except that a filter passing 2170-3905 cm^{-1} was used. Lower right: Same as the upper left, but during the idle period of the optical measurement the light source was turned off.

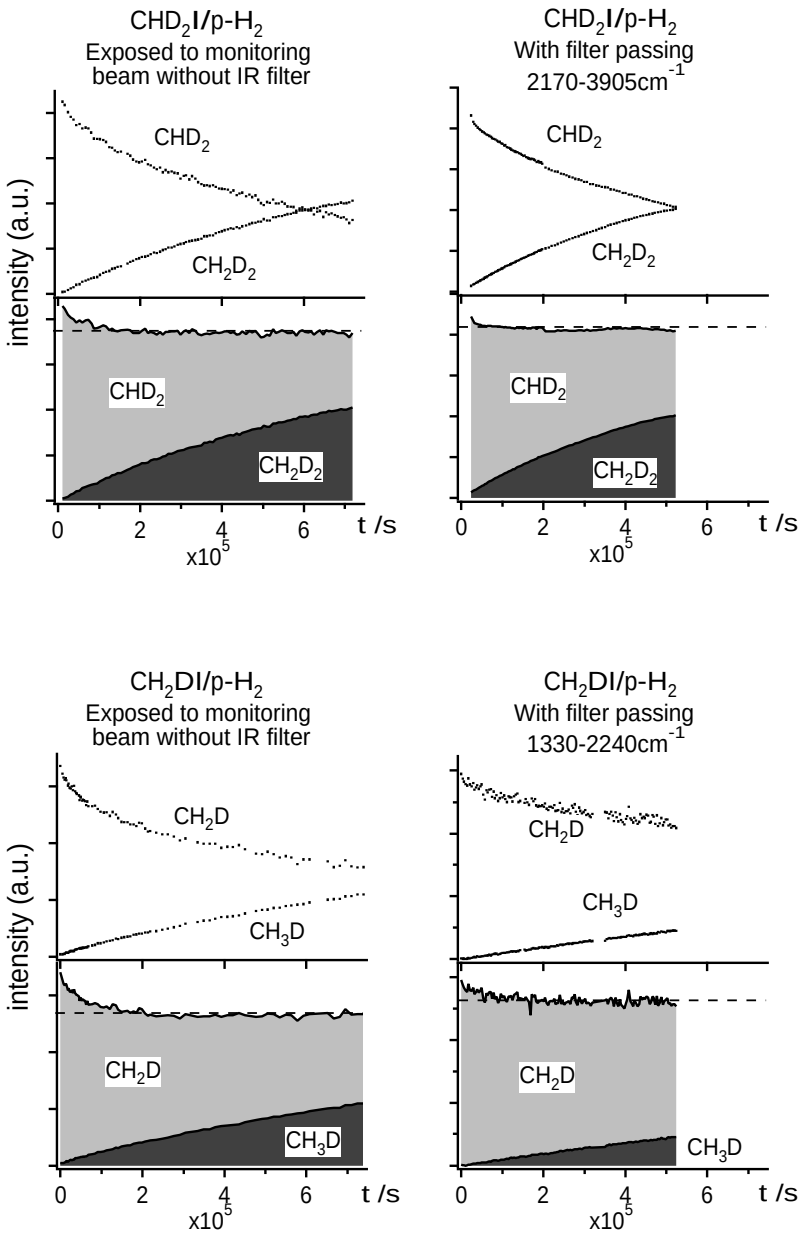

Figure 4.6: The temporal changes of CHD_2 and CH_2D_2 (the upper two panels) and the changes of CH_2D and CH_3D (the lower two panels). Upper left: The sample was exposed to the monitoring IR beam throughout the experiment with no filters being inserted. Upper right: Same as the left except that a filter passing 2170-3905 cm^{-1} was used. Lower left: The sample was exposed to the monitoring IR beam throughout the experiment with no IR filters being inserted. Lower right: Same as the left except that a filter pasing 1330-2240 cm^{-1} was used.

parent iodine by photolysis.

Table 4.2: Pseudo-first order rate constants for the rapidly dacaying component of the CD_3 radical in the CD_3I/p-H_2 system. The numbers in the table represent the pseudo first order rate constant (k) in units of 10^{-5}/sec. The decay corresponds to the area shown in gray exceeding the broken horizontal lines in Fig.4.5. Because of the temporal change of this component is rapid and weak the precision of the rate constants in Table 4.2 is inferior to that in Table 4.3.

	CD_3	CHD_2	CH_2D
no IR filter	1.8 ± 1.1	1.6 ± 2.0	1.5 ± 1.2
filter (2170-3905 cm^{-1})	4.9 ± 2.6	2.1 ± 4.1	–
filter (1330-2240 cm^{-1})	–	–	1.7 ± 5.7
filter (785-1390 cm^{-1})	6.6 ± 2.5	–	–
dark	3.0 ± 2.1	–	–

The fact that a horizontal line is attained by subtracting the above component decaying rapidly suggests that the major component of the radical is associated with the reaction (4.3), which requires that the sum of the radical and the methane produced therefrom remains constant. In the next section this major reaction (4.3) will be discussed after the examination of the geminate recombination between the radical and the iodine atom.

4.3.3 Reaction rate

Recombination between methyl radical and iodine atom

In order to substantiate the assumption of the additional reaction of the radical with the counterpart iodine atom we have surveyed the near infrared region of the photolyzed sample. In that region the magnetic dipole allowed transition of the iodine atom, $^2P_{1/2} \leftarrow ^2 P_{3/2}$, is known to exhibit a characteristic peak at 7640 cm^{-1}.[21] As a matter of fact, the peak was detected easily and showed the temporal

change as shown for the CD_3I system in the upper panel of Fig.4.7. Concomitantly, one of the absorption lines of CD_3I observed at 947.3 cm^{-1} increased as shown in the lower panel of figure 4.7. The rates of the decay and the increase are found to be in agreement each other within their standard deviations. Similar comparative measurements were done for all the iodide systems with no IR filter being set in between the sample and the monitoring IR beam. The observed decay rate of the decay of the iodine atom $1.0 \sim 1.1 \times 10^{-5}$ s^{-1} was found to be favorably comparable with the rate of the rapid decay of the radicals as listed in Table 4.2. These results suggest that some of the photolyzed iodides leave the geminately produced radicals and iodine atoms close to each other and are subjected to the following recombination.

$$R + I \rightarrow RI \tag{4.6}$$

$$(R = CD_3, CHD_2, CH_2D, CH_3)$$

We admit that there is no information on the distance between the reacting partners in reaction (4.6), but they may well be close enough to encounter at the low temperature of 5 K. The radicals far apart from the iodine atom are considered to be subjected to the tunneling reaction with the surrounding hydrogen molecules, which will be discussed in the next section.

Reaction between methyl radical and surrounding hydrogen

As repeatedly stated, one of the salient features of the p-H_2 matrix is that it allows *in situ* photolysis because of the negligibly small cage effect.[29,30] In the present systems too the major process must be the photolytic separation of the pair of the radicals and the counterpart iodine atom. The subsequent major process is obviously the tunneling reaction between the radicals and the surrounding hydrogen molecules in the reaction (4.3). The pseudo-first order reaction constant k in the

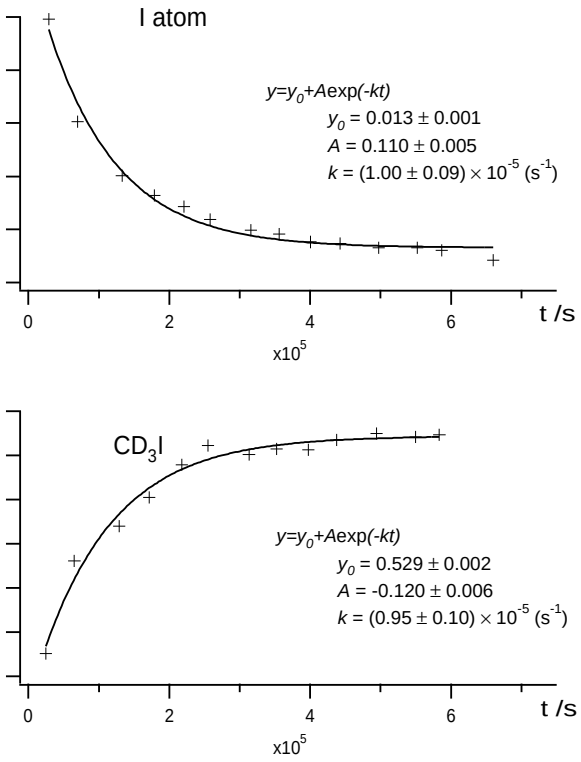

Figure 4.7: The temporal changes of the absorption of I atom (7638 cm^{-1}) and CD_3I (947.3 cm^{-1}) in solid p-H_2. The solid lines represents least squares fitting of the observed relative intensities to a single exponential function plus a residual y_0.

reaction (4.3) is determined by assuming that the number of methanes at time t, that is $N_{CH_4,t}$, is described by the following equation, where $N_{CH_4,\infty}$ stands for the number at an infinitely long period.

$$N_{CH_4,t} = N_{CH_4,\infty}[1 - \exp(-kt)] \tag{4.7}$$

The rate constant was determined by least-squares fitting to obtain the values in Table 4.3. The values are comparable with those of the slowly decaying component of the radicals within the exponential error. Since the intensity of the radicals consists of the rapidly and slowly decaying components, we adopt the values of the increasing methanes for the following analysis of the reaction (4.3). As the second

row of Table 4.3 shows, the rate constant obtained by monitoring the absorption spectra without using any IR filter diminishes as the degree of the deuteration in the radicals decreases. This tendency of the decrease in the rate constant with the decrease of the degree of the deuteration is also noticed in the experiments using the IR filters as is seen in the third through fifth rows of Table 4.3. As for the CD_3I system, we also tried to see any possible effect of the week long IR beam which might affect the reaction through the excitation of the reactions to their vibrational excited states by using different filters or the mode 3 stated in Sec.4.2. It turned out that the effects of the IR light source on the rate constant of CD_3 were roughly within 10 % as is seen in Table 4.3.

Table 4.3: Pseudo-first order rate constants for the increase in the intensity of the three methanes shown graphically in Figs. 4.5 and 4.6. The numbers in the table represent the pseudo first order rate constant (k) in units of 10^{-6}/sec. The second through sixth rows correspond to the three modes of the recording the spectra (see text in Sec.4.2).

	CD_3	CHD_2	CH_2D
no IR filter	3.24(5)	1.34(3)	0.97(4)
filter (2170-3905 cm^{-1})	3.47(3)	2.00(2)	–
filter (1330-2240 cm^{-1})	–	–	0.95(4)
filter (785-1390 cm^{-1})	3.46(4)	–	–
dark	3.0(1)	–	–

4.3.4 Discussion

In our previous paper the difference in the reactivity between CD_3 and CH_3 in the reaction (4.3) was associated to the difference in the enthalpy including the zero potential energies of the reactants and products.[9]

In the present extended study we have examined the validity of our previous approach. Figure 4.8 demonstrates the thermicity including the zero point vi-

bration energies for all the four isotopomeric systems. It is seen that as methyl radicals become heavier the value of $\delta E = E_f - E_i$ decreases. Thus, if the criterion of the occurrence of the reaction depends upon this difference as tentatively suggested in the previous paper, the demarcation line to divide the occurrence and non-occurrence of the reaction seems to be between CH_2D and CH_3 (see the upper horizontal bars in Fig.4.8).

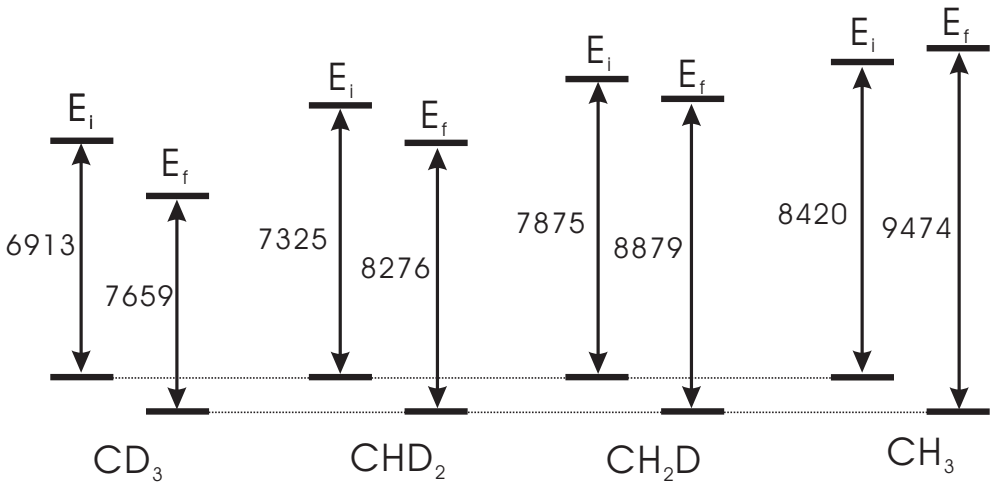

Figure 4.8: The thermicities of $R + H_2 \rightarrow RH + H$ for $R = CD_3$ through CH_3. The numbers for the vertical lines represent the sum of the zero-point vibrational energies of the reactants (initial) and products (final). The units are in cm^{-1}. In order to make the values consistent, calculated vibrational frequencies were used for all the methyl radicals,[26] while vibrational frequencies observed in the gas phase were used for all the methane molecules[24] and the hydrogen molecule.[27] The differences $\delta E = E_f - E_i$ are 746 cm^{-1}, 951 cm^{-1}, 1004 cm^{-1} and 1054 cm^{-1} for the CD_3, CHD_2, CH_2D and CH_3 systems, respectively. The horizontal bars at the bottom common to the four systems represent the energy levels of the potential minima for the initial (reactants) and the final (products) states. The upper horizontal bars show the levels with the zero point energies included. The figure is drawn such that the final state with the zero point energies (upper horizontal bar) is higher than the initial state for the CH_3 system, while the final states are lower than the initial states for all other systems.

The tunneling reaction rate should be analyzed on the basis of the transition

probability between the initial and final states of the reaction. According to the energy diagrams in Fig.4.8 including the sum of the zero-point vibrational energies of the reactants and products the energy mismatch among the three deuterated systems diminishes with the decrease in the degree of deuteration. This tendency may have relevance to the difference in the rate constants summarized in Table 4.3. Since the density of the final (product) state should be larger for heavier systems due to the smaller rotational constant, the chance that the initial and final states resonantly overlap may become larger for heavier systems. On the other hand, detailed analysis of the whole reaction path may also be necessary to understand the difference in the rate constants.[23] Detailed analysis of this point is worthy of further study.

As for the effect of the monitoring IR beam on the reaction rate, significant increase in the tunneling rate of CHD_2 was observed when the IR beam was filtered out except for the region of 2170-3905 cm^{-1} as is seen in Table 4.3. On the other hand, the effect is almost absent on the tunneling rate of both CD_3 and CH_2D. The effect of the monitoring IR beam on the reaction rate must be related to the vibrational quantum level dependence of the tunneling reaction, but the results indicated by Table 4.3 remain totally unexplained at the moment. The problem awaits further studies.

4.4 Conclusion

The significant conclusion of the present work can be summarized as follows,

1. All the deuterated methyl radicals react with *p*-H_2 molecules at 5 K by tunneling to produce methanes. The pseudo-first order reaction rate constants are determined to be about 3.5×10^{-6} s^{-1}, 2×10^{-6} s^{-1}, and 1×10^{-6} s^{-1} for the CD_3, CHD_2, CH_2D radicals, respectively. As an extrapolation, the rate

constant of the prototype system of CH_3 + H_2 is estimated roughly to be $10^{-7} \sim 10^{-8}$ s^{-1} or less.

2. The effect of the monitoring IR beam upon the above reaction is not quite remarkable except for CHD_2.

3. Most of the radical and its counterpoint iodine atom are separated enough upon the UV photolysis in solid p-H_2. However, some of the geminate pairs lie close enough to be subject to a rapid recombination to the parent iodide. The pseudo-first order rate constant is about one order of magnitude larger than the other reaction involving the surrounding hydrogen molecule.

Bibliography

[1] E. Herbst, *Annu. Rev. Phys. Chem.* **46**, 27 (1995).

[2] K. Toriyama, K. Nunome, and M. Iwasaki, *J. Am. Chem. Soc.* **99**, 5823 (1977).

[3] S. L. Baughcum, R. W. Duerst, W. F. Rowe, Z. Smith, and E. B. Wilson, *J. Am. Chem. Soc.* **103**, 6296 (1981).

[4] M. Petterson, E. M. S. Maçôas, L. Khriachtchev, J. Lundell, R. Fausto, M. Räsänen, *J. Chem. Phys.* **117**, 9095 (2002).

[5] E. D. Sprague, and F. Williams, *J. Am. Chem. Soc.* **93**, 787 (1971).

[6] A. Campion, and F. Williams, *J. Am. Chem. Soc.* **94**, 7633 (1972).

[7] T. Miyazaki, K-P. Lee, K. Fueki, and A. Takeuchi, *J. Phys. Chem.* **88**, 4959 (1984).

[8] T. Kumada, K. Komaguchi, Y. Aratono, T. Miyazaki, *Chem. Phys. Lett.* **261**, 463 (1996).

[9] T. Momose, H. Hoshina, N. Sogoshi, H. Katsuki, T. Wakabayashi, and T. Shida, *J. Chem. Phys.* **108**, 7334 (1998).

[10] T. Momose and T. Shida, *Bull. Chem. Soc. Jpn.* **71**, 1 (1998).

[11] D. P. Weliky, K. E. Kerr, T. J. Byers, Y. Zhang, T. Momose, T. Oka, *J. Chem. Phys.* **105**, 4461 (1996).

[12] T. Momose, T. Miki, T. Wakabayashi, T. Shida, M. -C. Chan, S. S. Lee, and T. Oka, *J. Chem. Phys.* **107**, 7707 (1997).

[13] T. Momose, H. Katsuki, H. Hoshina, N. Sogoshi, T. Wakabayashi, and T. Shida, *J. Chem. Phys.* **107**, 7717 (1997).

[14] T. Momose, M. Miki, M. Uchida, T. Shimizu, I. Yoshizawa, and T. Shida, *J. Chem. Phys.* **103**, 1400 (1995).

[15] S. Tam, M. E. Fajardo, H. Katsuki, H. Hoshina, T. Wakabayashi and T. Momose *J. Chem. Phys.* **111**, 4191 (1999).

[16] H. Hoshina, T. Wakabayashi, T. Momose, and T. Shida, *J. Chem. Phys.* **110**, 5728 (1999).

[17] H. Katsuki, and T. Momose, *Phys. Rev. Lett.* **84**, 3286 (2000).

[18] H. Katsuki, T. Nakamura, and T. Momose, *J. Chem. Phys.* **116**, 8881 (2002).

[19] M. Fushitani, N. Sogoshi, T. Wakabayashi, T. Momose and T. Shida, *J. Chem. Phys.* **109**, 6346 (1998).

[20] M. Fushitani, and T. Momose, *J. Chem. Phys.* **116**, 10739 (2002).

[21] M. Fushitani, T. Momose, and T. Shida, *Chem. Phys. Lett.* **356**, 375 (2002).

[22] K. Kraka, J. Gauss, and D. Cremer, *J. Chem. Phys.* **99**, 5306 (1993), and references cited therein.

[23] Y. Kurosaki, and T. Takayanagi, *J. Chem. Phys.* **110**, 10830 (1999).

[24] T. Shimanouchi, *"Molecular Vibrational Frequencies"* in NIST Chemistry WebBook, NIST Standard Reference Database Number 69, Eds. P.J. Linstrom and W.G. Mallard, March 2003, National Institute of Standards and Technology, Gaithersburg MD, 20899 (http://webbook.nist.gov).

[25] J. R. Riter, Jr., and D. F. Eggers, Jr., *J. Chem. Phys.* **44**, 745 (1966).

[26] J. L. Brum, R. D. Johnson III and J. W. Hudgens, *J. Chem. Phys.* **98**, 3732 (1993).

[27] G. Herzberg, *Molecular Spectra Molecular Structure, Vol. I, Spectra of Siatomic Molecules*, (Krieger Publishing, New York, 1991).

[28] H. Hoshina, M. Fushitani, and T. Momose, *to be published.*

[29] N. Sogoshi, T. Wakabayashi, T. Momose, and T. Shida, *J. Phys. Chem. A* **105**, 3077 (2001).

[30] T. Shida, and T. Momose, in *Sciences of Free Radicals (in Japanese)*, E. Hirota, ed., (Gakkai Shuppan Center, Tokyo, 1998).

Appendix A

Pair interaction between methyl radical and hydrogen molecule

A.1 Electronic interaction of pair molecules

When a pair molecules a and b are far apart and the electron exchange can be neglected, the total hamiltonian $\mathscr{H}$ is

$$\mathscr{H} = \mathscr{H}_a^{(0)} + \mathscr{H}_b^{(0)} + \mathscr{H}' \tag{A.1}$$

where $\mathscr{H}_a^{(0)}$, $\mathscr{H}_b^{(0)}$ is the unperturbed hamiltonian of free molecules a and b, and $\mathscr{H}'$ is the electronic interaction in between them which is,

$$\begin{aligned} \mathscr{H}' &= \sum_{i_a, i_b} e_{i_a} e_{i_b} R_{i_a, i_b}^{-1} \\ &= q_b \phi_b - \mu_{b,\alpha} F_{b,\alpha} - \frac{1}{3} \Theta_{b,\alpha\beta} F_{b,\alpha,\beta} \cdots \\ &= q_a \phi_a - \mu_{a,\alpha} F_{a,\alpha} - \frac{1}{3} \Theta_{a,\alpha\beta} F_{a,\alpha,\beta} \cdots \end{aligned} \tag{A.2}$$

where R_{i_a,i_b} is the distance from the element of charge e_{i_a} in molecule a to e_{i_b} in molecule b, q_a, $\mu_{a,\alpha}$, $\Theta_{a,\alpha\beta}$ are the charge, dipole moment and quadrupole moment opearators for the molecule a, ϕ_a is the electric potential at the origin of molecule

a due to the instantaneous charge distribution of molecule b,

$$F_{a,\alpha} = -\nabla_\alpha \phi_a \tag{A.3}$$

and

$$F_{a,\alpha\beta} = -\nabla_\alpha \nabla_\beta \phi_a \tag{A.4}$$

are the field and field-gradient operator, respectively. The Greek subscripts α, β in Eqs.(A.3) and (A.3) denote vector or tensor components and can be equal to x, y, z and a repeated Greek subscript denotes a summation over all the Cartesian components. For example, $\Theta_{\alpha\beta}F_{\alpha\beta}$ is expanded as follows.

$$\begin{aligned}
\Theta_{\alpha\beta}F_{\alpha\beta} &= \sum_{\alpha,\beta=x,y,z} \Theta_{\alpha\beta}F_{\alpha\beta} \\
&= \Theta_{xx}F_{xx} + \Theta_{xy}F_{xy} + \Theta_{xz}F_{xz} + \Theta_{yx}F_{yx} + \Theta_{yy}F_{yy} \\
&\quad + \Theta_{yz}F_{yz} + \Theta_{zx}F_{zx} + \Theta_{zy}F_{zy} + \Theta_{zz}F_{zz}
\end{aligned} \tag{A.5}$$

The interaction Hamiltonian $\mathscr{H}'$ can be written as a multipole series,

$$\begin{aligned}
\mathscr{H}' &= T_a q_a q_b + T_{a,\alpha}(q_b \mu_{a,\alpha} - q_a \mu_{b,\beta}) \\
&\quad + T_{a,\alpha\beta}\left(\frac{1}{3} q_b \Theta_{a,\alpha\beta} + \frac{1}{3} q_a \Theta_{b,\alpha\beta} - \mu_{a,\beta}\mu_{b,\alpha}\right) \\
&\quad + T_{a,\alpha\beta\gamma}\left(\frac{1}{15} q_b \Omega_{a,\alpha\beta\gamma} - \frac{1}{15} q_a \Omega_{b,\alpha\beta\gamma} - \frac{1}{3}\mu_{b,\alpha}\Theta_{a,\beta\gamma} + \frac{1}{3}\mu_{a,\alpha}\Theta_{b,\beta\gamma}\right) \\
&\quad + \cdots
\end{aligned} \tag{A.6}$$

where, if $\boldsymbol{R}$ is the vector from the origin of b to a, the tensor $\boldsymbol{T}$ is,

$$T_a = R^{-1} \tag{A.7}$$

$$T_{a,\alpha} = \nabla_\alpha R^{-1} = -R_\alpha R^{-3} \tag{A.8}$$

$$T_{a,\alpha\beta} = \nabla_\alpha \nabla_\beta R^{-1} = (3R_\alpha R_\beta - R^2\delta_{\alpha\beta})R^{-5} \tag{A.9}$$

$$T_{a,\alpha\beta\gamma} = -3[5R_\alpha R_\beta R_\gamma - R^2(R_\alpha \delta_{\beta\gamma} + R_\beta \delta_{\gamma\alpha} + R_\gamma \delta_{\alpha\beta})]R^{-7} \tag{A.10}$$

The electronic interaction of the molecules in the states of $\psi_{a_0}^{(0)}$ and $\psi_{b_0}^{(0)}$ may be obtained from perturbation theory and is,

$$\begin{aligned} W_{a_0,b_0} &= W_{a_0}^{(0)} + W_{b_0}^{(0)} + \langle \psi_{a_0}^{(0)} \psi_{b_0}^{(0)} | \mathscr{H}' | \psi_{a_0}^{(0)} \psi_{b_0}^{(0)} \rangle \\ &\quad - \sum_{i,j} \frac{|\langle \psi_{a_0}^{(0)} \psi_{b_0}^{(0)} | \mathscr{H}' | \psi_{a_i}^{(0)} \psi_{b_j}^{(0)} \rangle|^2}{(W_{a_i}^{(0)} - W_{a_0}^{(0)}) + (W_{b_j}^{(0)} - W_{b_0}^{(0)})} + \cdots \end{aligned} \tag{A.11}$$

where $\sum_{i,j}$ is the summation over all unperturbed states $\psi_{a_i}^{(0)} \psi_{b_j}^{(0)}$ except $\psi_{a_0}^{(0)} \psi_{b_0}^{(0)}$. The first order perturbed energy $\langle \psi_{a_0}^{(0)} \psi_{b_0}^{(0)} | \mathscr{H}' | \psi_{a_0}^{(0)} \psi_{b_0}^{(0)} \rangle$ is called *electrostatic energy* $\mathscr{U}_{elec}$, which has the values only when both molecules have electric charge.

The second order perturbation energy includes both the induction energy and dispersion energy. The sets of excited unperturbed states $\psi_{a_i}^{(0)} \psi_{b_0}^{(0)}$ and $\psi_{a_0}^{(0)} \psi_{b_j}^{(0)}$, in which the matrix elements of $\mathscr{H}'$ are diagonal in a and b, produce the *induction energy* $\mathscr{U}_{ind}$ and the remaining excited states constitute the *dispersion energy* $\mathscr{U}_{disp}$.

$$\mathscr{U}_{ind} = -\sum_{i \neq 0} \frac{|\langle \psi_{a_0}^{(0)} \psi_{b_0}^{(0)} | \mathscr{H}' | \psi_{a_i}^{(0)} \psi_{b_0}^{(0)} \rangle|^2}{W_{a_i}^{(0)} - W_{a_0}^{(0)}} - \sum_{j \neq 0} \frac{|\langle \psi_{a_0}^{(0)} \psi_{b_0}^{(0)} | \mathscr{H}' | \psi_{a_0}^{(0)} \psi_{b_j}^{(0)} \rangle|^2}{W_{b_j}^{(0)} - W_{b_0}^{(0)}} \tag{A.12}$$

$$\mathscr{U}_{disp} = -\sum_{i \neq 0, j \neq 0} \frac{|\langle \psi_{a_0}^{(0)} \psi_{b_0}^{(0)} | \mathscr{H}' | \psi_{a_i}^{(0)} \psi_{b_j}^{(0)} \rangle|^2}{(W_{a_i}^{(0)} - W_{a_0}^{(0)}) + (W_{b_j}^{(0)} - W_{b_0}^{(0)})}. \tag{A.13}$$

By using London approximation, Backingham simplified the dispersion energy in Eq.(A.13) as follows,

$$\begin{aligned} \mathscr{U}_{disp} &= -\frac{I^{(a)} I^{(b)}}{4(I^{(a)} + I^{(b)})} \Big[T_{b,\alpha\beta} T_{b,\gamma\delta} \alpha_{a,\alpha\gamma}^{(a)} \alpha_{b,\beta\delta}^{(b)} \\ &\quad + \frac{2}{3} T_{b,\alpha\beta} T_{b,\gamma\delta\epsilon} (\alpha_{\alpha\gamma}^{(a)} A_{\beta,\delta\epsilon}^{(b)} - \alpha_{\alpha\gamma}^{(b)} A_{\beta,\delta\epsilon}^{(a)}) + \cdots \Big] \end{aligned} \tag{A.14}$$

where $I^{a,b}$ equals to the first ionization potential energy, and $\boldsymbol{\alpha}^{a,b}$ and $\boldsymbol{A}^{a,b}$ are the dipole and quadrupole polarizability tensor of molecule a and b.

Hence, the pair interaction potential between two molecules can be written as

$$\mathscr{U}_{pair} = \mathscr{U}_{elec} + \mathscr{U}_{ind} + \mathscr{U}_{disp} \cdots . \tag{A.15}$$

When thinking about pair interaction between symmetric top molecules and p-H_2, $\mathscr{U}_{elec}$ and $\mathscr{U}_{ind}$ in Eq.(A.15) are zero because both molecules have neither electric charge nor permanent electric dipole moment. Hence Eq.(A.14) represents the pair potential in the classical approximation.

A.2 Dispersion interaction between CH_3 (CD_3) and p-H_2

From Eqs.(A.9) and (A.10), Eq.(A.14) is rewrited as

$$\begin{aligned}\mathscr{U}_{disp} &= -\frac{I^{(a)}I^{(b)}}{4(I^{(a)}+I^{(b)})}\Bigg[\frac{1}{R^{10}}\{3R_\alpha R_\beta - R^2\delta_{\alpha\beta}\}\{3R_\gamma R_\delta - R^2\delta_{\gamma\delta}\}\alpha^{(a)}_{\alpha\gamma}\alpha^{(b)}_{\beta\delta} \\ &\quad -\frac{3}{R^{12}}\{3R_\alpha R_\beta - R^2\delta_{\alpha\beta}\}\{5R_\gamma R_\delta R_\epsilon - R^2(R_\gamma\delta_{\delta\epsilon}+R_\delta\delta_{\epsilon\gamma}+R_\epsilon\delta_{\gamma\delta})\} \\ &\quad \times(\alpha^{(a)}_{\alpha\gamma}A^{(b)}_{\beta,\delta\epsilon} - \alpha^{(b)}_{\alpha\gamma}A^{(a)}_{\beta,\delta\epsilon})\Bigg]. \end{aligned} \tag{A.16}$$

By substituting x, y, z to $\alpha, \beta, \gamma, \delta, \epsilon$, Eq.(A.16) becomes

$$\begin{aligned}\mathscr{U}_{disp} &= -\frac{I^{(a)}I^{(b)}}{4(I^{(a)}+I^{(b)})}\Bigg[\frac{1}{R^6}(4\alpha^{(a)}_{zz}\alpha^{(b)}_{zz} - 4\alpha^{(a)}_{xz}\alpha^{(b)}_{xz} - 4\alpha^{(a)}_{yz}\alpha^{(b)}_{yz} + 4\alpha^{(a)}_{xx}\alpha^{(b)}_{xx} \\ &\quad +4\alpha^{(a)}_{yy}\alpha^{(b)}_{yy} + 4\alpha^{(a)}_{xy}\alpha^{(b)}_{xy}) - \frac{3}{R^7}(\alpha^{(a)}_{xx}A^{(b)}_{x,xz} - \alpha^{(b)}_{xx}A^{(a)}_{x,xz} + \alpha^{(a)}_{xz}A^{(b)}_{x,xx} \\ &\quad -\alpha^{(b)}_{xz}A^{(a)}_{x,xx}\cdots\cdots + \alpha^{(a)}_{zz}A^{(b)}_{z,zz} - \alpha^{(b)}_{zz}A^{(a)}_{z,zz})\Bigg] \end{aligned} \tag{A.17}$$

Here, the dipole polarizability $\alpha_{\alpha,\beta}$ can be rewrited as $\alpha_{\alpha,\beta} = \alpha\delta_{\alpha,\beta}$ because the tensor $\boldsymbol{\alpha}$ has only diagonal elements. The matrix elements $\alpha^{(H_2)}_{\alpha\alpha}$ of parahydrogen molecule has the values of $\alpha^{(H_2)}_{xx} = \alpha^{(H_2)}_{yy} = \alpha^{(H_2)}_{zz} = \alpha^{(H_2)}$ and the quadrupole polarizability of hydrogen molecule $A^{(H_2)}_{\alpha,\beta\gamma}$ equals to zero because the rotational wavefunction of the ground state of hydrogen molecule is completely spherical. Therefore,

$$\begin{aligned}\mathscr{U}_{disp} &= -\frac{I^{(H_2)}I^{(R)}}{4(I^{(H_2)}+I^{(R)})}\Bigg[\frac{1}{R^6}\alpha^{(H_2)}(4\alpha^{(R)}_{zz} + \alpha^{(R)}_{yy} + \alpha^{(R)}_{xx}) \\ &\quad -\frac{6}{R^7}\alpha^{(H_2)}(-A^{(R)}_{x,xz} - A^{(R)}_{y,yz} + A^{(R)}_{z,xx} + A^{(R)}_{z,yy} - 2A^{(R)}_{z,zz})\Bigg] \end{aligned} \tag{A.18}$$

where $\boldsymbol{\alpha}^{(R)}$ is the dipole polarizability tensor and $\boldsymbol{A}^{(R)}$ is the quadrupole polarizability tensor of methyl radical written out in the pair frame axes.

In order to estimate the potential energy from known parameters of molecular polarizability, the parameters $\boldsymbol{\alpha}^{(R)}$ and $\boldsymbol{A}^{(R)}$ must be transformed in the molecular fixed frame $\{X, Y, Z\}$.

The transformation of dipole polarizability from pair frame axis $\boldsymbol{\alpha}_{pair}$ to molecular fixed axis $\boldsymbol{\alpha}_{mol}$ is the similar transformation,

$$\begin{aligned}
\boldsymbol{\alpha}_{pair} &= \boldsymbol{\Phi}^{-1}\boldsymbol{\alpha}_{mol}\boldsymbol{\Phi} \\
&= \begin{pmatrix} \cos\phi\cos\theta\cos\chi - \sin\phi\sin\chi & -\cos\phi\cos\theta\sin\chi - \sin\phi\cos\chi & \cos\phi\sin\theta \\ \sin\phi\cos\theta\cos\chi + \cos\phi\sin\chi & -\sin\phi\cos\theta\sin\chi + \cos\phi\cos\chi & \sin\phi\sin\theta \\ \sin\theta\cos\chi & \sin\theta\sin\chi & \cos\theta \end{pmatrix} \\
&\quad \times \begin{pmatrix} \alpha_{XX} & 0 & 0 \\ 0 & \alpha_{YY} & 0 \\ 0 & 0 & \alpha_{ZZ} \end{pmatrix} \\
&\quad \times \begin{pmatrix} \cos\phi\cos\theta\cos\chi - \sin\phi\sin\chi & \sin\phi\cos\theta\cos\chi + \cos\phi\sin\chi & -\sin\theta\cos\chi \\ -\cos\phi\cos\theta\sin\chi - \sin\phi\cos\chi & -\sin\phi\cos\theta\sin\chi + \cos\phi\cos\chi & \sin\theta\sin\chi \\ \cos\phi\sin\theta & \sin\phi\sin\theta & \cos\theta \end{pmatrix}
\end{aligned} \tag{A.19}$$

where $\{\phi, \theta, \chi\}$ is the Euler angles relating the molecule fixed frame $\{X, Y, Z\}$ and pair fixed frame $\{x, y, z\}$. The dipole polarizabilities in Eq.(A.18) is transformed to the molecular fixed frame as

$$\begin{aligned}
4\alpha_{zz} + \alpha_{yy} + \alpha_{xx} &= 2(\alpha_{XX} + \alpha_{YY} + \alpha_{ZZ}) \\
&\quad + (2\alpha_{ZZ} - \alpha_{YY} - \alpha_{XX})\left(\frac{3}{2}\cos^2\theta - \frac{1}{2}\right)
\end{aligned} \tag{A.20}$$

Here, let us introduce the quantities

$$\alpha = \frac{1}{3}(\alpha_{XX} + \alpha_{YY} + \alpha_{ZZ}) \tag{A.21}$$

and

$$\gamma = \alpha_{ZZ} - \alpha_{XX} = \alpha_{ZZ} - \alpha_{YY} \tag{A.22}$$

where α is called the *isotropic* part of the polarizability and γ is called the *anisotropic* part of the polarizability. Finally, Eq.(A.20) becomes,

$$\begin{aligned} 4\alpha_{zz} + \alpha_{yy} + \alpha_{xx} &= 6\alpha + 2\gamma\left(\frac{3}{2}\cos^2\theta - \frac{1}{2}\right) \\ &= 6\alpha + 2\gamma D^2_{00}(\phi\theta\chi) \end{aligned} \tag{A.23}$$

where D^2_{00} is the Wigner's rotation matrix.

On the other hand, $\boldsymbol{A}$ is the quadrupole polarizability tensor defined as

$$\begin{pmatrix} \Theta_{xx} \\ \Theta_{xy} \\ \Theta_{xz} \\ \Theta_{yx} \\ \Theta_{yy} \\ \Theta_{yz} \\ \Theta_{zx} \\ \Theta_{zy} \\ \Theta_{zz} \end{pmatrix} = \begin{pmatrix} A_{xxx} & A_{yxx} & A_{zxx} \\ A_{xxy} & A_{yxy} & A_{zxy} \\ A_{xxz} & A_{yxz} & A_{zxz} \\ A_{xyx} & A_{yyx} & A_{zyx} \\ A_{xyy} & A_{yyy} & A_{zyy} \\ A_{xyz} & A_{yyz} & A_{zyz} \\ A_{xzx} & A_{yzx} & A_{zzx} \\ A_{xzy} & A_{yzy} & A_{zzy} \\ A_{xzz} & A_{yzz} & A_{zzz} \end{pmatrix} \begin{pmatrix} E_x \\ E_y \\ E_z \end{pmatrix} \tag{A.24}$$

where $\boldsymbol{E}$ is the electric field vector and $\boldsymbol{\Theta}$ is the quadrupole moment induced by $\boldsymbol{E}$.

As is in Eq.(A.19), similar transformation was opearated to the tensor $\boldsymbol{A}$.

$$\begin{aligned} \boldsymbol{A}_{pair} &= \boldsymbol{\Phi}^{-1}\boldsymbol{A}_{mol}\boldsymbol{\Phi} \\ &= \cdots . \end{aligned} \tag{A.25}$$

The quadrupole polarizabilities in Eq.(A.18) was transformed as

$$\begin{aligned} &-A_{xxz} - A_{yyz} + A_{zxx} + A_{zyy} - 2A_{zzz} \\ &\quad = 2(A_{XXX} - A_{XYY} - A_{YXY} - A_{YYX}) \\ &\qquad \times(\sin^3\theta\cos^3\chi - 3\sin^3\theta\cos\chi\sin^2\chi) \qquad \text{(A.26)} \\ &\quad = \frac{\sqrt{5}}{2}AD^{3*}_{03}(\phi\theta\chi) \qquad \text{(A.27)} \end{aligned}$$

where A is the quadrupole polarizability of D_{3h} molecule defined as

$$A = A_{XXX} - A_{XYY} - A_{YXY} - A_{YYX}. \tag{A.28}$$

By substituting Eq.(A.23) and Eq.(A.27) to Eq.(A.18), dispersion interaction $\mathscr{U}_{disp}$ is given as,

$$\begin{aligned}\mathscr{U}_{disp} &= -\frac{I^{(\mathrm{H_2})}I^{(R)}}{4(I^{(\mathrm{H_2})}+I^{(R)})}\alpha^{(\mathrm{H_2})}\Bigg[\frac{1}{R^6}\{6\alpha^{(R)}+2\gamma^{(R)}D^2_{00}(\phi\theta\chi)\} \\ &\quad -\frac{1}{R^7}3\sqrt{5}A^{(R)}D^{3*}_{03}(\phi\theta\chi)\Bigg] \end{aligned} \tag{A.29}$$

where $\alpha^{(R)}$,$\gamma^{(R)}$ and $A^{(R)}$ are the molecular polarizability of the methyl radical.

Acknowledgement

I express my sincere gratitude to Prof. T. Momose for his faithful advices and continuous encouragements. I also thank him for the proofreading of the manuscript and many comments which improved this work very much. I am heartily grateful to Prof. T. Shida for the proofreading and critical comments on the manuscript of Part II. I would like to thank Dr. T. Wakabayashi for his helpful advice on the manuscript of Chapter 3. Thanks are also due to Dr. N. Sogoshi, Dr. H. Katsuki, Dr. M. Fushitani and the colleagues of my laboratory for the support of the experiments and constructive discussions. The author was financially supported by Research Fellowships of the Japan Society for the Promotion of Science for Young Scientists. Finally, I would like to express my sincere thanks to my parents.

Hiromichi Hoshina

Kyoto June, 2003